THE GENETIC CHARACTER AND SPATIAL DISTRIBUTION OF PORE SYSTEMS IN MICROBIALITE CARBONATES

A Dissertation

by

MARCELO FAGUNDES DE REZENDE

Submitted to the Office of Graduate and Professional Studies of
Texas A&M University
in partial fulfillment of the requirements for the degree of

DOCTOR OF PHILOSOPHY

Chair of Committee,	Michael C. Pope
Committee Members,	Ethan Grossman
	Zoya Heidari
	Yuefeng Sun
Head of Department,	John R. Giardino

August 2015

Major Subject: Geology

ABSTRACT

Microbialite carbonate deposits are highly influenced by environmental settings, resulting in a large variety of depositional textures and fabrics. Pore systems in these deposits have a primary relation to the dominant depositional texture, which is later modified by diagenesis. Therefore, recognizing the textural controls on the pore system development and petrophysical characteristics is important to enhance the reservoir quality prediction in subsurface. Three microbialite carbonate deposits on different basins and ages were studied to address the effectiveness of these controls.

The first deposit, documented in chapter I, is a microbialite build-up formed in the Holocene lagoon Lagoa Salgada in Brazil. This deposit has undergone minimum diagenetic evolution, and textures and pore systems are directly correlated. Their textures and pore systems were evaluated by computed tomography and petrography. Stratigraphic interpretation and carbon and oxygen stable isotopes link these changes to depositional settings. The results show that large structure size, open packing and chaotic fabric form a better primary pore system.

The second deposit is the subsalt microbialite carbonates formed in lacustrine to lagoonal settings in the Santos Basin, Brazil. These carbonates have high heterogeneity in terms of textures and pore systems. Texture analysis indicated that particle size is a primary control on pore size and permeability, whereas sorting influences the porosity, and the permeability, and packing is a secondary control on porosity. Cements reduce

the final pore system, while dissolution enhances it. These results are presented in chapter II, and supplemented with log interpretation in Appendix A.

The third deposit, documented in chapter III, is an outcrop with lacustrine microbialite carbonates of the Eocene Green River Formation in Utah. Computed tomography and petrography were used to characterize pore systems and their relations to textures. In these deposits, pore systems derived from chaotic and open fabrics are better developed, with larger pores and higher connectivity than those derived from organized and tight fabrics. Stratigraphic relations indicate a strong depositional control on the distribution of microbialite textures throughout the outcrop.

ACKNOWLEDGEMENTS

I would like to thank my committee chair, Dr. Michael C. Pope, and my committee members, Dr. Ethan Grossman, Dr. Zoya Heidari, and Dr. Yuefeng Sun, for their guidance and support throughout the course of this research.

Thanks also go to my friends and colleagues and the faculty and staff of the departments of Geology and Geophysics and Petroleum Engineering for making my time at Texas A&M University a great experience. I also want to extend my gratitude to PETROBRAS, which sponsored this research, and the Brazilian National Agency of Petroleum, Natural Gas and Biofuels for authorizing the use of South Atlantic subsalt data.

Finally, thanks to my wife, my mother, my father and little Maggie for their encouragement, patience and love.

TABLE OF CONTENTS

Page

ABSTRACT ii

ACKNOWLEDGEMENTS iv

TABLE OF CONTENTS v

LIST OF FIGURES viii

LIST OF TABLES xx

CHAPTER I THREE-DIMENSIONAL PORE CONNECTIVITY EVALUATION IN HOLOCENE AND JURASSIC MICROBIALITE BUILD-UPS 1

Overview 1
Introduction 2
Geologic setting 4
Lagoa Salgada microbialites 4
Late Jurassic Smackover Formation thrombolite 6
Methods 7
X-ray computed tomography 7
Carbon and oxygen stable isotopes 11
Petrophysics 12
Petrography and cathodoluminescence 13
Results 13
Lagoa Salgada microbialite depositional textures 13
Stable isotopes 14
Smackover thrombolite primary porosity reconstruction 16
Discussion 19
Evolution of the Lagoa Salgada microbialite build-up 19
Evolution of the Lagoa Salgada microbialite porous media 24
Comparison to Late Jurassic thrombolite from Smackover Formation 31
Application of data to production 32
Conclusions 33

CHAPTER II IMPORTANCE OF DEPOSITIONAL TEXTURE IN PORE CHARACTERIZATION OF SUBSALT MICROBIALITE CARBONATES, OFFSHORE BRAZIL 35

Overview 35
Introduction 36
Geologic setting 39
Methods 41
Data 49
Carbonate textures 49
Pore system characteristics 50
Results 50
Discussion 63
Conclusions 66

CHAPTER III LATERAL CONTINUITY OF ROCK AND PETROPHYSICAL PROPERTIES IN A MICROBIALITE BUILD-UP IN THE GREEN RIVER FORMATION, UTAH 68

Overview 68
Introduction 69
Geologic setting 71
Methods 74
Petrography 75
Petrophysics 75
X-ray computed tomography 76
Image analysis 76
Results 77
Stratigraphy, build-up external geometry and facies distribution 77
Pore system characteristics of microbialites 87
Discussion 98
Texture controls on pore system in the Eocene Green River Formation microbialites 98
Reservoir quality lateral continuity in the Eocene Green River Formation microbialites 99
Applicability of data to production 101
Conclusions 103

REFERENCES 105

APPENDIX A 117

APPENDIX B 133

APPENDIX C 136

LIST OF FIGURES

Page

Figure I.1 Satellite maps show the location of the Lagoa Salgada (highlighted box), and the microbialite build-up sampling site on the western margin (white arrow) 5

Figure I.2 Schematic stratigraphic column for the Paraíba do Sul deltaic complex. The thickness of each interval changes laterally along the deltaic complex. Modified from Lemos (1995), and Dias and Kjerfve (2009) 8

Figure I.3 (A) Photograph of the microbialite build-up. The growth cycles, erosional surface (red dotted line) and sampling points for cores (red circles with white fill) and stable isotopes (yellow boxes) are shown. (B) Interpreted section labeled for different depositional textures (stromatolite, thrombolite, digitate stromatolites and grainstone). The green material that cover some areas on the sample are surface coloring by encrusting algae. 10

Figure I.4 Photomicrographs for the thrombolite (A and B), and stromatolite (C and D) textures (plain polarized light on left and cross polarized light on right). The thrombolite texture is massive and has a chaotic growth pattern. The stromatolite is laminated and with an organized growth pattern. Micritic peloids are the main building block for both textures. The peloids are bounded by calcium carbonate cements. The non-carbonate grains are quartz and undifferentiated feldspars 15

Figure I.5 Stratigraphic profile described for the microbialite build-up, $\delta^{13}C_{VPDB}$ and $\delta^{18}O$ ‰ $_{VPDB}$. The isotopic values increase towards the thrombolite intervals and decrease towards the stromatolites intervals indicating higher methanogenesis rate for the thrombolite intervals. The strong shift in the $\delta^{13}C$ ‰ and $\delta^{18}O$ ‰ values across the discontinuity resulted from a more humid climate condition that brought ^{16}O rich meteoric waters to the lagoon reducing, the evaporative trend and decreasing the rate of methanogenesis by more oxygenated bottom waters 17

Figure I.6 (A) Upper Jurassic Smackover Formation thrombolite, Little Cedar Creek Field, Alabama. The greyish colors are the microbial structures and the brownish colors are diagenetic cements. (B) Thin section image showing the microbial structures formed by syndepositional peloids cementation (dark components), mosaic and blocky calcite diagenetic cements (bright yellow colors) and pores (blue colors). (C) Cathodoluminescent thin section image. The microbial structures are dull, the calcite mosaic cement phase has low bright brown color and the blocky calcite cement has a zonation from low bright brown to bright yellow colors. (D) Reconstruction of the original microbial framework and subsequent cementation phases. The microbial structures are shown in brown, the calcite mosaic cement is shown in pink, the blocky calcite cement is shown in purple and the pores are shown in light blue 18

Figure I.7 “Time” slice series for the microbialite build-up. On the left plate, the horizontal and vertical arrows show the directions incremental height from the bottom to top. The slices are spaced 1.22 mm apart. This plate allows the interpretation of the build-up evolution, showing the upward shift and lateral distribution of internal depositional textures, and changes on the external morphologies, from individual to coalesced heads. A main flow channel and several secondary channels are partially filled with grains visible on these slice series. On the right plate selected slices to show specific features (red outlines), such as channels (white arrows), phases of head individualization and coalescence, and each depositional texture. These selected slices are numbered, and identified by color margins on the slice series. The first three slices are on the growth cycle 1 and the last three are on the growth cycle 2. Slice 37 is in the planar stromatolite interval, two individual heads are visible separated by a flow channel filled by grains. Slice 57 is in the first thrombolite interval, several round branches with an open packing define the main aspect of this depositional texture, the heads started to coalesce during this phase. Slice 80 is in the small digitate stromatolite, whose heads are totally coalesced and the channel between heads is closed. The packing is tight, which resulted in small isolated pores (black spots). Slice 94 is at the base of the large digitate stromatolite interval of cycle 2. The growth initiated as isolated heads, and a large channel filled by grains was developed in between heads. Slice 112 is at the top of the large digitate stromatolite interval, the individual heads are visible with a well-connected channel system. The tight packing and the vertical pore network orientation isolated the framework porosity that appears as dark circular zones in each head. Slice 149 is in the second thrombolite interval defined by round branches and open packing. The heads coalesced at this phase and enclose the channel system. The small digitate stromatolite cap the

microbialite build-up appears as a rim around the build-up on slices 112 and 149.....22

Figure I.8 Pore networks from CT scan rendering in different depositional textures. (A) Planar stromatolite has horizontally oriented pore network that is poorly connected vertically. (B) Thrombolite interval has large pore volume with chaotic porous network formed by fast growth rates and no preferential growth pattern. (C) Large digitate stromatolite has large and vertically oriented pores produced by the open growth pattern. Some pores resulted from enclosing of flow channels during the coalescence of different heads in this interval. (D) Small digitate stromatolite has vertically oriented pores that are poorly connected due the tight packing.....26

Figure I.9 Detail of pore geometries and pore throats of the thrombolite texture. The pores have very irregular geometries and a wide size distribution, thus small and simple pores occur besides large and complex pores. The pore throats also have irregular distribution and differing diameters. A set of pores may be connected by narrow and wide pore throats (black arrow).....27

Figure I.10. CT scan rendered volumes for the microbialite build-up. The pores shown in blue and the rock constituents are shown in green (high attenuation) and in red (low attenuation). The high attenuation is caused by dense carbonate areas (binding cement) and the low attenuation is caused by microporosity in peloid rich areas. The flow channels between coalescent heads connect different pore intervals and areas along the build-up 29

Figure I.11 CT scan rendered volume presented as the pore-rock boundary. The planar stromatolite appears at the base of the build-up with narrow horizontal pore geometries. The thrombolite is next visible texture, characterized by a chaotic and bright interval. This chaotic texture is due to a large volume of well-connected pores and chaotic fabric. The small digitate stromatolite appears as small vertical pores isolated in a dark interval after the thrombolite. These three intervals define the growth cycle 1. The upper part of the build-up indicates the growth cycle 2 has a lower volume of pores compared to the growth cycle 1. The limit between the 2 cycles is shown by a white dotted line. The large digitate stromatolite appears on the upper interval as large and vertical oriented bright areas. The thrombolite of the growth cycle 2 is visible on the

chaotic bright are above the large digitate stromatolite. Channels between heads appear on the image as wide and tall vertical features on the middle of the build-up. These channels connect the large digitate stromatolite with the thrombolite intervals, and the two growth cycles. The dark interval on top is the small digitate stromatolite low volume of pores, which capped the build-up.....30

Figure II.1 (A) Inset map - The eastern shore of Brazil and the Federation States are shown. (B) Location map of the Santos and Campos basin on the south-eastern Brazilian margin. The white circle marks the approximate study area in the zone of deep-water subsalt reservoirs (shaded dark grey area)...38

Figure II.2 Three common textures formed in the subsalt microbialite carbonates in the South Atlantic. (a) Microbial laminite, with plain to crinkle micritic laminae. (b) Medium shrub microbialite defined by shrubs with heights between 5 mm and 10 mm occurring in the upper half of the image. (c) Large shrub microbialite texture (shrubs > 10 mm). In most intervals microbial structures of different sizes coexist, so the textures are differentiated based on the dominance of one size class over the others 40

Figure II.3 Three possible pore system end-members formed by the depositional framework and diagenetic modifications. The three images show large digitate stromatolite texture, with the pore system end-members. Pores are shown in blue. The depositional pore system is characterized by a clear textural control on pore characteristics. The diagenetically enhanced pore system has depositional pores enlarged and new pores (intraparticle, moldic and vugs) formed by dissolution. The diagenetically reduced pore system has most of its pore space filled by cements (e.g. calcite). Hybrid pore systems have characteristics between the diagenetic end-members.....42

Figure II.4 Three main textural components formed in the subsalt microbialite carbonates in the South Atlantic. Dark areas are pores. All photomicrographs are with cross-polarized light. (a) Micritic laminae. (b) fibrous-radial spherulite. Crystals floating around the spherulite are dolomite. (c) Fan shaped radial shrub with peloids.....43

Figure II.5 Macroscopic and microscopic characteristics used to describe different microbial carbonate textures the relative precipitation rate for each texture. On the photo/depositional pore system pairs the red cross is an anchor for the field views. On the photo (left image) the greyish and white colours are carbonate and black areas are pore-system. The depositional pore system (right hand binary image) is shown in blue and the rock components in white.....46

Figure II.6 Data distribution for a set of 15 samples, showing the normalized structure size (a) and packing (b). The box thickness and whiskers indicates that the individual samples are different, regarding their internal variability for the analysed attribute. The boxes are built to show the number of measurements within the first and third quartiles. Longer boxes indicate that the sample has a high internal variability and shorter boxes indicate a lower variability in the sample. The black bar is the median value for each sample. The length of whiskers represents the lowest and highest values within 1.5 times the difference between the third and first quartile. Circles indicate measurements distant from the rest of the data, in this study they were not discarded as outliers. The area adjacent to each plug was described and categorized by texture and reference number: L = large shrub microbialite, M = medium shrub microbialite and S = small shrub microbialite. 52

Figure II.7 Microbialite carbonate textures are grouped based on shrub size, sorting, packing and morphology aspect. The dark areas represent the microbialite framework. This textural grouping is important because changes on these properties results in changes in the pore system characteristics such as pore size, pore-throat radius and tortuosity 53

Figure II.8 Pore geometry characteristics related to different microbialite carbonate textures. Usually, laminites have horizontal pores. Shrub microbialites have a variety of pore geometries from vertical to complex. The pore size, pore-throat radius and tortuosity are controlled by textural characteristics as shrub size, sorting and packing. The pore system is shown in white, and the rock framework in black. Modified after Hofmann (1976).....54

Figure II.9 Porosity v. permeability plot for each texture analysed from the subsalt microbialite reservoir units. There is a wide distribution of values with a

positive correlation. However, the regression line for each texture has different slopes. These relationships suggest that given moderate or less diagenetic modifications, texture also controls pore system characteristics and impacts petrophysical properties. Only samples with reservoir potential are shown. The grey areas represent samples with more dissolution features (top right area) and more cementation (bottom left area) described by petrography. The samples outside these areas have the depositional pore system less modified by diagenesis. The scale for shrubs is: small shrubs < 5 mm; medium shrubs between 5 mm and 10 mm; large shrubs > 10 mm 55

Figure II.10 (a) Plot of mean pore throat radius distribution per texture, including samples with pore systems classified as depositional, hybrid and diagenetically enhanced. (b) Plot of mean pore throat radius distribution per texture, without samples with pore systems classified as diagenetically enhanced. The pore-throat radius distribution is shifted towards larger values, as the texture change from laminites to large digitate stromatolite. The effect of diagenetic enhancement is identified where distributions show peaks for larger pore-throats for the laminite, small digitate stromatolite and medium digitate stromatolite. This diagenetic signal is not observed for the large digitate stromatolite texture. (c) Shrub size distribution compared to the pore-throat radius distribution in (a). These two properties measure distinct properties at different scales, but the similarity of the shift toward larger values between these properties distributions is suggestive that the size of the structures controls the pore and pore-throat sizes.....59

Figure II.11 (a) Comparison between shrub mean size (mm) and effective porosity (%) for shrub microbialite textures. The data are scattered showing no correlation between size and porosity. (b) Comparison between shrub mean size (mm) and absolute permeability (md). The data suggest that the shrub size is related to permeability as size controls the pore size and pore-throat radius 60

Figure II.12 (a) Comparison between shrub size sorting index and effective porosity (%) for shrub microbialite textures. Higher values indicate poorer sorting. (b) Comparison between shrub size sorting index and permeability (md). The relationships observed on both plots suggest that shrub size sorting impacts porosity and permeability. Poorly-sorted textures have their pore volume reduced, smaller pore-throats and higher

tortuosity because of the presence of shrubs of different sizes that occupy more space in a volume when compared to well-sorted textures ...61

Figure II.13 (a) Comparison between packing index and effective porosity (%) for each shrub microbialite texture. There are subtle trends for the shrub microbialite textures that correlates porosity increments to looser packing (higher packing index values), which are identifiable for each texture. The points that are plotted outside the main field are textures with a high concentration of large spaces between adjacent shrubs. (b) Comparison between packing index and permeability (md) for each shrub microbialite texture. The relationship between packing and permeability is not clear for this dataset 62

Figure II.14 Based on the relations of textural aspects, pore system characteristics and petrophysical properties, a general model is suggested for the microbialite carbonate textures analysed in this study. The numbers below the boxes are the total porosity calculated from bi-dimensional image analysis. The size of the shrubs for a given sorting controls major changes in the pore size and permeability, as result large structures allow larger pores and pore-throats. The porosity apparently is controlled by the shrub size sorting, because poorly-sorted textures have more shrubs with different sizes in comparison to well-sorted textures. This occurs because a relative reduction on the pore volume and pore throat radius, as well an increase the tortuosity of the pore system in poorly-sorted textures 65

Figure III.1 Inset map A – United States map with the states where the Great Green River Basin, Uinta Basin and Piceance Creek Basin are located. B – Regional map with the areal distribution of the Eocene lake basins (Great Green River Basin, Uinta Basin and Piceance Creek Basin), major uplifts and tectonic lineaments (modified after Smith et al., 2008). The white square shows the area of study in Utah, at the eastern border of the Uinta Basin.....71

Figure III.2 (a) Local map with the main roads and cities near the area of study in the Uintah County, UT (Map courtesy from the State of Utah). The red square indicates the area of study. (b) Satellite image showing the Three Mile Canyon Road and adjacent terrain (Image courtesy from Google and NASA). The areas highlighted in red are the microbialite build-ups

and detrital carbonates outcrops. The numbers 1 to 5 show the location of the stratigraphic sections in the outcrop 72

Figure III.3 Simplified stratigraphic section for units in the outcrop along Three Mile Canyon Road, showing lithology, sedimentary structures, grain types and the interpreted regressive-transgressive cycles. There are seven carbonate units interbedded with sandstone and shale deposits. The first unit is thicker and has a good lateral continuity of detrital and microbial carbonates throughout the outcrop. The passage from a transgressive period to the regressive periods was defined in the middle of a shale interval deposited before the first carbonate bed with gypsum crystal growth. It is based on the assumption that the maximum transgressive was reached at this stage and the lake water become more saturated in salts, favoring sulfate precipitation during rapid lake level falls, in a similar mechanism to the gypsum deposition in Dead Sea lakes proposed by Torfstein et al. (2008).....79

Figure III.4 Main microbialite external morphologies formed in this outcrop. (a) Panoramic image of the outcrop. The intervals highlighted in purple correspond to the microbialite build-ups and associated detrital carbonate deposits in the first carbonate unit. The numbers in red above the first interval are the location of the stratigraphic sections on the outcrop. The image has a 3x vertical exaggeration. (b) Laterally linked microbialite bioherms between the stratigraphic sections 4 and 5 (highlighted box on image (a). The white layer at the middle of the section is composed of intraclast packstone that represent a moment without microbialite growth. (c) Small microbialite heads formed on top of the section showed in the image b. They are coalesced in most areas, sometimes forming isolated depressions between them. (d) Meter-scale isolated microbialite head formed on top of the microbialite interval at section 1. Hammer for scale is 41 cm long. (e) Laterally linked microbialite at section 3. The center of this structure has thrombolite texture (light colors) and the outer layers formed a digitate stromatolite texture (dark colors). Hammer for scale is 41 cm long 82

Figure III.5 Shallow-water and exposure sedimentary structures. (a) Caliche and partially silicified intraclast grainstone filling a small depression on the top of the lowest carbonate unit. The S on the image marks the silicified interval. (b) Close-up of the highlighted area in a. There is a noticeable stratification in this caliche/grainstone deposit. The cavities are

grainstone layers more susceptible to dissolution and erosion. The bar on this image has a length of 1 cm. (c) Thin section image showing the caliche infiltration into the grainstone pore space and partial carbonate replacement by silica. The bar on this image has a length of 0.25 mm. (d) Intraclast chips of mudstone and desiccation cracks formed on the top of the first carbonate unit. (e) Tufa formed around a tree root on the top of the seventh carbonate unit. (f) Close-up image on the area highlighted in e, showing the root marks impressed on the carbonate surface.....83

Figure III.6 Stratigraphic section for the first carbonate unit in this outcrop, showing the vertical and lateral distribution of facies, the depositional texture, grain and framework components and main unconformities. The microbialite and detrital carbonate intervals are laterally continuous, with internal and vertical changes in texture and petrophysical characteristics. Detrital carbonate deposits are more frequent at the area between sections 1 and 2, and microbialite deposits occur more often between the sections 3 and 5. The unconformities define the limits of different stratigraphic events. The texture scale of each section mnemonics are: Sh – shale, P – packstone, G – grainstone, St – stromatolite and Th – thrombolite. 85

Figure III.7 Microbialite carbonate microfabrics. (a) Peloid and peloidal shrubs – structures formed by peloids. (b) Mixed microfabric with peloids, shrubs and crystalline carbonate precipitate. (c) Crystal shrubs – structures formed by calcite crystals (light color material filling the pore space on the image). This component was only identified in this unit as a diagenetic phase.....86

Figure III.8 Porous microbialite textures in the lowest carbonate unit. Each row is a separate texture. The images on left are hand samples, the middle images are high-resolution scans of thin sections, and the images on the right side close-ups on the areas marked by squares in the middle image. (a) Thrombolite texture formed by mixed peloid and crystalline carbonate, with chaotic shrub fabric and open pore system. (b) Thrombolite texture formed by peloid layers and crystalline carbonate bridges, with chaotic shrub and branches fabric and open pore system. (c) Digitate stromatolite texture formed by layers of mixed peloid and crystalline carbonate, with vertically oriented fabric, tight packing and a relatively open pore system. (d) Digitate stromatolite texture formed by layers of

mixed peloid and crystalline carbonate, with vertically oriented fabric, tight packing and a closed pore system.. 89

Figure III.9 Pore filling material and diagenetic cements. (a) Desiccation crack filled by detrital carbonate material partially replaced by silica (polarized light). (b) Bioturbation structure partially filled by intraclast skeletal grainstone (plane light) (c) Coarse dolomite with dirty nuclei formed in the dissolved pore space within an oncolite/pisolite grain (plane light). (d) Dolomite formed in pores between peloid shrubs and as replacement of carbonate mud (polarized light). (e) Dolomite formed around peloid and shrub filling the pore space between them (plane light). (f) Crystal shrubs (arrow) and amorphous material (greyish). They were precipitated around most part of the pore border (plane light) (g). Microcrystalline silica partially filling pores (polarized light). (h) Blocky calcite cement an intraclast, skeletal grainstone (polarized light). The components are labeled on the image as: c – cement, i – intraclast and s – skeletal grain 90

Figure III.10 Porosity versus permeability plot for the digitate stromatolite, thrombolite, and intraclast pisolite grainstone. The microbialite results show a positive correlation trend that is caused by changes in the pore system from closed to open as the texture packing becomes looser and the textures fabric more chaotic. The grainstone samples have a slight separation from the microbialite trend that could be caused by difference in the pore system between the detrital and microbialite carbonate.....92

Figure III.11 CT scans, rock/pore and pore system volumes. The rock components are showed as grey and white on the CT scans (left) and yellow and orange on the rock/pore volumes (center). White and orange colors represent denser material or with areas with less microporosity. The pores are represented in black on the CT scans and blue on the rendered volumes (right side). The red polygons on the CT images mark the limits of the volumes shown. The first two samples have thrombolite texture and the other two have digitate stromatolite texture. The thrombolite samples have a much higher pore volume when compared to the digitate stromatolite samples. The pore system connectivity is also better in the thrombolite samples than in the digit stromatolite samples. However, there are differences between samples with similar texture, as visible on the pore system volumes between samples P3T and P5T, and P1S and

P2S. Sample P3T has the best pore system of all samples analyzed by CT, with a high proportion of well-connected pores. These characteristics result in very high permeability values for this sample (50000 darcys). Conversely, the pore system of sample P2S has more isolated pores that result in the lowest permeability values measured in these samples (3.75 millidarcys). The mnemonic of each sample indicates the section number (P1, P2, P3, P4 or P5) and its dominant depositional texture (T for thrombolite and S for digitate stromatolite)....94

Figure III.12 Pore size distribution determined by CT image analysis for the samples P1S, P2S, P3T and P5T. The thrombolite samples have a higher frequency of large pores when compared with the digitate stromatolite samples, which are dominated by small pores. Pores sizes below 0.25 mm were below the CT equipment resolution. The mnemonic of each sample indicates the section number (P1, P2, P3 or P5) and its dominant depositional texture (T for thrombolite and S for digitate stromatolite).....95

Figure III.13 Distribution of pores with 2, 3, and 4 pore-throats for the samples P1S, P2S, P3T and P5T. The samples with thrombolite texture have a higher number of connected pores, often connected by 3 and 4 pore-throats, in comparison to the samples with digitate stromatolite texture. The sample P3T has the higher number of connected pores, with 3 and 4 pore- throats of all samples analyzed, which helps to explain its very high permeability. The mnemonic of each sample indicates the section number (P1, P2, P3 or P5) and its dominant depositional texture (T for thrombolite and S for digitate stromatolite).....96

Figure III.14 Connectivity density per volume (Conn. D) versus permeability plot for the samples P1S, P2S, P3T and P5T, showing a strong positive correlation between the sample pore system connectivity and the permeability measured in plugs. The mnemonic of each sample indicates the section number (P1, P2, P3 or P5) and its dominant depositional texture (T for thrombolite and S for digitate stromatolite)....97

Figure III.15 Stratigraphic section of the first carbonate unit interpreted in terms of reservoir quality. Purple and red colors represent better reservoir intervals and green and yellow colors indicate poor reservoir intervals, considering the following permeability range: green < 10 md; yellow

<100 md; red <1000 md and purple >1000 md. Intervals sampled for petrophysical analysis are marked with an x to the left of each measured section. All other intervals were classified based on the interpretation of thin sections, field descriptions and comparison to similar samples with petrophysical measurements and their textural characteristics. There is good lateral continuity in relation to the reservoir quality in this unit, since the texture controls the pore system and its porosity and permeability are well-defined for these microbialite deposits in the Eocene Green River Formation. The intervals with better reservoir quality are associated with thrombolite texture or digit stromatolite with open packing and low pore filing by detrital sediments. They occur more often on locations where the microbialite development was favored, and form layers that can be laterally correlated in terms of depositional characteristics and reservoir quality. The texture scale of each section mnemonics are: Sh – shale, P – packstone, G – grainstone, St – stromatolite and Th – thrombolite.....100

LIST OF TABLES

Page

Table I.1 Depositional texture and pore network characteristics described for each interval on the build-up 16

Table III.1 Carbonate depositional textures, their framework components, fabric and pore system characteristics, in the Three Mile Canyon Road outcrop, Eocene Green River Formation 84

CHAPTER I

THREE-DIMENSIONAL PORE CONNECTIVITY EVALUATION IN HOLOCENE AND JURASSIC MICROBIALITE BUILD-UPS[1]

Overview

Microbial carbonates have complex pore networks formed by their biological growth framework, which later may be modified by diagenetic alteration. A proper evaluation of the porous media characteristics and their evolution is essential to better characterize microbial carbonate reservoirs. However, conventional methods of fundamental rock characteristic description are insufficient to elucidate the heterogeneity of pore networks and textural shifts. X-ray computed tomography allows a better evaluation of these fundamental characteristics, which integrated with stratigraphic analysis enhances understanding of the volume and connectivity of pore networks in different microbial textures.

A three-dimensional evaluation of a Holocene microbialite from Brazil provides insights about how the primary pore network is related to textural changes in microbialite successions, which in ancient deposits may be reduced or enhanced by diagenesis. Conventional methods such as petrography, carbon and oxygen stable isotopes analysis and laboratory measurements for porosity and permeability were

[1] This chapter was published in the American Association of Petroleum Geologists Bulletin, Volume 97, p. 2085 – 2101. Copyright ©2013. Reprinted by permission of the AAPG whose permission is required for further use.

integrated with computed tomography images and three-dimensional rendering to provide a high-resolution history of the evolution of porosity and permeability within this microbialite.

The pore network differences are related to the microbial textural evolution driven by environmental changes. The depositional textures control the petrophysical properties based on fundamental rock characteristics such as: structure size, structure packing and framework fabric. Those fundamental characteristics influence the pore volume and number of pore throats. Large structures, open packing, and chaotic framework fabric result in a better connected pore network, whereas small structures, tight packing and organized fabric result in less connected pore networks. Comparative pore geometry analysis of Late Jurassic Smackover Formation thrombolites show that their depositional textures also had high primary porosity values. If the microbial textures and petrophysical properties are environmentally controlled, their prediction in the subsurface is possible by refined depositional models.

Introduction

The principal goal of reservoir characterization is to construct three-dimensional images of petrophysical properties (Lucia, 2007). The evaluation and quantification of porous media are essential steps for this construction (Bowers et al., 1995). In carbonate reservoirs the analysis of the evolution of the porous media also is important, since they record textural shifts and they are easily modified by diagenetic processes. These steps become critical when working on microbial carbonates, because the porosity within

biological framework of these rocks generally has complex geometries and complex network connection patterns.

Carbonate reservoirs are influenced by depositional and diagenetic processes which control texture, fabric and pore geometries (Choquette and Pray, 1970; Tucker and Wright, 1990; Moore, 2001). Pores related to microbial textures have properties that reflect biological processes rather than mechanical sedimentation of loose grains (Ahr, 2008). These pore networks require detailed descriptions of the fundamental characteristics, such as texture and fabric, for an appropriate evaluation of the petrophysical properties (Verwer et al., 2011). Conventional methods of fundamental rock characteristic description are insufficient to elucidate the heterogeneity of pore networks in microbial carbonates. Computed Tomography (CT scan) volumes are a powerful tool that allows for the recognition of fundamental rock characteristics and the pore network elements to a degree not matched by conventional methods. Two-dimensional (2D) and three-dimensional (3D) reconstructions better resolve the heterogeneity of pore and pore throat geometries and how these influence pore network changes in conventional and complex reservoirs (Ehrlich et al., 1991; Anselmetti et al., 1998; Xu et al., 1999; Akin and Kovscek, 2003; Ashbridge et al., 2003; Hidajat et al., 2004; Okabe, 2004; Ketcham and Iturrino, 2005; Glemser, 2007; Okabe and Blunt, 2007; Padhy et al., 2007; Al-Kharusi and Blunt, 2008; Čapek et al., 2009).

The results of a 3D reconstruction of a Holocene microbialite build-up, whose diagenetic processes are minor and do not affect the depositional patterns provides a better understanding of how the pore networks evolve within the depositional framework

evolution. This analysis integrates conventional methods such as petrography, carbon and oxygen stable isotopes, and laboratory measurements for porosity and permeability, with CT scan image analysis and 3D rendering to provide high-resolution history of the evolution of porosity and permeability within this microbialite.

The results of this analysis were compared with a cathodoluminescence petrographic analysis of the pore network in a Late Jurassic Smackover Formation thrombolite and indicate that the thrombolites primary pore networks have similar characteristics that are controlled by their depositional textures. The Late Jurassic Smackover Formation thrombolite depositional porosity was estimated to be very high, up to 59%. However, subsequent diagenetic events reduced the final porosity of the Smackover Formation thrombolite to a range of 6 to 12%. The diagenetic alterations of the rock framework may be influenced by the primary pore geometry and pore connectivity (Morse and Mackenzie, 1990) that are related to the microbial texture. Thus, it is important to understand how the microbial texture controls the primary pore network characteristics under different environmental conditions.

Geologic setting

Lagoa Salgada microbialites

Holocene microbialites (figure I.1) grew on the west side of an isolated coastal lagoon (Lagoa Salgada) located in the Paraíba do Sul deltaic complex, in Campos dos Goytacazes, Rio de Janeiro, Brazil (Srivastava, 1999; Silva e Silva et al., 2007). The lagoon was formed 3850 ±200 BP (Srivastava, 1999) by sea level rise and the formation

of coastal barriers by longshore spit progradation (Dias and Kjerfve, 2009; Dominguez, 2009). The lagoon formed within a seasonal climate, and its water chemistry fluctuated from normal to hypersaline in response to the low precipitation rates from February to April. These conditions were dominant until the 1980s, when the lagoon was connected to a nearby river for agricultural purposes (Srivastava, 1999).

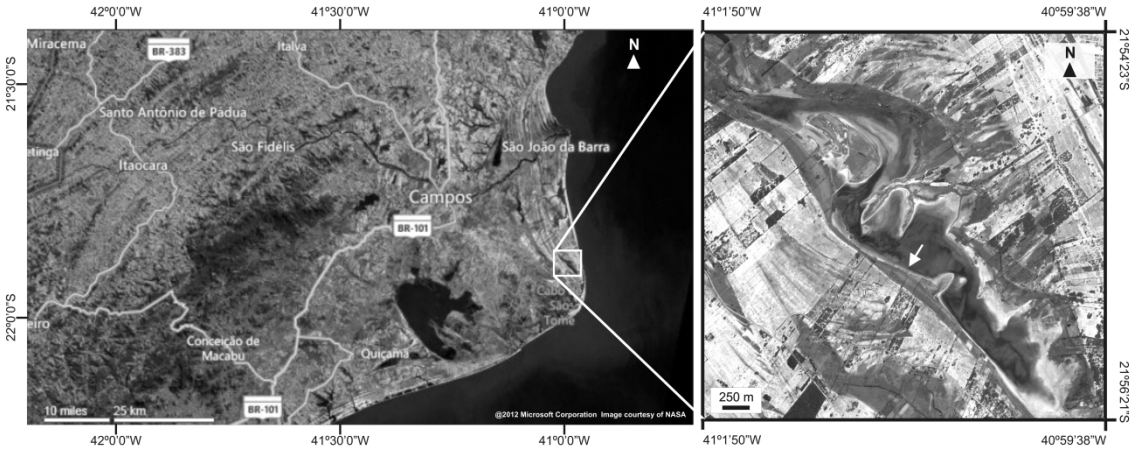

Figure I.1. Satellite maps show the location of the Lagoa Salgada (highlighted box), and the microbialite build-up sampling site on the western margin (white arrow).

Deltaic sediments (figure I.2) were deposited unconformably above Neogene continental sandstone of the Barreiras Formation, and they grade upward from medium to coarse marine sandstone into prodeltaic mudstone that is overlain by fine to medium deltaic and beach ridge sands (Lemos, 1995; Dias and Kjerfve, 2009). The lagoon sediments are skeletal grains, microbialite build-ups, microbial mats and mudstone

(Srivastava, 1999). The microbialites (figure I.1) formed only on the west side of the lagoon as a rim of laterally continuous bioherms, with irregular width. These microbialites vary in thickness, and morphology from thin laminated crusts to 0.6 meter thick coalescent build-ups (Srivastava, 1999). The microbialite in this study began growing on a cemented hardground surface that formed on the top of sandstone rich in brackish and marine fossils (Dias, 1981; Srivastava, 1999; Iespa *et al.*, 2008) at 2260 ±80 BP, and ceased growth at 290 ±80 BP (Coimbra *et al.*, 2000).

The microbialite growth rate varied in accordance to seasonal variations in climate and aerobic conditions (Vasconcelos and McKenzie, 1997; Coimbra et al., 2000). These changes are related to the major differences in the framework texture (Coimbra et al., 2000). Texture attributes such as size, fabric and packing of the microbial framework structures allow for the differentiation of the depositional textures. Carbonate mudstone and accumulations of microbialite fragments, gastropod, bivalve, ostracod, and vertebrate fragments commonly are associated with the microbialites (Srivastava, 1999), and occasionally occur in channels between the microbialite build-ups. The diagenetic processes in these microbialites are early carbonate rim cementation and meteoric dissolution (Iespa et al., 2008).

Late Jurassic Smackover Formation thrombolite

The Late Jurassic Smackover Formation records carbonate deposition on a carbonate ramp (Ahr, 1973), during a major transgression during the formation of oceanic crust in the Gulf of Mexico and thermal subsidence due to cooling (Nunn et al.,

1984; Mancini et al., 1999). Smackover Formation reefs consist of cyanobacteria (microbial buildups) or a more diverse coral-algal assemblage (Baria et al., 1982). In Little Cedar Creek Field, southeast Alabama, the Smackover Formation microbial buildup consists of microbial mats at its base and thrombolite (reservoir facies) in the top. The thrombolite is composed mainly by peloids, and rare skeletal grains (benthic foraminifera and green algae).

Methods

A microbialite build-up (figure I.3) 25 cm (9.84 inches) high and 30 cm (11.81 inches) wide from the Lagoa Salgada was described, scanned by computed tomography and sampled for petrography, stable isotopes, porosity, and horizontal permeability. All data was integrated to allow an improved geological interpretation of the pore networks at different scales.

X-ray computed tomography

X-ray computed tomography is used to scan rock samples, and render volumes in voxel units (Ketcham and Carlson, 2001; Mees *et al*., 2003; Van Geet *et al*., 2003; Ketcham and Iturrino, 2005). The main purpose of this technique is to predict the petrophysical parameters and model their results (Akin and Kovscek, 2003; Van Geet *et al*., 2003; Hidajat *et al*., 2004; Glemser, 2007; Okabe and Blunt, 2007), a major objective in the reservoir characterization. Nevertheless, the use of the geologic information is reduced to lithology and pore type classification. Adding geologic

information can produce better predictive models related to depositional and diagenetic settings (Grochau et al., 2010).

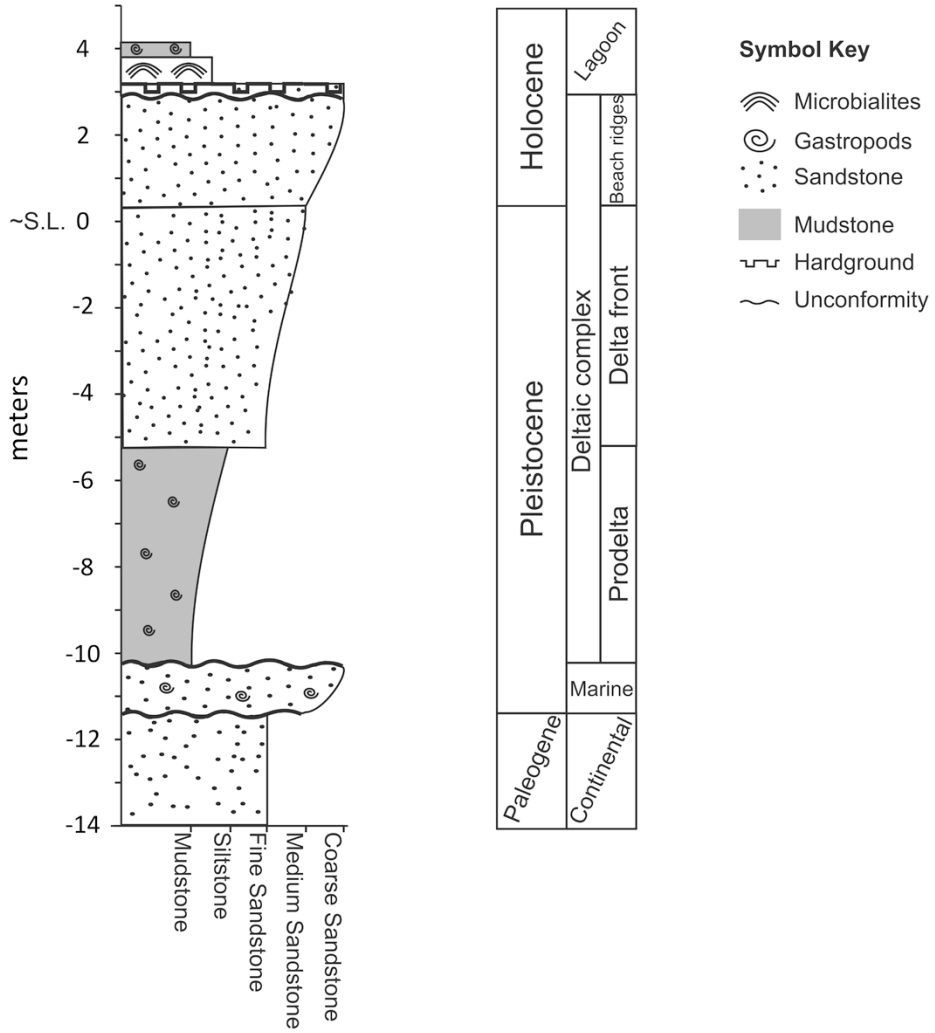

Figure I.2. Schematic stratigraphic column for the Paraíba do Sul deltaic complex. The thickness of each interval changes laterally along the deltaic complex. Modified from Lemos (1995), and Dias and Kjerfve (2009).

A set of 384 axial slices were obtained with spacing of 1.25 mm (0.05 inches) in a 16 channel *BrightSpeed GE*® CT scanner, with X-ray voltage set at 130 kV, current at 100 mA, and image resolution of 0.5 x 0.5 mm (0.02 x 0.02 inches). The data from the CT scanner at the *PETROBRAS* Research Center in Rio de Janeiro was converted, using in-house algorithms, to SEGY file format to use seismic volume interpretation software from commercial and in-house developers. This allowed a numeric and well defined segmentation for the volumes of the pore networks and the rock framework.

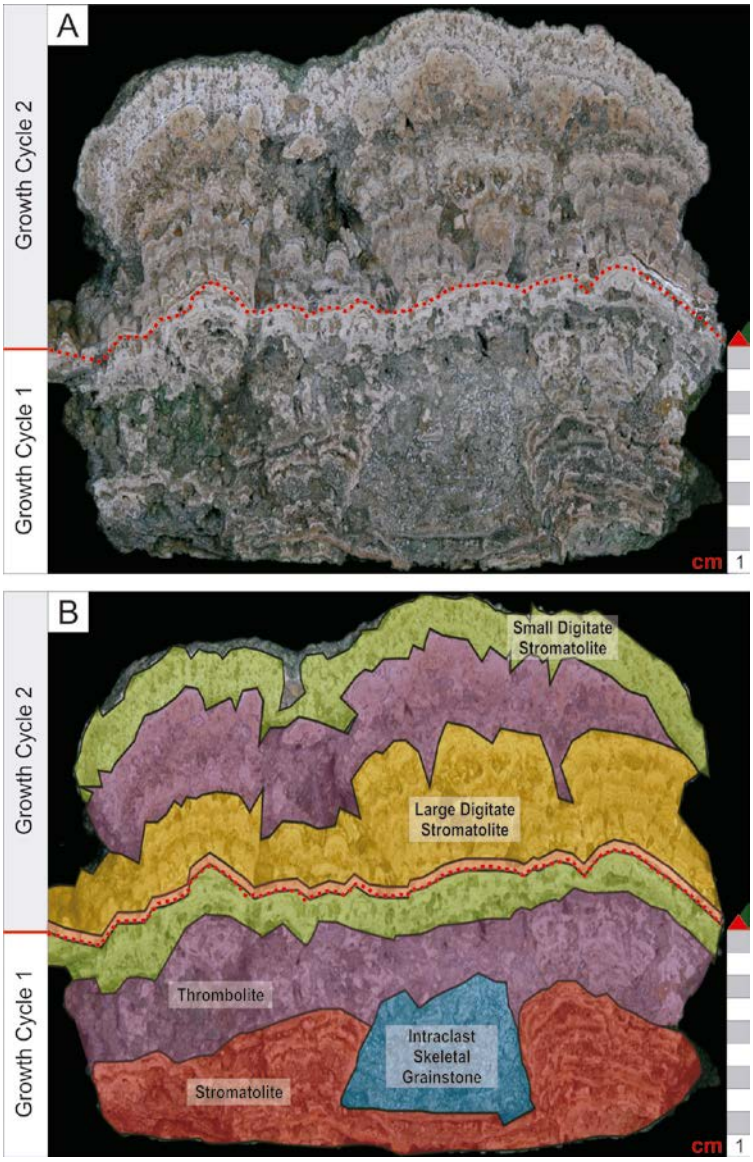

Figure I.3. (A) Photograph of the microbialite build-up. The growth cycles, erosional surface (red dotted line) and sampling points for cores (red circles with white fill) and stable isotopes (yellow boxes) are shown. (B) Interpreted section labeled for different depositional textures (stromatolite, thrombolite, digitate stromatolites and grainstone). The green material that cover some areas on the sample are surface coloring by encrusting algae.

Once the volumes were segmented and rendered, the total porosity was quantified for the entire sample and for each sub-volume of interest, using the software algorithms for volume quantification. The method to calculate the porosity from CT slices is well known and is based on the difference of attenuation coefficients of the rock and fluid (Withjack, 1988; Ketcham and Iturrino, 2005). The precision on these pore volumes was limited to millimeters due to the tomograph resolution.

Sagittal (horizontal) slices were reconstructed from the 3D matrix of attenuation values obtained by CT scanning. These slices cut the sample horizontally, producing simulated time-slice maps. These maps were useful to explain the vertical evolution of depositional elements and pore networks. Furthermore, using the sagittal (horizontal), coronal (vertical), and axial (vertical) planes the fundamental rock properties such as size, internal morphology and packing were described, measured and correlated to changes in the porous media properties.

Carbon and oxygen stable isotopes

Continental carbonates are sedimentary deposits highly influenced by their environmental settings. Small changes in climate conditions and water chemistry result in large differences between two contiguous deposits (Alonso-Zarza and Tanner, 2010). Thus, a good stratigraphic interpretation of continental carbonate deposits must evaluate all the environmental variables, which is complicated by the overprinting influence of subsequent meteoric, marine or burial diagenesis.

In carbonate rocks, the porous media derive from the depositional texture and later dissolution and cementation during diagenesis (Lucia, 2007; Ahr, 2008). Continental carbonates due to their higher susceptibility to environmental changes also may have abundant vertical heterogeneity. Therefore, the $\delta^{13}C$ and $\delta^{18}O$ analysis for these rocks are essential to constrain the environmental interpretation of the depositional controls on the pore media.

Eleven bulk rock samples were collected vertically at regularly spaced intervals (~2 cm; 0.8 inches each) along a profile of the microbialite build-up (figure I.1). The samples were analyzed at the *PETROBRAS* Research Center stable isotope facility using an automated carbonate device (KIEL IV) linked to a dual inlet Delta V Plus Thermo® Finnigan isotope ratio mass spectrometer. Results are presented as values compared to VPDB. The analytical precision for this set of samples was $\delta^{13}C = 0.05‰_{VPDB}$ and $\delta^{18}O = 0.10‰_{VPDB.}$

Petrophysics

Two horizontal cores, 1.5 inch long and 1 inch wide, were analyzed under a pressure of 500 psi using the Corelab® Ultrapore-300 p300 porosimeter and the Corelab® Ultra-perm 400 permeameter at the *PETROBRAS* Research Center. These two cores were drilled where the depositional texture is homogeneous, insuring the measured values correspond to differences in texture and pore geometries.

Petrography and cathodoluminescence

Standard petrography and cathodoluminescence analysis were used to characterize microfabrics, diagenetic features and porosity in a representative sample for the Smackover Formation thrombolite, 2.54 cm (1 inch) diameter plug taken from core. Cathodoluminescence analysis was performed using Technosyn® cold cathode luminescence equipment, model 8200 MK II. Operating conditions for the analysis were 10 KeV accelerating voltage and 300 μA current. The differences in the cement morphology and cathodoluminescence color and intensity were used as criteria to reconstruct the primary porosity network of the Jurassic thrombolite.

Results

Lagoa Salgada microbialite depositional textures

Four microbial depositional textures are differentiated in the Lagoa Salgada microbialite: planar stromatolite, thrombolite, small digitate stromatolite, and large digitate stromatolite and (figure I.3). While these four depositional textures are representative of the microbialite at this site, different textures may occur in other microbialite deposits. The microbial structures are composed of micritic peloids and bound skeletal fragments, oncolite, quartz grains, and syndepositional calcite cement. The thrombolites have a massive internal structure and the stromatolites laminated (figure I.4). The planar stromatolites are characterized by crinkly laminations, with horizontal fabric, open packing, and structure size smaller than 5 mm (0.2 inches). The porosity in the planar stromatolite texture is fenestral with simple pore geometry, pore

size mean less than 1.5 mm (0.05 inches), and a low number of pore throats (0 to 2). The thrombolites are composed by interconnected and morphologically irregular branches, with chaotic fabric, open packing and structure size large than 2 cm (0.8 inches) (figures I.3 and I.4). The pore geometry within the thrombolite intervals is complex, with pore size mean higher than 5 mm (0.2 inches), and a high number of pore throats (2 to 6). The digitate stromatolite grew vertically divergent touching digits, with tight internal packing (figures I.3 and I.4). The structure size varies from small digits, with height lower 1 cm (0.39 inches) to large digits, with height higher than 1 cm (0.39 inches). The pore geometry is simple, with low to medium number of pore throats (0 to 4). The mean pore size is 1.5 mm (0.05 inches) in the small digitate stromatolites and higher than 3 mm (0.12 inches) in the large digitate stromatolite. These data are summarized on table I.1.

Early carbonate rim cementation and meteoric dissolution are the most evident diagenetic modifications in these microbialite build-ups. However, neither of these events substantially modified the depositional texture, because they are not expressive on thin sections, and the microbial framework boundaries are very well preserved (figure I.4).

Stable isotopes

Carbon and oxygen isotope values for bulk rock, in the Holocene microbialite build-up range from 7.7 to 18.7‰ $\delta^{13}C_{VPDB}$, and -0.8 to -3‰ $\delta^{18}O_{VPDB}$, with an average of 14.7‰ $\delta^{13}C_{VPDB}$, and -1.8‰ $\delta^{18}O_{VPDB}$ (figure I.5). These enriched ^{13}C values suggest that the carbonate precipitation occurred from bacterial methanogenesis (Talbot and Kelts, 1990). The dominant mineral phase for this microbialite is calcite, with minor

concentrations of aragonite near the base of the sample as determined by infrared spectroscopy.

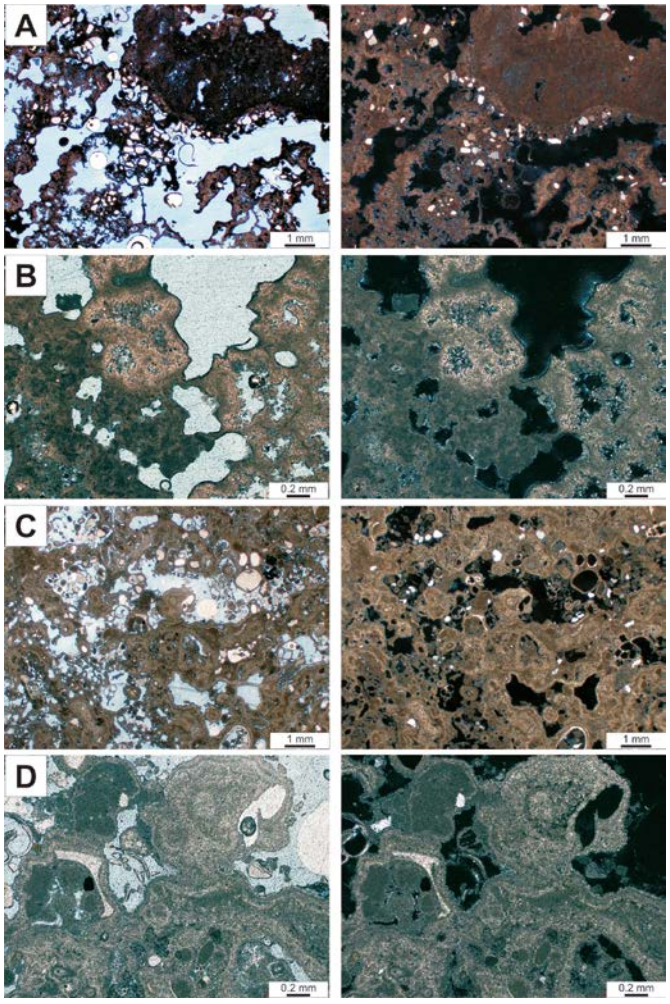

Figure I.4. Photomicrographs for the thrombolite (A and B), and stromatolite (C and D) textures (plain polarized light on left and cross polarized light on right). The thrombolite texture is massive and has a chaotic growth pattern. The stromatolite is laminated and with an organized growth pattern. Micritic peloids are the main building block for both textures. The peloids are bounded by calcium carbonate cements. The non-carbonate grains are quartz and undifferentiated feldspars.

Table I.1. Depositional texture and pore network characteristics described for each interval on the build-up.

Growth Cycle	Depositional Texture	Fabric	Packing	Structure Size	Pore Geometry	Mean Pore Size	Number of Pore Throats	Pore Network Connectivity
1	Planar Stromatolite	horizontal	open	Small (<0.5 cm)	Simple	1.5 mm	0 to 2	Low
1	Thrombolite	chaotic	open	Large (>2 cm)	Complex	> 5 mm	2 to 6	High
1	Small Digitate Stromatolite	vertical	very tight	Small (<1 cm)	Simple	1.5 mm	0 to 2	Low
2	Large Digitate Stromatolite	vertical	tight	Large (>1 cm)	Simple	> 3 mm	0 to 4	Medium
2	Thrombolite	chaotic	open	Large (>2 cm)	Complex	> 5 mm	2 to 6	High
2	Small Digitate Stromatolite	vertical	very tight	Small (<1 cm)	Simple	1.5 mm	0 to 2	Low

*Structure size was measured on the sample. Pore size and number of pore throats were measured in the rendered volume. Fabric, packing, pore geometry and pore network connectivity are qualitative characteristics by visual estimative.

Smackover thrombolite primary porosity reconstruction

The initial pore space of the Smackover Formation thrombolite sample, calculated by analyzing petrography and cathodoluminescent images was 40% (figure I.6), similar to the porosity value of the Holocene thrombolite. The first cementation phase was mosaic calcite cement that reduced the initial pore space 6%. The final cementation phase was blocky calcite cement that reduced the porosity by up to 27%. As a result, after these cementation phases 33% of the initial pore space was filled and the final porosity is 7%.

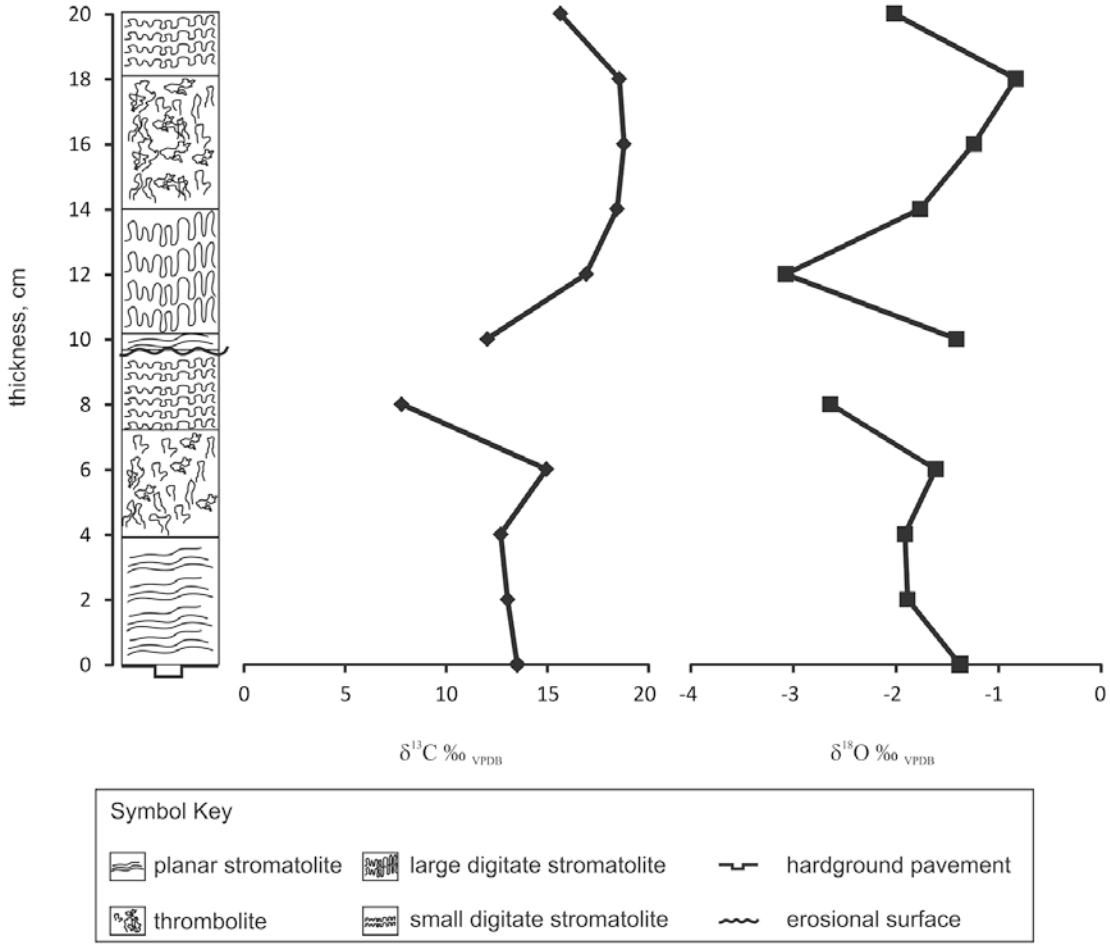

Figure I.5. Stratigraphic profile described for the microbialite build-up, $\delta^{13}C_{VPDB}$ and $\delta^{18}O$ ‰ $_{VPDB}$. The isotopic values increase towards the thrombolite intervals and decrease towards the stromatolites intervals indicating higher methanogenesis rate for the thrombolite intervals. The strong shift in the $\delta^{13}C$ ‰ and $\delta^{18}O$ ‰ values across the discontinuity resulted from a more humid climate condition that brought ^{16}O rich meteoric waters to the lagoon reducing, the evaporative trend and decreasing the rate of methanogenesis by more oxygenated bottom waters.

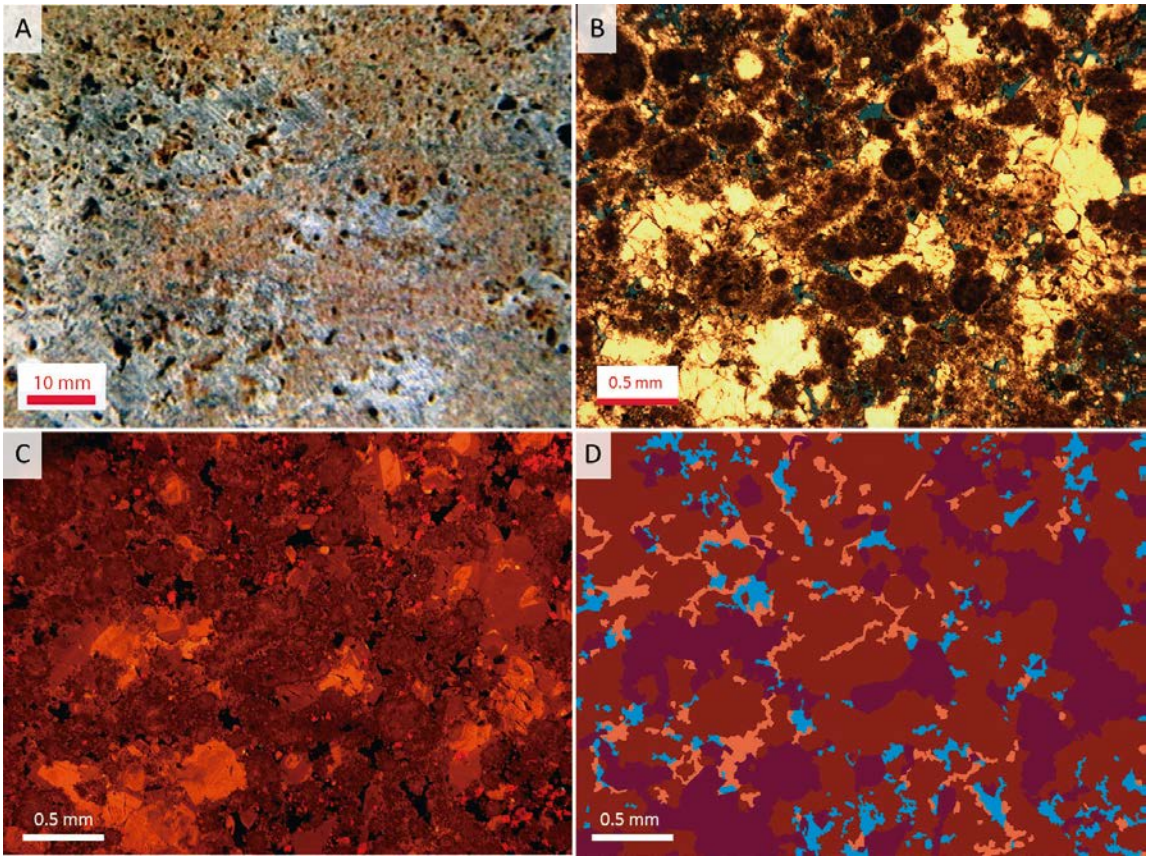

Figure I.6. (A) Upper Jurassic Smackover Formation thrombolite, Little Cedar Creek Field, Alabama. The greyish colors are the microbial structures and the brownish colors are diagenetic cements. (B) Thin section image showing the microbial structures formed by syndepositional peloids cementation (dark components), mosaic and blocky calcite diagenetic cements (bright yellow colors) and pores (blue colors). (C) Cathodoluminescent thin section image. The microbial structures are dull, the calcite mosaic cement phase has low bright brown color and the blocky calcite cement has a zonation from low bright brown to bright yellow colors. (D) Reconstruction of the original microbial framework and subsequent cementation phases. The microbial structures are shown in brown, the calcite mosaic cement is shown in pink, the blocky calcite cement is shown in purple and the pores are shown in light blue.

Discussion

Evolution of the Lagoa Salgada microbialite build-up

Microbial growth initiated in the Lagoa Salgada when the enclosed water body achieved high salinity and low levels of dissolved oxygen. These environmental conditions allowed reactions of methanogenesis and carbonate precipitation by microbial metabolism (Kelts and Talbot, 1990; Vasconcelos and McKenzie, 1997; Konhauser, 2007; Pueyo et al., 2011). Changes in the environmental conditions controlled the microbial growth rates, depositional textures, and the carbon and oxygen stable isotopic values (Coimbra et al., 2000).

Strong evaporative conditions and anoxic bottom waters prevailed during the driest periods, increasing microbial growth and methanogenesis rates, which resulted in rapid carbonate precipitation with high values of $\delta^{13}C$ and $\delta^{18}O$. The rapid carbonate precipitation formed a more chaotic fabric by disorganized accretion processes, producing the thrombolite textures (Konhauser, 2007). As the environment returned to humid conditions, the influx of meteoric waters reduced the potential for methanogenesis, and this resulted in slower growth rates (Coimbra et al., 2000), lower $\delta^{13}C$ and $\delta^{18}O$ values and well organized fabric, including well defined lamination and tighter packing that characterize the stromatolite textures. Planar stromatolites formed during the initial growth phase, when the environmental conditions reached proper levels to stabilize the microbial community.

As a result of environmental fluctuations, two growth cycles, separated by an erosional surface, formed the microbialite build-up. Both cycles have their own characteristics in terms of succession of the depositional textures and thickness of each interval.

The first cycle (figure I.3) starts with a phase of planar stromatolite development on a hardground pavement cemented by calcium carbonate. These stromatolites evolve upward into a columnar external morphology that initiated on topographic highs (e.g. ripple marks and bivalve shells) of the hardground pavement. Flow channels formed between the columns (figures I.3 and I.7), and they generally are filled by skeletal grains (e.g. gastropods). The $\delta^{13}C$ and $\delta^{18}O$ values are low and decrease upward (figure I.5), which may record a relative increase on humidity during this depositional phase.

The second growth phase is characterized by chaotic branching thrombolites (figures I.3, I.4 and I.7), with massive internal texture. These branches grew with well-spaced packing, producing a large and well-connected pore network. This phase was previously interpreted to result from the destruction of the original laminated texture by feeding organisms (Srivastava, 1999; Silva e Silva et al., 2007; Iespa et al., 2008). However, the highest $\delta^{13}C$ and $\delta^{18}O$ values (figure I.5) suggest a high rate of methanogenesis, better microbial productivity and rapid carbonate precipitation during this phase (Sumner, 2001; Konhauser, 2007; Conrad et al., 2011), producing the chaotic thrombolite texture. Lower humidity environmental conditions also are suggested by the higher growth rates (Coimbra et al., 2000), and the lack of skeletal grains within the thrombolite (figure I.4).

Figure I.7. "Time" slice series for the microbialite build-up. On the left plate, the horizontal and vertical arrows show the directions incremental height from the bottom to top. The slices are spaced 1.22 mm apart. This plate allows the interpretation of the build-up evolution, showing the upward shift and lateral distribution of internal depositional textures, and changes on the external morphologies, from individual to coalesced heads. A main flow channel and several secondary channels are partially filled with grains visible on these slice series. On the right plate selected slices to show specific features (red outlines), such as channels (white arrows), phases of head individualization and coalescence, and each depositional texture. These selected slices are numbered, and identified by color margins on the slice series. The first three slices are on the growth cycle 1 and the last three are on the growth cycle 2. Slice 37 is in the planar stromatolite interval, two individual heads are visible separated by a flow channel filled by grains. Slice 57 is in the first thrombolite interval, several round branches with an open packing define the main aspect of this depositional texture, the heads started to coalesce during this phase. Slice 80 is in the small digitate stromatolite, whose heads are totally coalesced and the channel between heads is closed. The packing is tight, which resulted in small isolated pores (black spots). Slice 94 is at the base of the large digitate stromatolite interval of cycle 2. The growth initiated as isolated heads, and a large channel filled by grains was developed in between heads. Slice 112 is at the top of the large digitate stromatolite interval, the individual heads are visible with a well-connected channel system. The tight packing and the vertical pore network orientation isolated the framework porosity that appears as dark circular zones in each head. Slice 149 is in the second thrombolite interval defined by round branches and open packing. The heads coalesced at this phase and enclose the channel system. The small digitate stromatolite cap the microbialite build-up appears as a rim around the build-up on slices 112 and 149.

Figure I.7. Continued.

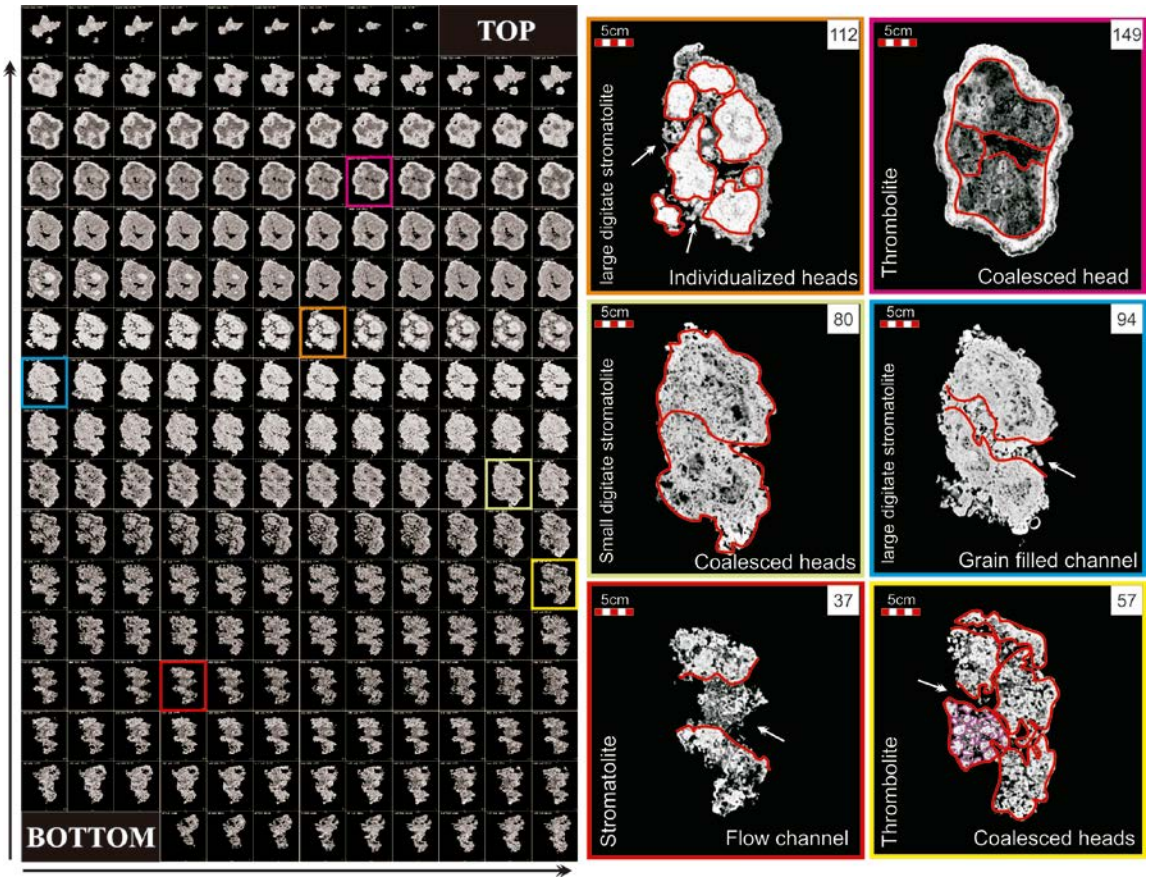

Small digitate stromatolites record the final growth phase of the first cycle (figure I.3). The digits touch each other in a tight vertical growth framework. They spread laterally and cover the thrombolite structures formed earlier, allowing the individual build-ups to coalesce (figure I.7). This growth behavior suggests a time of more stressful environmental conditions for the microbial community, with reduction of the methanogenesis rate expressed as lower values of 7.7‰ $\delta^{13}C‰_{VPDB}$ and -2.6‰ $\delta^{18}O_{VPDB}$ (figure I.5). This cycle of microbial growth was interrupted and the system

underwent erosional processes. Intraclasts and skeletal grains accumulated as sediments in ponds and cavities along the structures.

The second growth cycle begins with a thin planar stromatolite that acted as a veneer covering the erosional surface and grain deposits. Following this initial phase, large digitate stromatolites formed when the system began to return to arid conditions. Each set of digits formed an individual build-up with flow channels between them (figure I.7). The $\delta^{13}C$ and $\delta^{18}O$ values increase upward in a trend of intensification of methanogenesis rate and evaporative conditions (figure I.5). The $\delta^{18}O$ profile has a shift near the base of the cycle from relative high values to low -1.4 to -3.0‰ $\delta^{18}O_{VPDB}$ (figure I.5); this shift is related to influx of ^{16}O-rich meteoric waters.

The digitate stromatolite graded upward to thrombolite with massive internal structure and a less oriented growth pattern (figures I.3 and I.4). Individual build-ups and well-connected flow channels persisted in this third phase (figure I.7). This textural change is coincident with a narrow range of more positive values in stable isotopes (18.7 to 18.5 $\delta^{13}C$ ‰ $_{VPDB}$ and -1.2 to -0.8 $\delta^{18}O$ ‰ $_{VPDB}$) within this second growth cycle (figure I.5). The final growth phase is recorded by the development of small digitate stromatolites. Similar to the final phase of the first cycle, the small digitate stromatolites grew in a tightly packed vertical growth pattern. During this phase, coalescence of individual build-ups shaped the build-up external domal morphology.

Evolution of the Lagoa Salgada microbialite porous media

The texture and fabric of each interval created differences in pore geometries and pore connection patterns, in the growth framework porosity at each interval, which are best evaluated on CT scan volumes. Furthermore, depositional elements such as flow channels connect different porosity areas and textural intervals. The planar stromatolite and thrombolite of the first cycle, and the large digitate stromatolite and small digitate stromatolite of the second cycle were isolated in the volume. The best-connected pore network occurs in the thrombolite interval, because even though it has more complex pore geometries, it also has a higher number of connected pores, resulting from the chaotic fabric and open packing. The stromatolite intervals with their oriented fabrics and tight packing have the worst pore connection patterns, which are horizontal in the planar stromatolites and vertical in the digitate stromatolites. The size and packing of the structures also control the pore connectivity in these intervals. In small digitate stromatolites, which have small structure sizes and tight packing, the pore volume and amount of connected pores are very low in comparison to the other stromatolite intervals on the build-up (figure I.8).

Stromatolite

The planar stromatolites have a simple horizontal pore geometry that interferes with the vertical connections between porous layers in this interval (figure I.8a). The pores also are segmented laterally or show narrow and few pore throats. The porosity

estimation for a 2 x 16 cm (0.8 x 6.3 inches) CT scan volume defined on this depositional texture is 11%.

Thrombolite

The thrombolite interval has the highest porosity with a well-connected pore network, inherited from its chaotic depositional fabric and high growth rate (figure I.8b). This pore network is enhanced when flow channels connect the space between the branches. The pore geometries are irregular, without a preferential orientation, and usually with four or more pore throats. These pore throats also vary in width, and a set of pores may have narrow pore throats besides wide pore throats (figure I.9). The porosity and permeability values are 40.6% and 6.9 Darcys, respectively for a plug in the first thrombolite interval. The porosity value obtained by a 3 x 16 cm (1.18 x 6.3 inches) CT scan volume was 31.5%. The high permeability value – lacking compaction and cementation – is due to the well-connected pore network of this depositional texture.

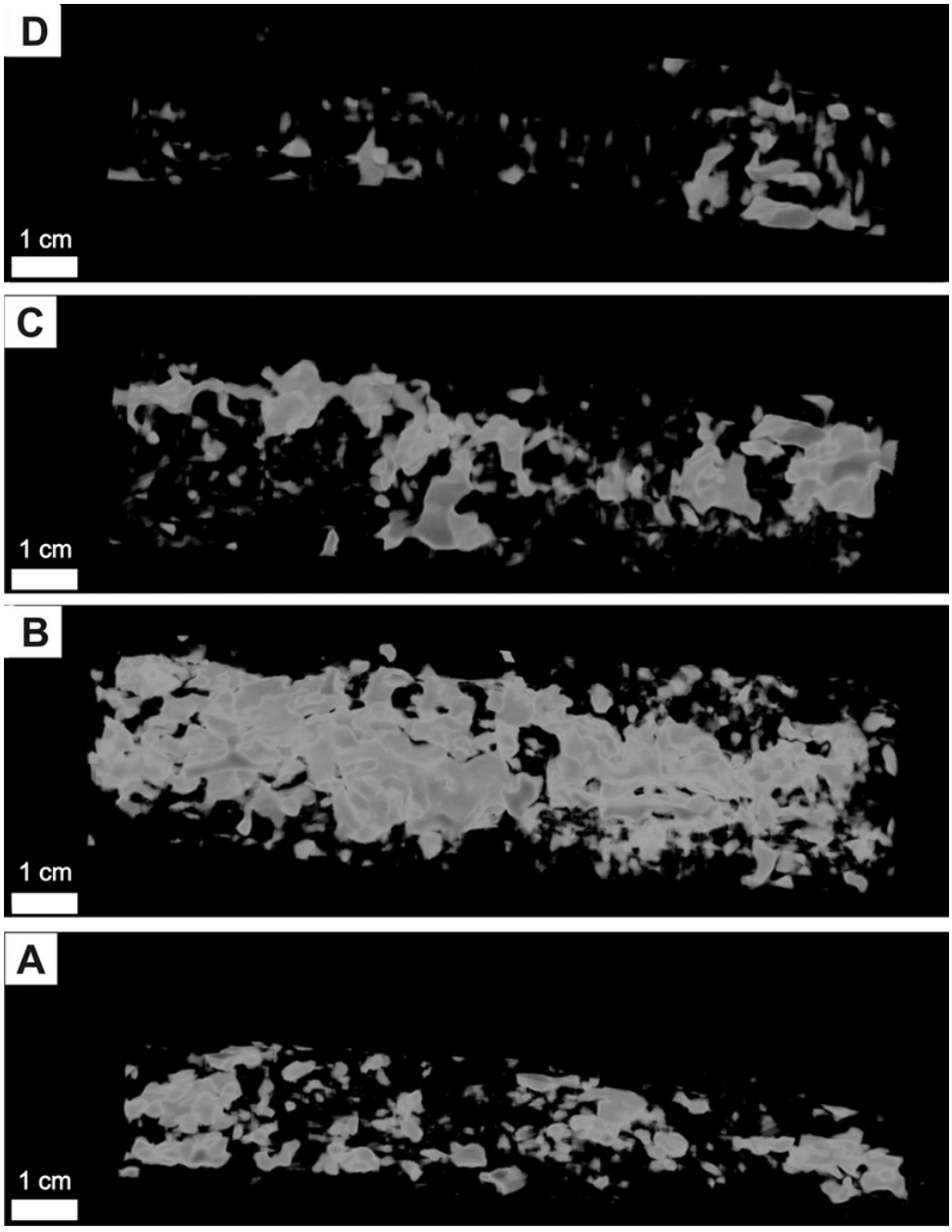

Figure I.8. Pore networks from CT scan rendering in different depositional textures. (A) Planar stromatolite has horizontally oriented pore network that is poorly connected vertically. (B) Thrombolite interval has large pore volume with chaotic porous network formed by fast growth rates and no preferential growth pattern. (C) Large digitate stromatolite has large and vertically oriented pores produced by the open growth pattern. Some pores resulted from enclosing of flow channels during the coalescence of different heads in this interval. (D) Small digitate stromatolite has vertically oriented pores that are poorly connected due the tight packing.

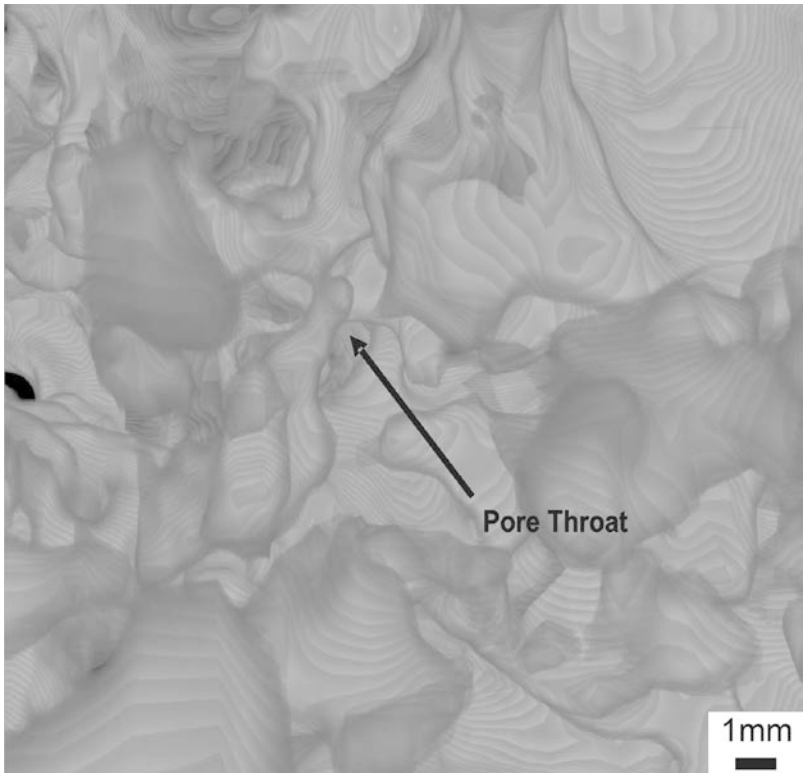

Figure I.9. Detail of pore geometries and pore throats of the thrombolite texture. The pores have very irregular geometries and a wide size distribution, thus small and simple pores occur besides large and complex pores. The pore throats also have irregular distribution and differing diameters. A set of pores may be connected by narrow and wide pore throats (black arrow).

Large digitate stromatolite

The large digitate stromatolite interval has a vertically oriented and laterally disconnected pore network (figure I.8c). The pores are usually large, being the space between large sets of packed digits. However, the number of pore throats is low and those are usually narrow, reducing the connectivity between the pores. The porosity and permeability values for a plug in this texture are 30.7% and 92.1 millidarcys, respectively. The porosity obtained on a 3 x 16 cm (1.18 x 6.3 inches) CT scan volume

on the same area where the plug was obtained is 12.1%. These diverse values indicate the complex nature of microbial pore network due to textural heterogeneity. The difference in horizontal permeability from the thrombolite interval to this interval reflects the change from an irregular and well-connected pore network to a poorly connected vertically oriented pore network.

Small digitate stromatolite

The small digitate stromatolites have few vertical oriented pores, which are barely connected due to their tight packing (figure I.8a). The small and narrow size of the digits and less space between them produced less pore space when compared to other textures. The porosity obtained in a 2 x 16 cm (0.8 x 6.3 inches) CT scan volume in this interval is 2.1%. However, channels between individual build-ups and areas with higher number of pores may link some of this more isolated porosity with the well-connected pore network of other intervals, as seen on the entire CT scan volume (figures I.10 and 11).

This evaluation of how the porous network evolved was also done for the entire build-up, providing insights into how depositional elements act as channels to connect different areas and intervals with diverse textures and pore networks (figures I.6, I.10 and I.11). The porosity obtained from the CT scan volume of the entire sample is 25%. This value considers the presence of flow channels and other textures, such as the loose skeletal grains dispersed within some of these channels. Whereas the thrombolite intervals have higher porosity with large, chaotic and well-connected pores, they do not

represent by itself the entire volume and pore connectivity of the sample. The digitate stromatolite and the planar stromatolite textures reduced the overall porosity value, and due to their poorly connected and strongly oriented pore network will likely decrease the average permeability for the entire sample. The textural and pore network characteristics of the entire sample are given in Table I.1. Since these textures evolved from differing environmental conditions, it is possible to evaluate the primary porosity and predict the pore connectivity and model petrophysical properties.

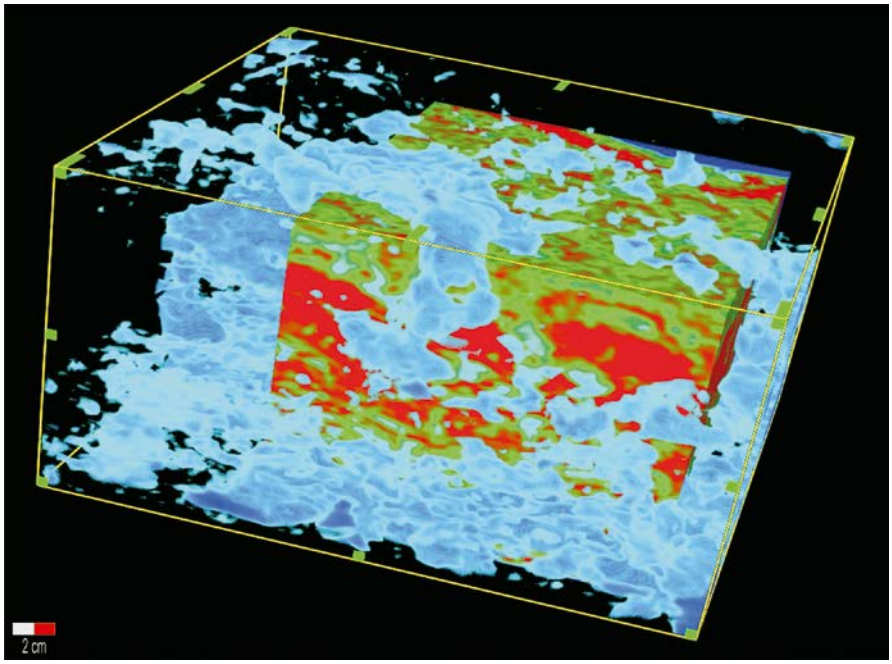

Figure I.10. CT scan rendered volumes for the microbialite build-up. The pores shown in blue and the rock constituents are shown in green (high attenuation) and in red (low attenuation). The high attenuation is caused by dense carbonate areas (binding cement) and the low attenuation is caused by microporosity in peloid rich areas. The flow channels between coalescent heads connect different pore intervals and areas along the build-up.

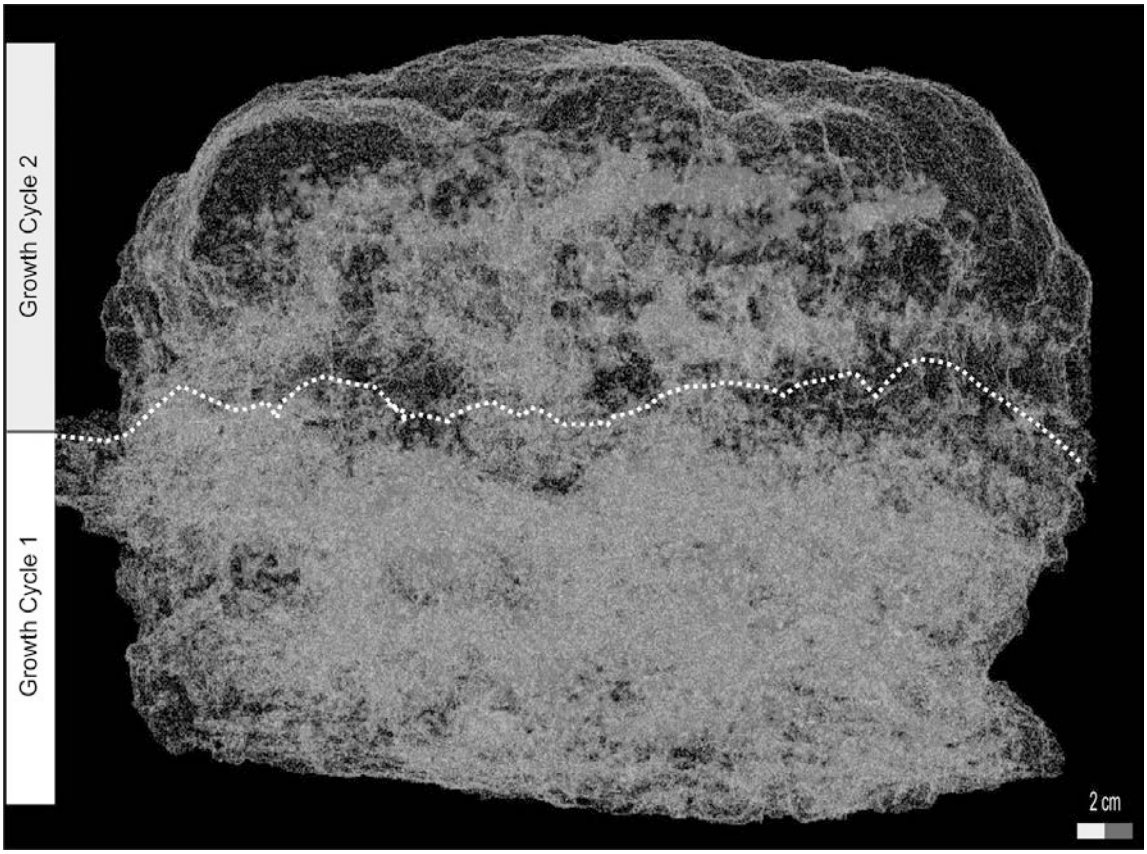

Figure I.11. CT scan rendered volume presented as the pore-rock boundary. The planar stromatolite appears at the base of the build-up with narrow horizontal pore geometries. The thrombolite is next visible texture, characterized by a chaotic and bright interval. This chaotic texture is due to a large volume of well-connected pores and chaotic fabric. The small digitate stromatolite appears as small vertical pores isolated in a dark interval after the thrombolite. These three intervals define the growth cycle 1. The upper part of the build-up indicates the growth cycle 2 has a lower volume of pores compared to the growth cycle 1. The limit between the 2 cycles is shown by a white dotted line. The large digitate stromatolite appears on the upper interval as large and vertical oriented bright areas. The thrombolite of the growth cycle 2 is visible on the chaotic bright are above the large digitate stromatolite. Channels between heads appear on the image as wide and tall vertical features on the middle of the build-up. These channels connect the large digitate stromatolite with the thrombolite intervals, and the two growth cycles. The dark interval on top is the small digitate stromatolite low volume of pores, which capped the build-up.

Comparison to Late Jurassic thrombolite from Smackover Formation

The comparison between ancient and recent microbialites can clarify some aspects of diagenetic evolution on these bioherms. Analyses of a Late Jurassic Smackover Formation thrombolite, deposited in ancient Gulf of Mexico embayments (Baria et al., 1982), were compared to the Holocene thrombolite intervals in the microbialite build-up from Lagoa Salgada. This sample of the Jurassic Smackover Formation thrombolite has a microbial texture formed by irregular branches, chaotic fabric, and open packing that is similar to the Holocene thrombolite, (compare figures I.3, I.4 and I.6a). The original framework components of the Jurassic Smackover Formation thrombolite and the Holocene build-up are peloids and syndepositional cement.

The Holocene thrombolite interval has a porosity value of 40.6%, whereas the Smackover Formation thrombolite has porosity values ranging from 6 to 12%. Analyzing petrographic and cathodoluminescence images of a sample from the Jurassic thrombolite (figures I.6b and I.c), the diagenetic history and the evolution of the porosity in this sample were reconstructed (figure I.6d). It was possible to observe how each diagenetic event modified the primary pore network (figure I.6d). The initial porosity on the Holocene thrombolite and in the Smackover Formation thrombolite are similar (c.a. 40%), with irregular pore geometry inherited from the thrombolite depositional texture, chaotic fabric and open packing.

Application of data to production

Microbialite porous media are very complex and difficult to describe using traditional methods (e.g. general attributes and petrography), so volumetric techniques, such as CT scan, are necessary to fully understand 3-D porous media. Furthermore, pore volumes provide insights into the amount of connected and non-connected pores, pore-pore throat ratio, and allow their results to be upscaled during reservoir modeling exercises.

The fundamental characteristics of structure size, structure packing and framework fabric help to predict the major changes on petrophysical properties. The differences in calculated porosity and measured porosity in the thrombolite, large digitate stromatolite, small digitate stromatolite and planar stromatolite indicate the importance of accurately defining fundamental characteristics for studies of porous media. Differences in permeability in the thrombolite and the large digitate stromatolite also are related to textural changes. Thus, the bigger the structures and the more chaotic is the fabric, better are the chances for high permeability and porosity to develop, whereas tight packing of microbial fabrics reduces both porosity and permeability.

Once the controls on the depositional texture and external morphology are understood, computed models may be generated to build 3-D models for the evolution of microbialites and their porous media. During reservoir characterization projects much is done to build sedimentary, stratigraphic and petrophysical models, but in complex

reservoirs such as microbialites, they must be integrated to increase the quality of these projects aiming to more completely exploit the resource.

Conclusions

The pore networks of the microbialite build-ups analyzed formed under environmental and microbial influence, resulting in complex pore-pore throat relations, which were driven by the changes in depositional textures. In this case, the depositional pore networks changed as the microbial structures evolved. The depositional textures provide insights of pore network characteristics such as pore geometry and connectivity, based on the attributes of structure size, structure packing and framework fabric. Thus, refined depositional models become very important to the microbial reservoir characterization, and can add valuable information to the petrophysical evaluation.

Two growth cycles occurred during the formation of the Lagoa Salgada microbialite build-up. The vertical succession of depositional textures shows a gradual increase in microbial production and carbonate precipitation, which transitions from organized to chaotic fabrics, and also towards the enlargement of structures and more open packing. The environmental changes are recorded in the $\delta^{13}C$ and $\delta^{18}O$ profiles, which pass upward from low values in the basal stromatolites to high values in the thrombolite intervals in the middle and return to low values to the top for both cycles.

Internal flow channels occur between build-ups, and they formed lateral and vertical connection pathways along the microbialite build-ups. These channels may be

effective at reducing flow barriers and enhancing the vertical permeability in microbialite reservoirs.

The comparison between the Holocene thrombolite and the Jurassic thrombolite indicates they had comparable primary pore networks, with similar porosity values, which were controlled by similar depositional textures. Thus, the identification of microbialite depositional textures, and their relationship to environmental changes, provides insights into understanding some primary pore network characteristics such as pore geometry and pore connectivity. This information, when related to diagenetic modifications of the rock framework, improves the correlation of the fundamental rock characteristics and petrophysical properties that is useful for rock type classification, formation analysis and reservoir modeling.

CT scan volumes provide important detail about the pore networks that enhance the recognition of fundamental rock characteristics and porous media properties to a degree not matched by basic description and petrography. These types of scans are highly recommended for geological description of microbialites to better exploit these complex reservoirs.

CHAPTER II

IMPORTANCE OF DEPOSITIONAL TEXTURE IN PORE CHARACTERIZATION OF SUBSALT MICROBIALITE CARBONATES, OFFSHORE BRAZIL[2]

Overview

Microbialite carbonates (e.g. stromatolites, thrombolites, shrubs and spherulites) are sedimentary deposits highly influenced by their environmental settings such as water depth, water chemistry and relative energy. Lower Cretaceous subsalt microbialite carbonates, in the Santos Basin (Brazil), have complex pore systems produced by their growth framework, which are related to carbonate precipitation by biotic and abiotic processes and also influenced by subsequent cementation and dissolution. Complex pore systems and high spatial reservoir heterogeneity result in reservoirs having total porosity ranging from 2 to 27% and permeability from less than 0.01 millidarcys to 4.9 Darcys. Differences in textural characteristics such as shrub size, sorting and packing lead to different pore systems that subsequently control the petrophysical properties. Cements and dissolution also modify these texturally controlled pore systems by respectively reducing or enhancing the pore volume and pore-throats. The shrub size is a primary control on changes in the pore size and affects the permeability, whereas the shrub sorting influences the primary porosity, and secondarily the permeability. Packing acts

[2] This chapter was published in the Geological Society of London Special Publications, Volume 418, First published online February 26, 2015. Copyright ©2015. Reprinted by permission of the Geological Society of London whose permission is required for further use.

as a secondary control on porosity. As result, a sample with small shrubs, well-sorted and tight packing has lower permeability for the same range of porosity than a sample with the same characteristics, but larger shrubs.

Introduction

Microbialite units have been intensely studied in recent years to address questions about the nature of the carbonate precipitation (Dupraz *et al.* 2009), the distribution and geometry of microbialite deposits (Harris *et al.* 2013) and the importance of establishing the relations between fundamental rock characteristics and petrophysical properties in hydrocarbon reservoirs formed or dominated by microbial induced carbonate precipitation (Tonietto & Pope 2013). A central element in these studies is the pore system. In microbialites, pores are formed or modified by biological, depositional and diagenetic processes, which leads to complex pore systems (Parcell 2002; Ahr 2008). Internal factors of each process can cause differentiation in texture and fabric of carbonate rocks that also affects pore system characteristics, such as pore and pore-throat sizes (Lønøy 2006; Lucia 2007; Ahr 2008; Verwer *et al.* 2011). Thus, the relative importance of these processes in the pore system development is the key to understanding the petrophysical properties within these reservoir rocks (Melim *et al.* 2001; Parcell 2002; Mancini *et al.* 2004; Ahr 2008).

However, microbialite textures and fabrics are heterogeneous as a result of diverse depositional environments, biotic and abiotic processes (Monty 1976; Burne & Moore 1987; Riding 2000; Riding 2011), and subsequent diagenetic modifications. This

heterogeneity obscures the direct link between microbialite textures, pore system and petrophysical properties. Textural controls on pore system characteristics and petrophysical properties in detrital carbonate rocks were outlined previously (McCreesh *et al.* 1991; Luo & Machel 1995; Dürrast & Siegesmund 1999; Melim *et al.* 2001). An approach to better understand these microbialite reservoirs is to describe their basic textural elements and mode of occurrence, relating them to differences in pore systems and petrophysical properties for each texture (Melim *et al.* 2001; Ahr 2008; Rezende *et al.* 2013).

Such an approach is used here to evaluate Lower Cretaceous subsalt microbialite carbonate units in the Santos Basin (figure II.1) formed in transitional to marine settings (Dias 2005). There is an ongoing scientific debate about the origin and nature of microbialite carbonates in terms of biotic and abiotic processes that lead to carbonate precipitation (Chafetz & Guidry 1999; Pope *et al.* 2000; Dupraz *et al.* 2009; Rainey & Jones 2009; Mancini *et al.* 2013). Herein, these subsalt carbonate deposits are assumed as microbialites, which are defined as deposits formed by association between biotic and abiotic carbonate precipitation processes and detrital particles (Burne & Moore, 1987).

These carbonates are highly heterogeneous in terms of texture, pore systems and diagenetic history. Plugs were selected in core sections with well-defined textures and fabrics to determine their porosity, permeability and capillary pressures to understand how fundamental rock characteristics relate to the interconnected pore network in these microbialites. The results suggest that textural aspects such as size, sorting, packing and

morphology of structures are fundamental controls on the porosity, permeability and pore-throat distribution within this reservoir.

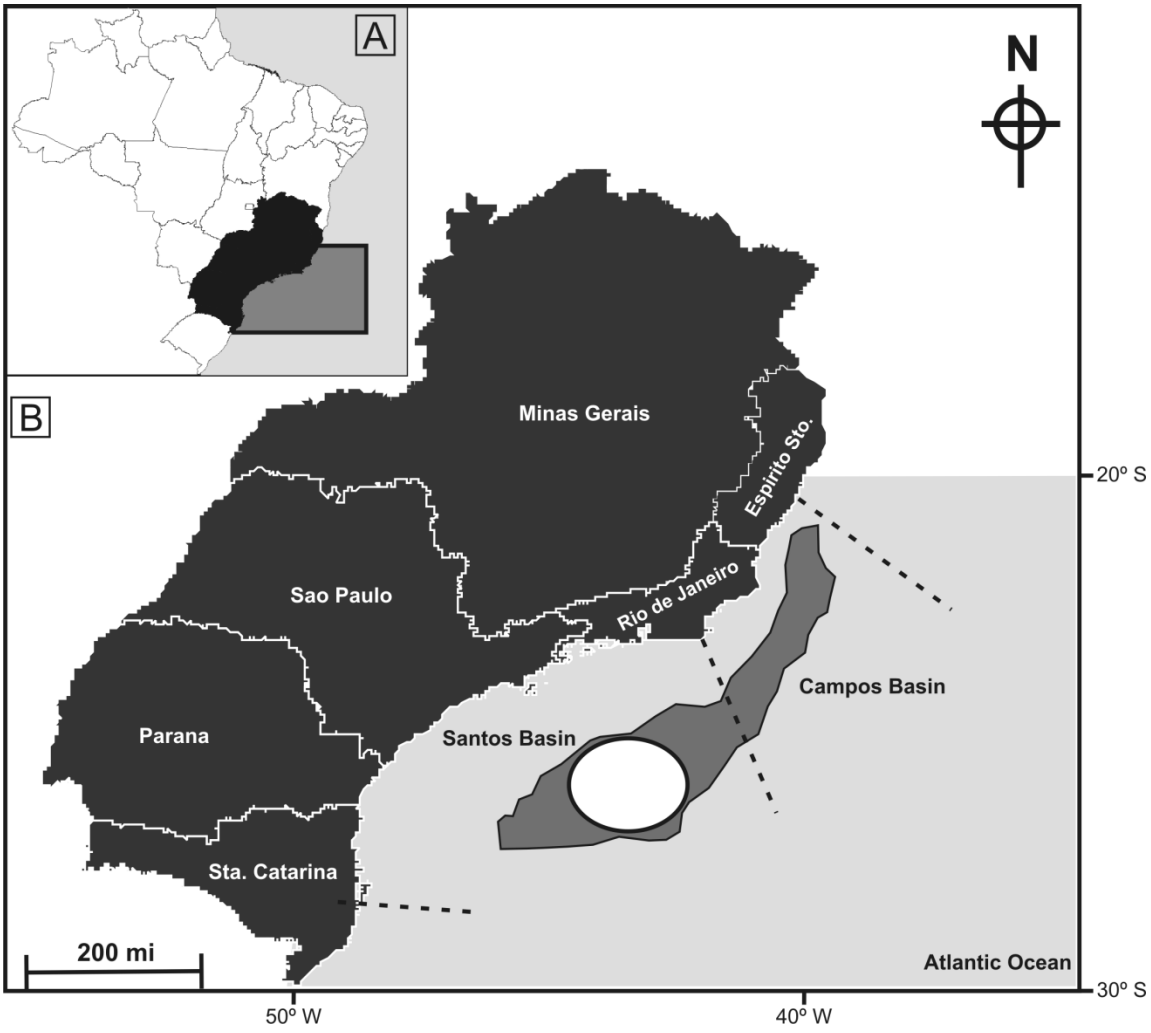

Figure II.1. (A) Inset map - The eastern shore of Brazil and the Federation States are shown. (B) Location map of the Santos and Campos basin on the south-eastern Brazilian margin. The white circle marks the approximate study area in the zone of deep-water subsalt reservoirs (shaded dark grey area).

Geologic setting

Extensive Lower Cretaceous subsalt carbonate deposits (figure II.1) formed in shallow water environments in a compartmentalized sag basin along the south-eastern Brazilian coast (Bueno 2004; Dias 2005; Campos Neto *et al.* 2007; Moreira *et al.* 2007; Araújo *et al.* 2009;). Paleontological data suggest that Tethyan waters entered the basin through seaways to the north (Araí 2009). Microbialites and detrital carbonates formed in these shallow water environments in a transitional phase between previous continental settings characterized by fan deltas and lacustrine deposits (e.g. coquina banks) and overlying marine salt deposits (Winter *et al.* 2007). In the Santos Basin these carbonate deposits are included in the Barra Velha Formation (Moreira *et al.* 2007).

Harsh hypersaline environmental conditions prevailed in these shallow environments because of evaporation in this arid setting (França *et al.* 2007; Araújo *et al.* 2009; Beglinger *et al.* 2012). Furthermore, the sedimentary basins were compartmentalized into proximal areas with siliciclastic sediments and distal areas where siliciclastic input was minimal and carbonate deposition flourished (Dias 2005; França *et al.* 2007; Moreira *et al.* 2007; Gomes *et al.* 2013).

These subsalt microbialite carbonate deposits have different external morphologies and textures (Terra *et al.* 2009). The external morphologies of these microbial carbonates were related to water depth, water chemistry and environmental energy (Dias 2005; Araújo *et al.* 2009;). Furthermore, depositional textures in these microbialite deposits have diverse textural variations in size, morphology, sorting and

packing (Terra *et al.* 2009). The microbialite textures in the dataset presented herein range from microbial laminite to shrub microbialite with distinct morphological aspects (figure II.2). This textural diversification was caused by changes in environmental processes that drove microbial growth and carbonate precipitation (Schmid 1996; Konhauser 2007; Dupraz *et al.* 2009).

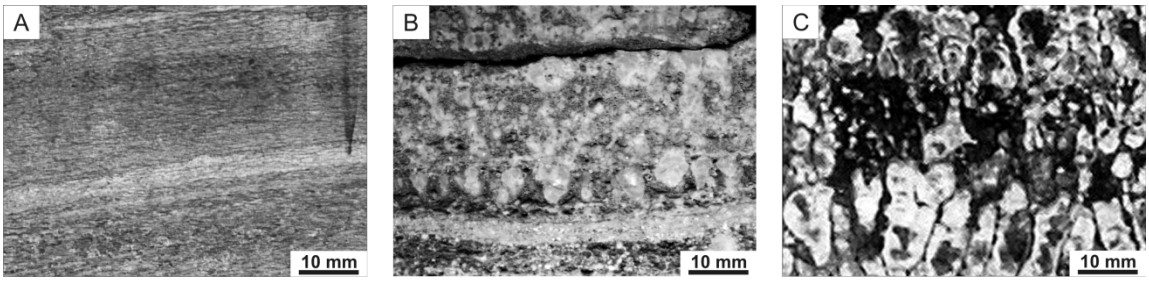

Figure II.2. Three common textures formed in the subsalt microbialite carbonates in the South Atlantic. (a) Microbial laminite, with plain to crinkle micritic laminae. (b) Medium shrub microbialite defined by shrubs with heights between 5 mm and 10 mm occurring in the upper half of the image. (c) Large shrub microbialite texture (shrubs > 10 mm). In most intervals microbial structures of different sizes coexist, so the textures are differentiated based on the dominance of one size class over the others.

Syndepositional and diagenetic processes are common in these microbial carbonates, which led to a shift from depositional to diagenetically modified pore systems (figure II.3). Usually, dissolution is the major process that enhances the pore system in these carbonates, by enlarging depositional pores or creating new pores (Araújo *et al.* 2009). Dolomite, calcite and silica occur as cements and replacive phases.

These cements formed as result of syndepositional and burial processes and they normally reduce the depositional pore system. In most cases however, the pore system in these rocks is classified as a hybrid between depositional and diagenetically enhanced or reduced using the classification proposed by Ahr (2008).

Methods

A large variety of textures are currently described for these subsalt carbonates from the Santos Basin (Terra *et al.* 2009). While this variation is important in understanding the depositional conditions, it also makes the correlation between texture and petrophysical properties more complex. This added complexity occurs because a large number of textures can have similar pore system characteristics. To simplify the correlation procedure, depositional textures were re-classified by sampling based on their morphometric aspects (Hofmann 1976), height to width ratio (h/w). This classification scheme considers lamina, spherulite and shrub as the basic textural elements in these microbialite carbonates (figure II.4). To simplify the textural classification criteria and evaluate the effect of shrub size and sorting on the pore system, shrub microbialite textures were divided in three size classes (small – less than 5 mm height; medium – between 5 to 10 mm height; and large – greater than 10 mm height).

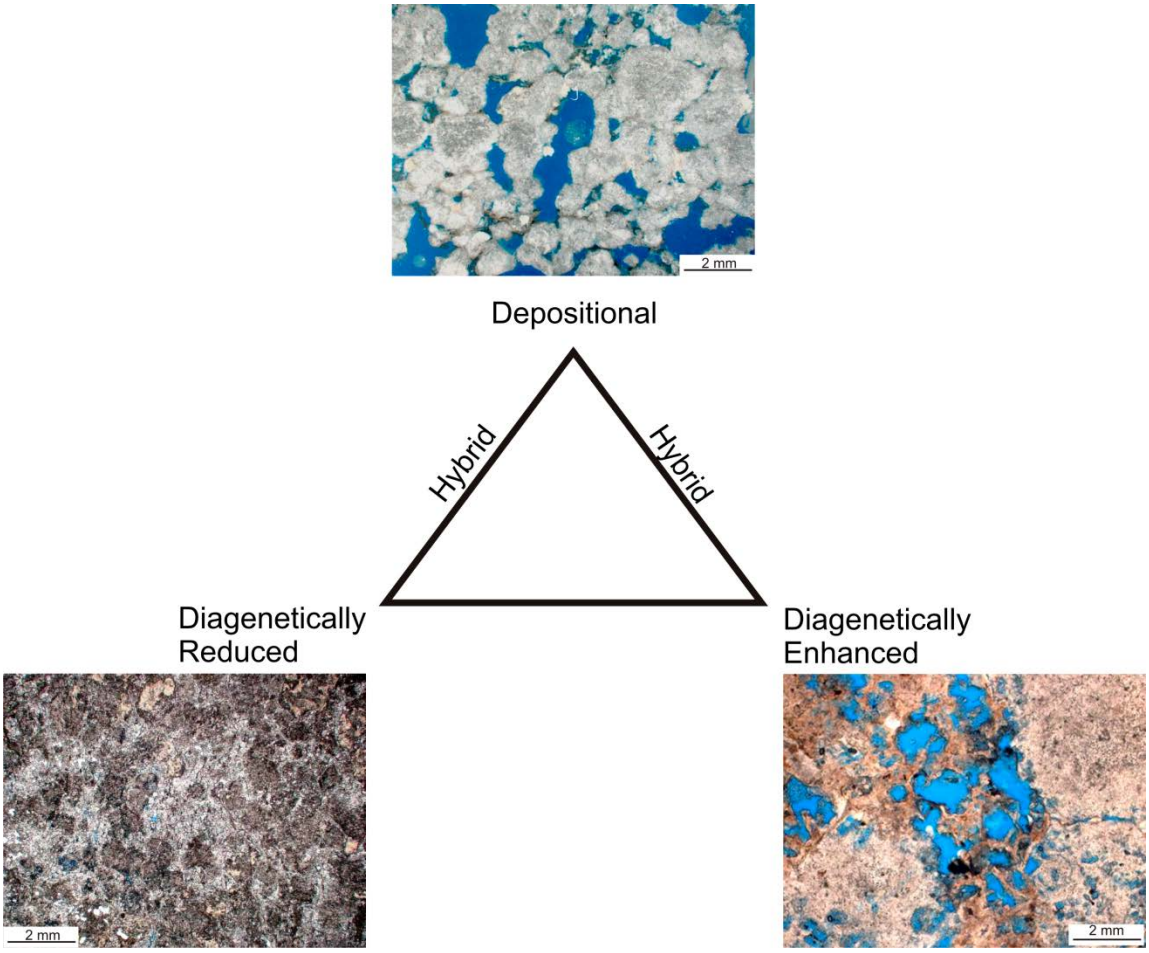

Figure II.3. Three possible pore system end-members formed by the depositional framework and diagenetic modifications. The three images show large digitate stromatolite texture, with the pore system end-members. Pores are shown in blue. The depositional pore system is characterized by a clear textural control on pore characteristics. The diagenetically enhanced pore system has depositional pores enlarged and new pores (intraparticle, moldic and vugs) formed by dissolution. The diagenetically reduced pore system has most of its pore space filled by cements (e.g. calcite). Hybrid pore systems have characteristics between the diagenetic end-members.

46 core plugs were selected from three wells in different hydrocarbon fields of the Lower Cretaceous subsalt microbial carbonates. This selection was based on textural homogeneity and diagenetic modification by rock description and thin-section petrography. The main macroscale and microscale characteristics for each texture described in these cores and the assumptions related to carbonate precipitation rate are summarized in figure II.5. These assumptions are based on previous works that relate more complex morphologies and rapid structure development to environmental conditions considered more suitable for microbial growth and biotic/abiotic carbonate precipitation to nutrient availability and high carbonate saturation respectively (Dupraz *et al.* 2006).

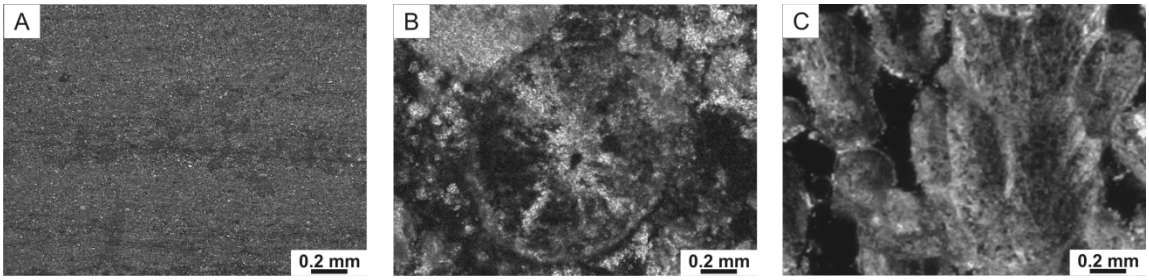

Figure II.4. Three main textural components formed in the subsalt microbialite carbonates in the South Atlantic. Dark areas are pores. All photomicrographs are with cross-polarized light. (a) Micritic laminae. (b) fibrous-radial spherulite. Crystals floating around the spherulite are dolomite. (c) Fan shaped radial shrub with peloids.

Cored intervals with very high textural heterogeneity, regarding differences in shrub size sorting, morphology and packing were avoided so as to illustrate a more straightforward correlation between individual textural aspects, pore system characteristics and petrophysical properties. Intervals where the depositional pore system was strongly reduced or obliterated by cements were discarded from the dataset, because in these intervals the relationship between pore system characteristics and petrophysical properties is defined by the presence of cement within the pores. However, intervals with dissolution features such as the presence of vugs and dissolved particles were sampled to evaluate the enhancement effect of dissolution in the depositional pore system. This sampling strategy results in 46 core plugs, 38.1 mm long and 25.4 mm wide that were described and their effective porosity and absolute permeability measured. These petrophysical analyses were performed under reservoir pressure regime, using the Corelab® Ultrapore-300 helium porosimeter and the Corelab® Ultra-perm 400 gas (nitrogen) permeameter. The permeability measurements were corrected to Klinkenberg gas slippage effect.

Five plugs for each of the four depositional textures analysed (e.g. laminite, small shrub microbialite, medium shrub microbialite and large shrub microbialite) were selected in a range of pore systems from purely depositional to diagenetic enhanced from the initial selection of 46 plugs. The criteria to select these plugs were based on texture and diagenetic enhancement and petrophysical properties. Samples with similar characteristics in each textural class were removed from the original dataset. These 20 plugs were described in detail for textural and pore system characteristics and they also

were analysed by mercury injection porosimetry to measure capillary pressure and calculate the pore-throat radius distribution.

Mercury injection capillary pressure (MICP) were measured with a Micromeritics® AutoPore IV 9500 porosimeter on clean and dry 1 cubic centimetre fragments. The incremental pressure was measured up to 60,000 psia. The pore-throat radius distribution was obtained from this pressure data. Explanations about laboratory procedures and calculations are extensively detailed in Luo & Machel (1995) and Basan *et al.* (1997). All petrophysical measurements on the selected samples were performed at the *PETROBRAS* Research Centre, Rio de Janeiro, Brazil.

Texture		Image		Macroscale characteristics							Microscale characteristics		Relative carbonate precipitation rate
		Photo	Binary	Main internal sctucture	Internal structure size	Internal structure morphology	Packing	Shrub size sorting	Fabric	Pore System	Peloids/Crystals	Micrite/Cements	
Microbialite	Microbial laminite	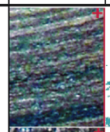		Lamina	Not aplicable	Simple	Tight	Not aplicable	Horizontal	Simple	High	High	Slow
	Small shrubs			Shrub	Smaller than 5 mm height	Commonly complex branches	Commonly tight	Well to Moderate	Vertical	Complex	Moderate	High	Slow
	Medium shrubs		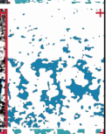	Shrub	Between 5 mm and 10 mm height	Simple to complex branches	From loose to tight	Moderate	Vertical	Complex	Low	Low	Moderate
	Large shrubs	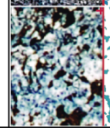		Shrub	Higher than 10 mm height	Simple to complex branches	From loose to tight	Moderate to Poor	Vertical	Complex	Low	Low	Fast

Figure II.5. Macroscopic and microscopic characteristics used to describe different microbial carbonate textures the relative precipitation rate for each texture. On the photo/depositional pore system pairs the red cross is an anchor for the field views. On the photo (left image) the greyish and white colours are carbonate and black areas are pore-system. The depositional pore system (right hand binary image) is shown in blue and the rock components in white.

The 15 samples selected from the three microbialite textures were described by petrography for texture, fabric, microbial components, mineralogy, pore system characteristics and diagenetic features, as shown in the figure II.5. The shrubs had their attributes, such as size (height and width) and packing (ratio between shrub width and adjacent spacing) measured and the morphological aspects (simple or complex branches) classified on the area adjacent to the plugs (up to 10 cm). Each shrub attribute was measured 80 times to allow a minimum quantitative modal analysis and further correlation to petrophysical properties. Height and width were measured assuming the longer linear lengths (vertical and horizontal) as a value for these attributes. The space between shrubs was assumed as the longer linear length for the space between two adjacent shrubs.

The spatial distribution of shrubs in these microbialite carbonates occurs as a three-dimensional arrangement that is not completely defined by means of two-dimensional measurements. However, the basic textural characteristics such as shrub size, packing and morphologic aspects may suffice to identify the basic textural controls on the pore system characteristics and the petrophysical properties in these subsalt microbialite carbonate units.

The standard deviation (σ) calculated for the shrub attributes data series was used as an internal variability index to address how each sample differs from others in the same texture class. The σ calculation intentionally did not exclude possible outliers because in these rocks the presence of these may modify the pore system and alter the petrophysical parameters. The shrub size was defined by its height. The shrub size

variability index of each sample was used as a measure for sorting (shrub size sorting index). It was determined using the normalized height, which was calculated by the ratio between each measured value and a fixed maximum size in each sample. This procedure allows the evaluation of the shrub size sorting for different height ranges in a same decimal scale. Higher values for shrub size sorting index means poorer sorted textures and low values means better sorted textures.

The ratio between the length of a space adjacent to a shrub and the width of the shrub was used as measure of packing. In this ratio, lower values define closely spaced shrubs and higher values define more separated shrubs. The packing variability index of each sample was calculated based on the distribution of this space and width ratio, and represents the internal dispersion in a sample from tight to loose packing. Thus, a texture with packing index close to 1 has tighter packing and a packing index close to 0 has looser packing.

The shrub normalized size and the packing index distributions (figure II.6) indicate that these samples are texturally heterogeneous. Therefore, measuring textural and shrub morphometric attributes can provide insights into the importance of the microbialite texture to pore system characterization. However, this high textural heterogeneity and the three-dimensional (3D) aspect of the pore system also affects a proper assessment of a representative elementary volume (REV) that accounts for fluid flow and the measurement of the permeability in these microbialite carbonates. It occurs because of the small dimension of samples analysed, as well the scale of morphometric

measurements on cores does not include all the elements of the 3D interconnected pore network.

Data

Carbonate textures

Three basic microbialite textural components are described as lamina, spherulite, and shrub (figure II.4). Since these three basic elements coexist in a sample, the microbialite texture was determined by its dominant component by rock description and petrographic analysis. This procedure results in a simplified textural classification (figure II.5) that contains four textures: microbial laminite and three classes of microbialite shrub (small, medium and large). The differentiation between shrub textural classes was based on the shrub mean size distribution. Spherulites occur dispersed in the microbial laminite and shrub microbialite textures, and are a common textural component, but in none of our samples was it dominant.

Lamina developed as micritic and peloidal horizontal layers (figure II.4a) with planar to crinkly morphologies. Spherulites usually have diameters less than 5 mm and are composed of calcite with variable nucleus composition (figure II.4b) and an internal radial-fibrous pattern. The shrubs have diverse morphologies from simple to complex branches and variable sizes from spherulite/small shrubs less than 5 mm in height to large shrubs greater than 10 mm, usually constructed of a combination of micritic peloids and fibrous fan-shaped calcite (figure II.4c). In addition, the textures were

grouped based on size sorting, tight or loose packing and complex or simple morphology (figure II.7).

Pore system characteristics

The pore system of each sample was classified as depositional, hybrid or diagenetically enhanced or reduced (figure II.3) based on the genetic classification proposed by Ahr (2008). This classification describes the amount of the pore geometry characteristics inherited from the *in situ* microbialite carbonate texture and its subsequent diagenetic alteration. Additionally, the pore geometry was described in relation to it spatial organization (e.g. horizontal, vertical or complex) and size (figure II.8). The impact of caves and channels, diagenetic vugs and fractures larger than the plugs, on the petrophysical properties in these microbial carbonates was not evaluated because of sample size limitations.

Results

The porosity and permeability data for the selected samples have a wide range of values (ϕ = 5.5 to 27%; κ = 3 millidarcys [md] to 4.9 Darcys [d]). Generally, intervals with a higher degree of cementation have the lowest porosity and permeability values for any microbialite texture analysed (figure II.9). Conversely, the diagenetically enhanced intervals (e.g. pore enlargement, particle dissolution and vug creation) have the highest porosity and permeability values (figure II.9). Furthermore, each texture described (e.g. laminite, small shrub microbialite, medium shrub microbialite, and large shrub

microbialite) has a positive correlation for porosity and permeability values, but differing slopes (figure II.9).

Figure II.6. Data distribution for a set of 15 samples, showing the normalized structure size (a) and packing (b). The box thickness and whiskers indicates that the individual samples are different, regarding their internal variability for the analysed attribute. The boxes are built to show the number of measurements within the first and third quartiles. Longer boxes indicate that the sample has a high internal variability and shorter boxes indicate a lower variability in the sample. The black bar is the median value for each sample. The length of whiskers represents the lowest and highest values within 1.5 times the difference between the third and first quartile. Circles indicate measurements distant from the rest of the data, in this study they were not discarded as outliers. The area adjacent to each plug was described and categorized by texture and reference number: L = large shrub microbialite, M = medium shrub microbialite and S = small shrub microbialite.

Figure II.6. Continued.

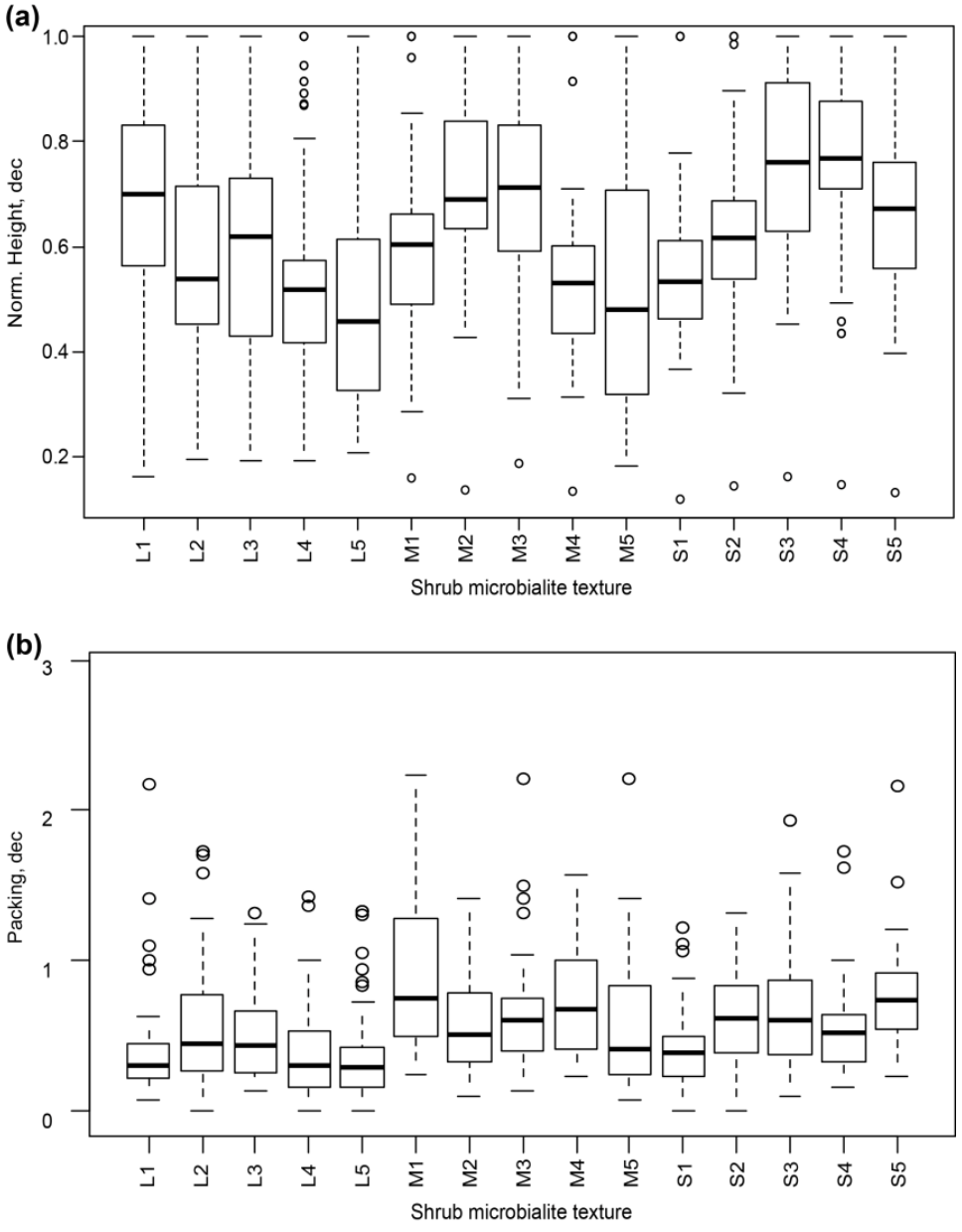

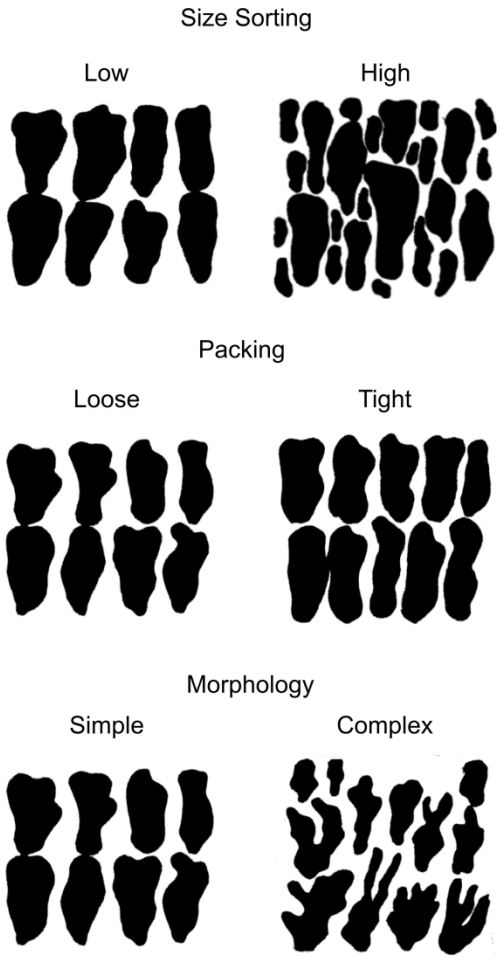

Figure II.7. Microbialite carbonate textures are grouped based on shrub size, sorting, packing and morphology aspect. The dark areas represent the microbialite framework. This textural grouping is important because changes on these properties results in changes in the pore system characteristics such as pore size, pore-throat radius and tortuosity.

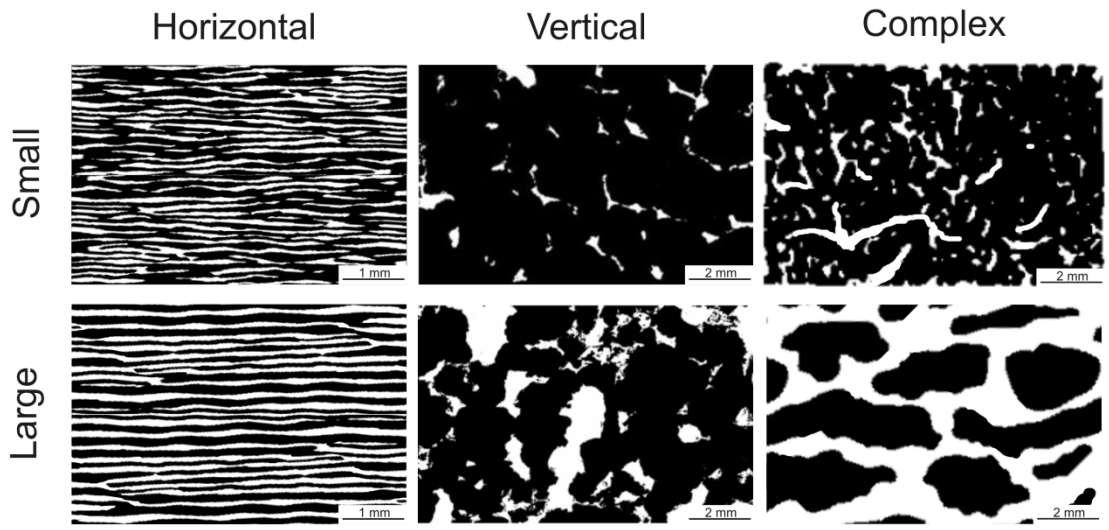

Figure II.8. Pore geometry characteristics related to different microbialite carbonate textures. Usually, laminites have horizontal pores. Shrub microbialites have a variety of pore geometries from vertical to complex. The pore size, pore-throat radius and tortuosity are controlled by textural characteristics as shrub size, sorting and packing. The pore system is shown in white, and the rock framework in black. Modified after Hofmann (1976).

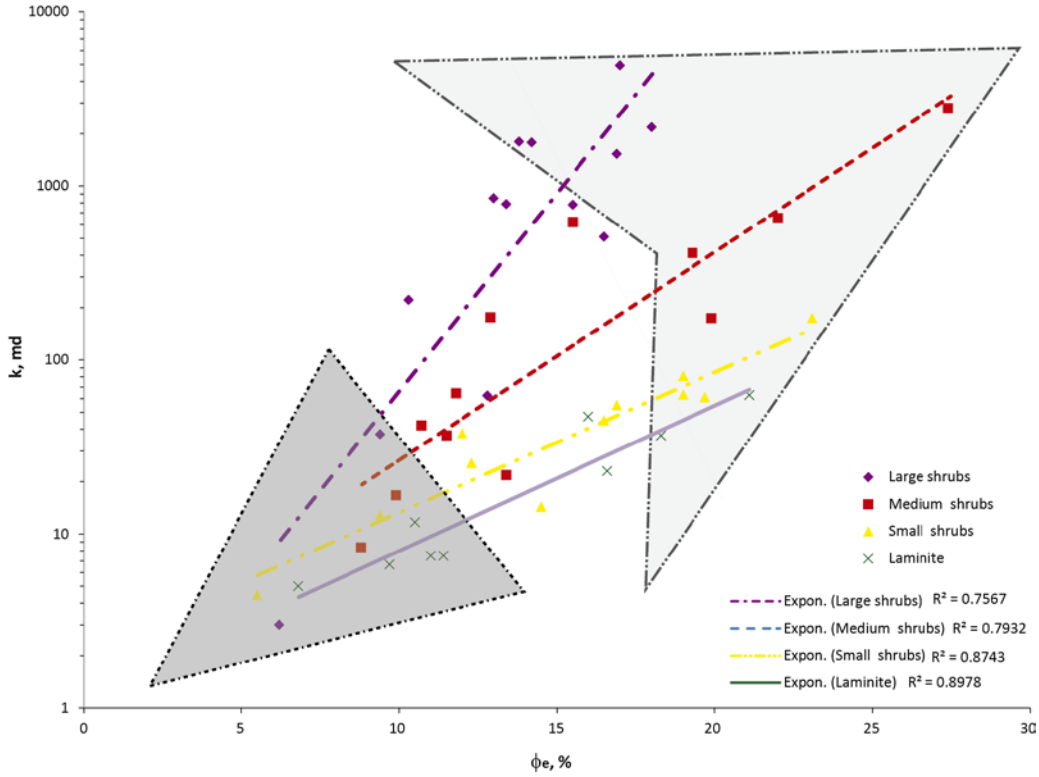

Figure II.9. Porosity v. permeability plot for each texture analysed from the subsalt microbialite reservoir units. There is a wide distribution of values with a positive correlation. However, the regression line for each texture has different slopes. These relationships suggest that given moderate or less diagenetic modifications, texture also controls pore system characteristics and impacts petrophysical properties. Only samples with reservoir potential are shown. The grey areas represent samples with more dissolution features (top right area) and more cementation (bottom left area) described by petrography. The samples outside these areas have the depositional pore system less modified by diagenesis. The scale for shrubs is: small shrubs < 5 mm; medium shrubs between 5 mm and 10 mm; large shrubs > 10 mm.

The mean pore-throat distribution for four sets of MICP samples in each microbialite texture shows a progressive trend of higher pore-throat radii from the laminite towards the large shrub microbialite (figure II.10a). This trend still occurs when samples with diagenetic enhanced pore systems are removed from the calculation of the mean pore-throat radius distribution (figure II.10b). Only the small shrub microbialite shows a bimodal distribution that is caused by a higher proportion of laminae associated with the small shrubs in some samples.

A clear separation on the correlation trends for the four textures analysed in this dataset indicates that the larger shrub microbialite texture has higher permeability values for the same porosity value than the other textures (figure II.9). This characteristic is corroborated by the largest pore-throat radii measured on the larger shrub microbialite textures in comparison to the other textures analysed (figure II.10a).

The link between shrub size and pore-throats in these subsalt carbonate units also occurs when pore-throat radius distribution is compared to the shrub size distribution for the three shrub microbialite textures (figure II.10c). Pore-throat radius and shrub size have a similar distribution at different observational scales. The laminite texture does not have any measurable shrubs to allow a comparison between shrub size and pore-throat radii distribution.

However, no correlation occurs between the mean structure size and porosity in the shrub microbialite textures (figure II.11a). Conversely, the permeability shows a positive correlation with an increase in the mean structure size (figure II.11b). A positive

correlation also occurs for each of the shrub microbialite textures, but with some dispersion in the small and large shrub microbialite textures (figure II.11b).

When porosity is plotted versus the shrub size sorting index (figure II.12a) a slight negative correlation trend is observed. Samples with poorer sorting have lower porosity values, whereas samples with better sorting have higher porosity. Thus, the shrub size sorting is a primary control on porosity. The dispersion of low porosity values in the shrub size sorting and porosity plot (figure II.12a) represents the reduction of pore volume in samples with a higher proportion of cement in the pore system. Furthermore, the shrub size sorting index shows a slight negative correlation with permeability for each shrub microbialite texture class (figure II.12b), which suggests that in addition to shrub size, sorting is a secondary control on permeability. Consequently, a better shrub sorting leads to higher permeability values.

Packing is a tertiary control on porosity in these shrub microbialite textures, as indicated by the subtle positive trends between packing index and porosity for each texture (figure II.13a). The packing control on porosity is expressed by higher porosity values towards looser packing. The samples of small and medium shrub microbialites with the highest porosity values are the most affected by diagenetic dissolution in their classes. The presence of pores larger than the average shifts the packing index to higher values. The relationship between packing and permeability is not defined because of large data scattering (figure II.13b).

Figure II.10. (a) Plot of mean pore throat radius distribution per texture, including samples with pore systems classified as depositional, hybrid and diagenetically enhanced. (b) Plot of mean pore throat radius distribution per texture, without samples with pore systems classified as diagenetically enhanced. The pore-throat radius distribution is shifted towards larger values, as the texture change from laminites to large digitate stromatolite. The effect of diagenetic enhancement is identified where distributions show peaks for larger pore-throats for the laminite, small digitate stromatolite and medium digitate stromatolite. This diagenetic signal is not observed for the large digitate stromatolite texture. (c) Shrub size distribution compared to the pore-throat radius distribution in (a). These two properties measure distinct properties at different scales, but the similarity of the shift toward larger values between these properties distributions is suggestive that the size of the structures controls the pore and pore-throat sizes

Figure II.10. Continued.

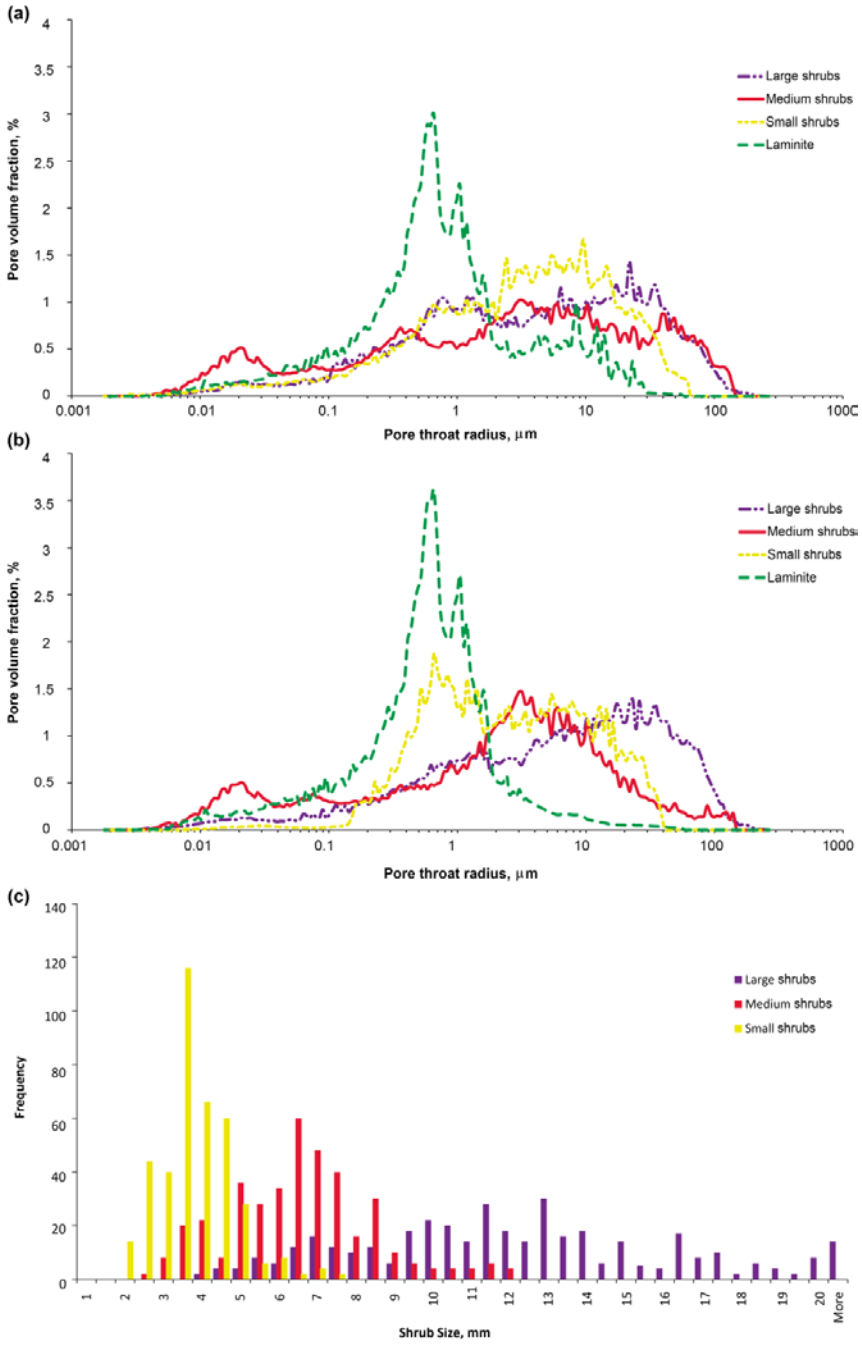

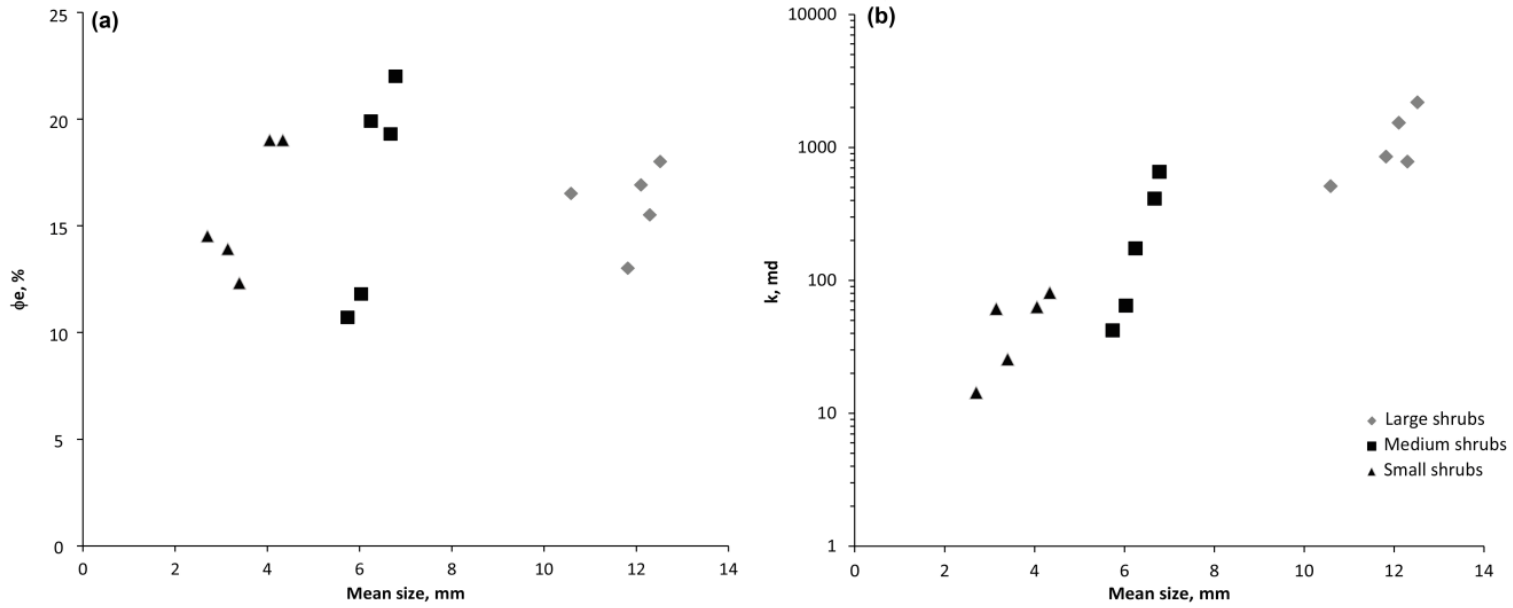

Figure II.11. (a) Comparison between shrub mean size (mm) and effective porosity (%) for shrub microbialite textures. The data are scattered showing no correlation between size and porosity. (b) Comparison between shrub mean size (mm) and absolute permeability (md). The data suggest that the shrub size is related to permeability as size controls the pore size and pore-throat radius.

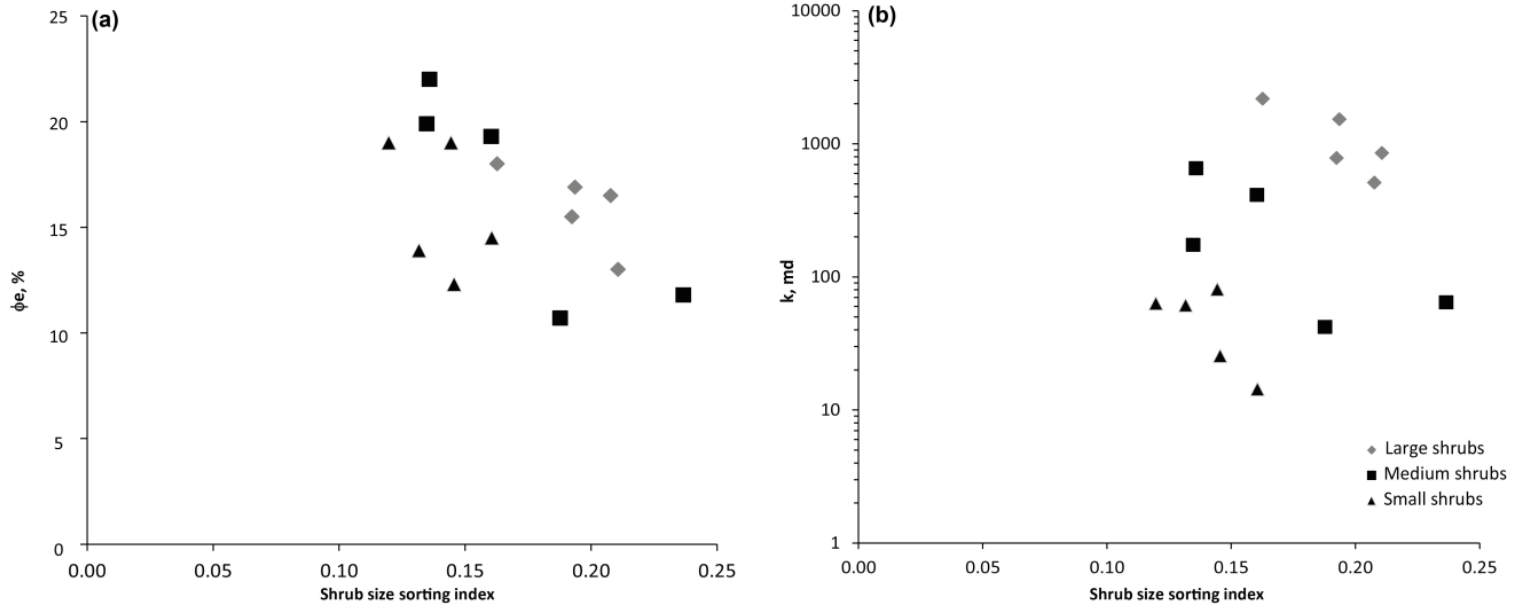

Figure II.12. (a) Comparison between shrub size sorting index and effective porosity (%) for shrub microbialite textures. Higher values indicate poorer sorting. (b) Comparison between shrub size sorting index and permeability (md). The relationships observed on both plots suggest that shrub size sorting impacts porosity and permeability. Poorly-sorted textures have their pore volume reduced, smaller pore-throats and higher tortuosity because of the presence of shrubs of different sizes that occupy more space in a volume when compared to well-sorted textures.

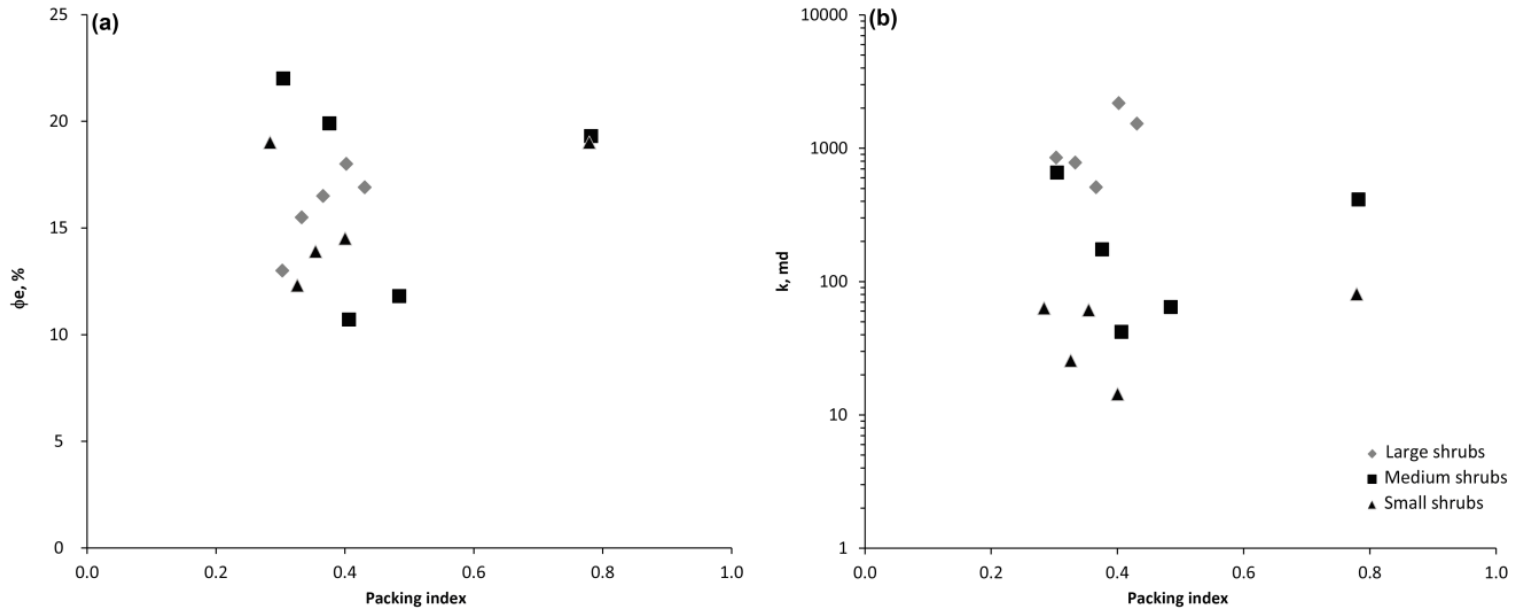

Figure II.13. (a) Comparison between packing index and effective porosity (%) for each shrub microbialite texture. There are subtle trends for the shrub microbialite textures that correlates porosity increments to looser packing (higher packing index values), which are identifiable for each texture. The points that are plotted outside the main field are textures with a high concentration of large spaces between adjacent shrubs. (b) Comparison between packing index and permeability (md) for each shrub microbialite texture. The relationship between packing and permeability is not clear for this dataset.

Discussion

Textural characteristics such as fabric, shrub size, sorting and packing in the Lower Cretaceous subsalt microbialites in the Santos Basin control the development of the depositional pore system and influence their petrophysical properties. Four microbialites textures (e.g. microbial laminite, small shrub microbialite, medium shrub microbialite and large shrub microbialite) are defined in terms of textural characteristics and petrophysical properties (figure II.8). The data scattering observed in this porosity and permeability relationship is related to the textural heterogeneity observed in these samples (figure II.6).

The size of shrubs controls changes in the pore-throat size (figure II.10) and consequently affects the permeability (figure II.11b), whereas the shrub size sorting controls porosity (figures II.12a). Additionally, shrub size sorting is a secondary control on permeability (figure II.12b) as result of an increased pore system tortuosity in poorly-sorted textures. The effect of packing is perceptible on porosity by increased porosity towards textures with looser packing in each texture (figure II.13a). However, its influence on permeability is unclear in this dataset. Generally, the textural differences identified herein as large shrub size, well sorting and loose packing result in higher porosity and permeability values in the shrub microbialite textures (figure II.14), because of the textural control of the pore system characteristics (i.e. pore, pore-throat size, and tortuosity).

The role of complex versus simple textural component (e.g. shrub) morphology needs further evaluation because complex morphologies may result in intricate pore networks with dead-end pores and tortuous pathways, which may cause permeability reduction. Additionally, a more detailed morphometric description is needed to determine how much this actually affects the petrophysical properties in these microbialites. Whereas, shrub size, sorting and packing defined by two-dimensional measurements can provide a basic means to understand the textural controls on the pore system, more precise relations can be obtained by the use of three-dimensional methods (e.g. computed tomography) to access both texture and pore system characteristics.

These textural controls are valid in depositional to hybrid pore systems, when the depositional pore systems were not completely altered by cementation and dissolution (figures II.9, II.10). In these latter cases, the textural controls on the pore system characteristics may be totally obscured and the petrophysical properties related to the effect of diagenetic modifications on the pore system. Overall, the highest permeability and porosity values are related to diagenetically enhanced pore systems (figures II.9, II.10a and II.10b) because of enlargement of depositional pores, creation of new pores, such as vugs and intraparticle pores.

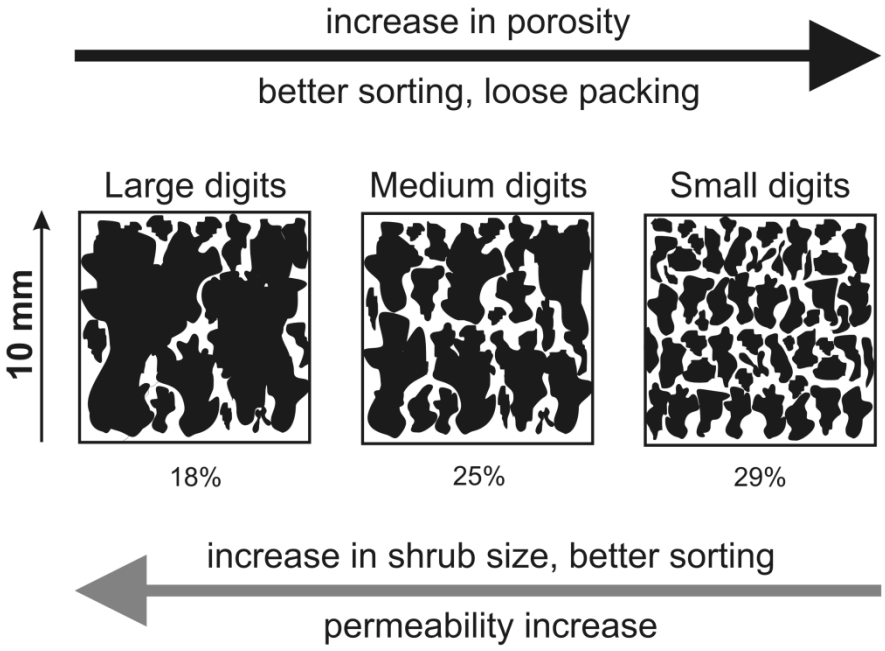

Figure II.14. Based on the relations of textural aspects, pore system characteristics and petrophysical properties, a general model is suggested for the microbialite carbonate textures analysed in this study. The numbers below the boxes are the total porosity calculated from bi-dimensional image analysis. The size of the shrubs for a given sorting controls major changes in the pore size and permeability, as result large structures allow larger pores and pore-throats. The porosity apparently is controlled by the shrub size sorting, because poorly-sorted textures have more shrubs with different sizes in comparison to well-sorted textures. This occurs because a relative reduction on the pore volume and pore throat radius, as well an increase the tortuosity of the pore system in poorly-sorted textures.

Future work will focus on the upscaling of both depositional and diagenetic textures and pore system to well-log evaluation. For this purpose, changes on mineralogical content associated with diagenetic processes may provide a better interpretation about how different processes (e.g. dolomitization and silicification) are related to changes in pore system characteristics. Furthermore, spatial distribution of

textures obtained from outcrops can provide more predictable outcomes about lateral variability of both microbial carbonate texture and its pore system.

Conclusions

Lower Cretaceous subsalt microbialite carbonates in the Santos Basin have pore system characteristics (e.g. pore size and pore-throat radius) defined by textural characteristics, shrub size, sorting and packing. Four microbialite textures defined by differences in fabric and shrub size have distinct porosity and permeability relationships, and pore-throat size distributions.

The shrub size in these microbialites is the main control on permeability. Larger structures result in large pores and pore-throats, leading to higher permeability values. Furthermore, the shrub size sorting controls porosity and is a secondary control on permeability. This control relates to the observation that textures with poorer shrub sorting means that more shrubs can occupy the available space per unitary volume, which reduces the total porosity, impacts the pore-throat radii and increases the pore system tortuosity. Packing also affects the porosity by reducing the space available between digits. However, its effects on permeability are unclear. As a result, a texture defined by well-sorted small shrubs that are tightly packed has lower permeability for the same range of porosity than a texture with the same characteristics, but larger shrubs.

These depositional pore systems characteristics were later altered by diagenetic processes that reduced or enhanced porosity and permeability. In this study, hybrid pore systems, diagenetically enhanced by dissolution, have higher porosity and permeability

values than purely depositional pore systems. This enhancement is visible on the pore-throat radius distribution that increases towards larger radii in samples with dissolution. Conversely, the precipitation of cements into the pore system reduces both porosity and permeability. The lowest porosity and permeability values are related to samples with high proportion of cements in the pore system.

CHAPTER III

LATERAL CONTINUITY OF ROCK AND PETROPHYSICAL PROPERTIES IN A MICROBIALITE BUILD-UP IN THE GREEN RIVER FORMATION, UTAH

Overview

Eocene Green River Formation microbialite carbonate build-ups are common as proximal lacustrine deposits. Build-up outcrops offer good opportunities to address questions regarding the depositional controls on the pore system development and its petrophysical properties. They also provide understanding of the spatial distribution and lateral continuity of microbialite facies and their reservoir rocks quality. A detailed study of one of these microbialite build-ups outcrops, along Three Mile Canyon Road, Uintah County, Utah, presents clear results that demonstrate that porosity and permeability in this build-up are strongly controlled by the microbialite depositional texture and the resultant primary pore system. Thrombolite texture produced open and chaotic fabrics and results in pore systems with better porosity and permeability values, than digit stromatolite texture which has organized fabrics, but is tighter. Petrophysical measurements on plugs drilled in the microbialites with these textures have porosity values ranging from 17.2% and 30.6% and permeability as low as 3.75 millidarcys to over 50 darcys. X-ray computed tomography scans of the rock textures provide more information showing that the thrombolite texture has better pore systems with larger pore sizes, higher number of pore throats and a better connectivity density per volume when compared to the digit stromatolite texture. The microbialite intervals are laterally

continuous through tens of meters in terms of depositional characteristics and reservoir quality. The interbedding with detrital carbonates is common, which allows the recognition of stratigraphic relations between these types of carbonate deposits, and the periods that favored microbialite growth and open pore system development. These relations provide useful insights that could be used to build more detailed reservoir models, using geologic and petrophysical information.

Introduction

Several studies recently characterized sedimentology, stratigraphy, depositional models and petrophysical characterization of microbialite and abiotically precipitated carbonate rocks in continental depositional settings (Pope and Grotzinger, 2000; Parcell, 2002; Bohacs et al., 2013; Chafetz, 2013; Rezende et al., 2013; Sarg et al., 2013; Seard et al., 2013; Tonietto and Pope, 2013). The aim of these studies was to improve our knowledge of microbial and abiotic carbonate deposits, providing better understanding of rock properties for the exploitation of microbial or abiotic hydrocarbon reservoirs, such as those along the south Atlantic Margins (Mancini et al., 2013; Rezende and Pope, 2015). However, to build refined 3-dimensional (3D) reservoir models, more information about the 3D depositional architecture and lateral distribution of sedimentary environments and their petrophysical properties is necessary (Fitch et al., 2015). Outcrops provide 3D access to the deposits, allowing for the recognition of textures and morphologies at different scales and lateral and vertical changes in the distribution of these properties.

The Eocene Green River Formation provides excellent examples of microbialite and associated carbonate facies formed in lacustrine settings (Awramik and Buchheim, 2012; Seard et al., 2013). Extensive outcrops in this unit in Utah, Colorado and Wyoming provide information about the origin of these carbonate rocks, their fabrics, morphologies, depositional conditions and stratigraphic evolution (; Tänavsuu-Milkeviciene and Sarg, 2012; Sarg et al., 2013; Seard et al., 2013; Frantz et al., 2014; Swierenga, 2014). However, more detailed reservoir characterization studies are still necessary to address the presence and characteristics of pores, their spatial distribution and connectivity, the lateral continuity of rock properties, the position of the best reservoir facies in the deposit and the distribution of external morphologies.

This study details a laterally continuous microbialite outcrop of the Eocene Green River Formation on the western margin of the Uinta Basin in Utah (figures III.1 and III.2) mapped out the lateral and vertical facies distribution and their rock properties. This paper discusses the genetic character, textural controls and lateral continuity of pore networks in these Green River Formation microbialite carbonates. The variation of petrophysical parameters is related to changes in texture, fabric, pore network and cement content. Shrub microbialites, thrombolites and stromatolites are laterally continuous and vertically connected throughout the outcrop. Their distribution and interbedding with other carbonate rocks is related to the relative position in the depositional setting, such that microbialite textures with better reservoir characteristics developed in areas and intervals with minor influence of transport or detrital sediments.

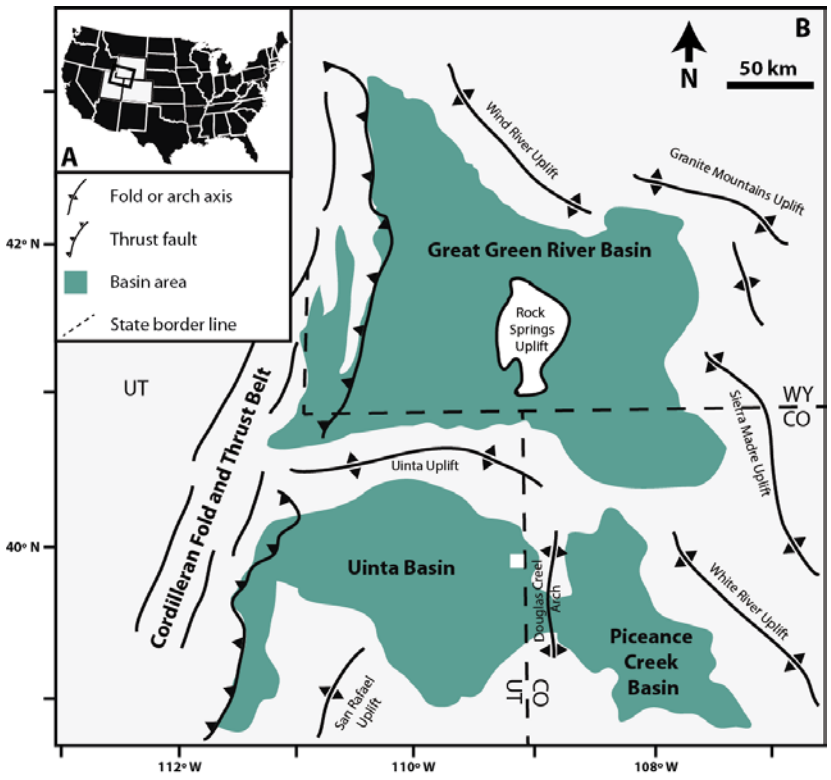

Figure III.1. Inset map A – United States map with the states where the Great Green River Basin, Uinta Basin and Piceance Creek Basin are located. B – Regional map with the areal distribution of the Eocene lake basins (Great Green River Basin, Uinta Basin and Piceance Creek Basin), major uplifts and tectonic lineaments (modified after Smith et al., 2008). The white square shows the area of study in Utah, at the eastern border of the Uinta Basin.

Geologic setting

During the Late Cretaceous to Eocene a series of isolated non-marine basins separated by emergent basement uplifts formed in the western US (Figure III.1), as result of the Laramide Orogeny (Beck et al., 1988; Dickinson et al., 1988). These basins formed in mid-latitude temperate to sub-tropical climates (Sloan, 1994; Morrill et al., 2001; Sewall and Sloan, 2006). As a result of tectonic and climatic variations, the non-

marine environments in these basins episodically expanded and contracted (Surdam and Stanley, 1979; Carroll and Bohacs, 1999; Smith et al., 2008). Fluvial drainages were tectonically blocked at times to form large freshwater or saline lakes with interfingering lacustrine and fluvial deposits along the basin margins (Dickinson et al., 1988; Roehler, 1992; Pietras et al., 2003; Smith et al., 2008).

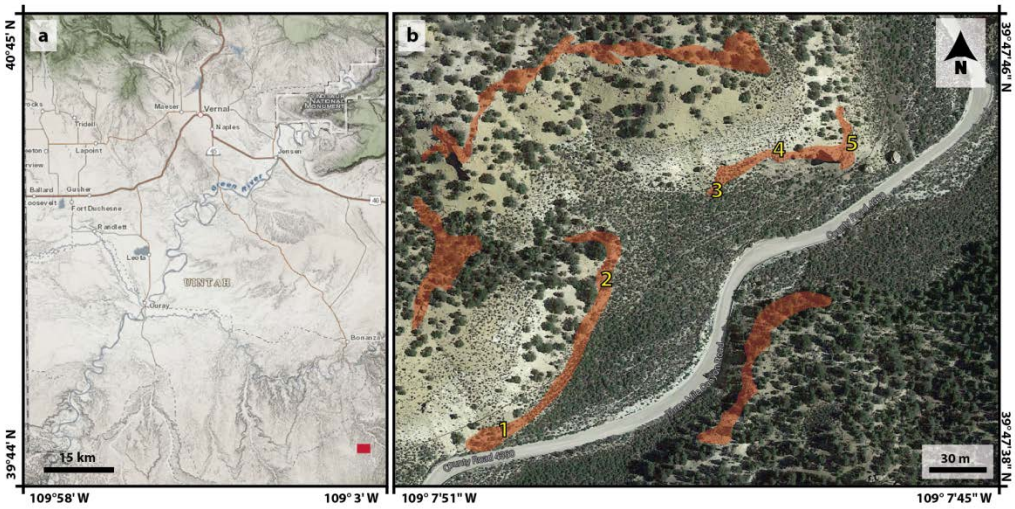

Figure III.2. (a) Local map with the main roads and cities near the area of study in the Uintah County, UT (Map courtesy from the State of Utah). The red square indicates the area of study. (b) Satellite image showing the Three Mile Canyon Road and adjacent terrain (Image courtesy from Google and NASA). The areas highlighted in red are the microbialite build-ups and detrital carbonates outcrops. The numbers 1 to 5 show the location of the stratigraphic sections in the outcrop.

In this tectonic setting, the Uinta Basin and Piceance Creek Basin were separated from the Greater Green River by the Uinta uplift (Bradley, 1964; Roehler, 1992). However, during times of prolonged pluvial periods and/or periods of active volcanism

in the northern end of the Greater Green River Basin, sediment and water influxes increased, and proximal areas were filled with volcanic sediments and the lake levels rose (Surdam and Stanley, 1980; Keighley et al., 2003; Smith et al., 2008). These regional events caused the overflow of the lake systems and expansion of its areal extent (Keighley et al., 2003; Smith et al., 2008). As a result, these basins became hydrologically connected, causing changes in lake stratification, water chemistry and distribution of depositional environments (Desborough, 1978; Surdam and Stanley, 1980; Boyer, 1982; Keighley et al., 2003; Smith et al., 2008). In the Uinta and Piceance Creek basins, the Green River Formation (GRF) is defined by rocks that record transitions from open, freshwater lakes to closed, saline lakes (Smith et al., 2008). The rocks deposited in these lakes are siltstone, sandstone, kerogen-rich carbonate mudstone, evaporite, and shallow-water carbonate (Sarg et al., 2013).

This paper focuses on microbialite build-ups and shallow-water carbonates within the lower part of the Eocene Green River Formation along the eastern border of the Uinta Basin (Figure III.1). Previous studies considered the microbialites as nearshore deposits of littoral environments in a transgressing lake system (Roehler, 1993; Bohacs et al., 2000; Osmond, 2000; Sarg et al., 2013; Tänavsuu-Milkeviciene and Sarg, 2012). The microbialites are interbedded with lacustrine shale, and pisoid/ooid, oncolite, intraclast and skeletal grainstone/packstone. One of the microbialite build-ups produces oil and gas in an interval with maximum thickness of 30.50 meters in the West Willow Creek Field (Osmond, 2000).

The microbialite build-up of the Eocene Green River Formation, documented in this paper, crops out along the Three Mile Canyon, near the town of Bonanza, Utah (Figure III.2). The external geometries in this build-up vary along the outcrop from laterally linked mounds to isolated heads. It pinches-out two miles to the northeast into profundal mudstones and oil shale (Swierenga, 2014). High wave energy in the littoral zone favored the formation of ooids, pisoids, oncolites and sublittoral-generated intraclasts. In protected environments, lower energy allowed microbial colonies to grow and *in situ* carbonate precipitation occurred. Open growth framework fabrics formed porous textures and well-connected pore networks within some intervals of these microbialite build-ups (Sarg et al., 2013; Swierenga, 2014).

Methods

Five stratigraphic sections were measured and described (Figure III.2) to document the vertical and lateral changes in facies, depositional textures and fabrics along the microbialite build-up outcrop. The distance between sections 1 to 3 is ~80 m and between sections 3 to 5 is ~45 m. This distance difference between the profiles is because of the lack of rock exposure due to erosion and sediment/soil coverage between the sections 1 to 2 and 2 to 3.

Twenty eight samples were collected at regularly spaced intervals (~10 cm) from the base to the top of the section 1 in the microbialite carbonate outcrop. These samples were used to prepare petrographic thin-sections to study the microfabrics, diagenesis and pore system in the microbialite carbonate. This section was chosen for this sampling strategy because it was the most accessible section and has a higher number of facies.

An additional ten samples, each with at least 10 cm^3, were collected throughout the five sections for petrophysical analysis and petrography at arbitrary locations. These samples were selected based on presence of visible pores and less visible weathering conditions. Four of these samples, with more than 20 cm^3, were also used for X-ray computed tomography. The larger samples allowed a better 3D evaluation by image analysis of the relations between depositional textures, sedimentary features and pore systems in a more representative elementary volume (REV). These relations are fundamental for petrophysical evaluation, and in microbialites they commonly are bigger than the scale sampled by plugs (Rezende et al., 2013; Corbett et al., 2015).

Petrography

Standard petrography and high-resolution scanning were used to characterize microfabrics and the pore system of the samples collected. The large size of microbialite fabrics meant 2 x 3 inch thin sections were prepared for twenty seven samples to provide better fabric characterization. Conventional 1 x 2 inch thin sections were prepared for detrital carbonates and small microbialite samples. All samples were impregnated with blue-epoxy resin to better define the pore system. High-resolution images of thin sections were made using the Nikon Super CoolScan 8000 scanner, with 4000 dpi true optical-resolution and density range of 4.2 in the Department of Geology and Geophysics at Texas A&M University.

Petrophysics

Ten horizontal cores, 1.5 inch long and 1 inch wide, were analyzed under a pressure of 800 psi using the Corelab® CMS 300 plug analysis equipment at the

Corelab® unit in Houston. Porosity was determined using Boyle's Law technique by measuring grain volume at ambient conditions and pore volume at indicated net confining stress. Permeability measurements were corrected to Klinkenberg gas slippage effect. These cores were drilled where the depositional texture is homogeneous, insuring the measured values correspond to the intended texture and pore system.

X-ray computed tomography

X-ray computed tomography of four microbialite samples was obtained by making sets of axial slices with spacing of 1 mm, using a 16 channel Aquilion RXL Toshiba® CT scanner, with X-ray voltage set at 130 kV, current at 75 mA, and spatial resolution of 0.25 mm, in the Department of Petroleum Engineering at Texas A&M University. The data from the X-ray CT scanner were rendered using the open source visualization and image computing software 3D Slicer® (Pieper et al., 2004; Pieper et al., 2006), available at www.slicer.org. This software also was used for volume manipulation (scalar transform and measuring), and threshold segmentation between rock and pore space.

Image analysis

The sets of CT scans images for each sample were cut for regular polygons to eliminate the empty space outside the boundaries of the samples. Each image in these sets was converted to black and white colors (binarized) using the open source image analysis software ImageJ® 1.49p, available at imagej.nih.gov/ij. The stack of each set of binarized images was used to calculate the pore connectivity density per volume (Odgaard and Gundersen, 1993; Toriwaki and Yonekura, 2002), the pore size by 3D

particle thickness distribution and the number of pore throats by 3D skeleton (medial axis of a particle) analysis (Lee et al., 1994). These calculations were processed using the BoneJ® 1.4.0 plugin (Doube et al., 2010) for ImageJ, available at bonej.org. The precision of the pore image measurements is limited to millimeters because of the tomograph resolution.

Results

Stratigraphy, build-up external geometry and facies distribution

The microbialite outcrop extends for ~240 m on both sides of the Three Mile Canyon Road (figure III.2). It consists of a vertical succession of fluvial-deltaic sandstone, microbialite build-ups and detrital carbonate bars and lacustrine shale deposited in a transgressive-regressive cycle (figure III.3). Seven carbonate units composed of microbialite and detrital carbonate occur interbedded with sandstone and shale. The first carbonate unit (Fifgures III.3 and III.4a), which is detailed in this paper, has an average thickness of 2.6 m. It was deposited on an erosive unconformity over the underlying massive sandstone bed. The five carbonate units within the shale have a maximum thickness of 10 cm, and the upper carbonate unit varies in thickness from 10 cm to 50 cm on the hilltop (figure III.3).

The microbialite build-up external geometry changes laterally from coalesced meter scale bioherms (figures III.4b and III.4c) in the southeast towards laterally linked, but morphologically isolated meter scale heads (figures III.4d and III.4e) in the northwest. The top of the microbialite build-up preserves its depositional upper surface, showing a change in morphological aspects from coalesced submetric heads (figure

III.4c) to isolated metric heads (figure III.4d). Intraclast packstone/grainstone, oncoid/pisoids packstone/grainstone and skeletal packstone/grainstone fill channels and depressions between heads and form beds that cover the build-up surface all over the outcrop (figure III.4b).

Shallow-water and exposure related sedimentary structures occur throughout the outcrop and are more frequent towards the uppermost levels of each build-up. Silica caliche (figures III.5a, III.5b and III.5c), desiccation cracks (figure III.5d), and brecciated beds are common features in the first microbialite carbonate unit. The caliche deposits formed thin intervals (~5 cm maximum thickness), as filling sediments in small ponds and channels (figures III.5a and III.5b). Tufa deposits formed by carbonate precipitation around tree roots (figures III.5e and III.5f) in the sixth carbonate unit.

The facies distribution along the outcrop records a shift from detrital carbonate facies that occur more often on the section 1, and become less frequent towards the section 5, where the microbialite facies are dominant (figure III.6). Four shallowing upward cycles were defined by: (1) unconformity surfaces, (2) progressive development worsening of the microbialite texture framework components, (3) grain type proportion (higher proportion of pisolites/ooids towards the top of cycles, and intraclasts and oncoids on the base of cycles), (4) subaerial exposure structures (brecciation, rip-up clasts, mud cracks, caliche formation) and (5) vertical shift of facies from thrombolite to digitate stromatolite to laminated stromatolite.

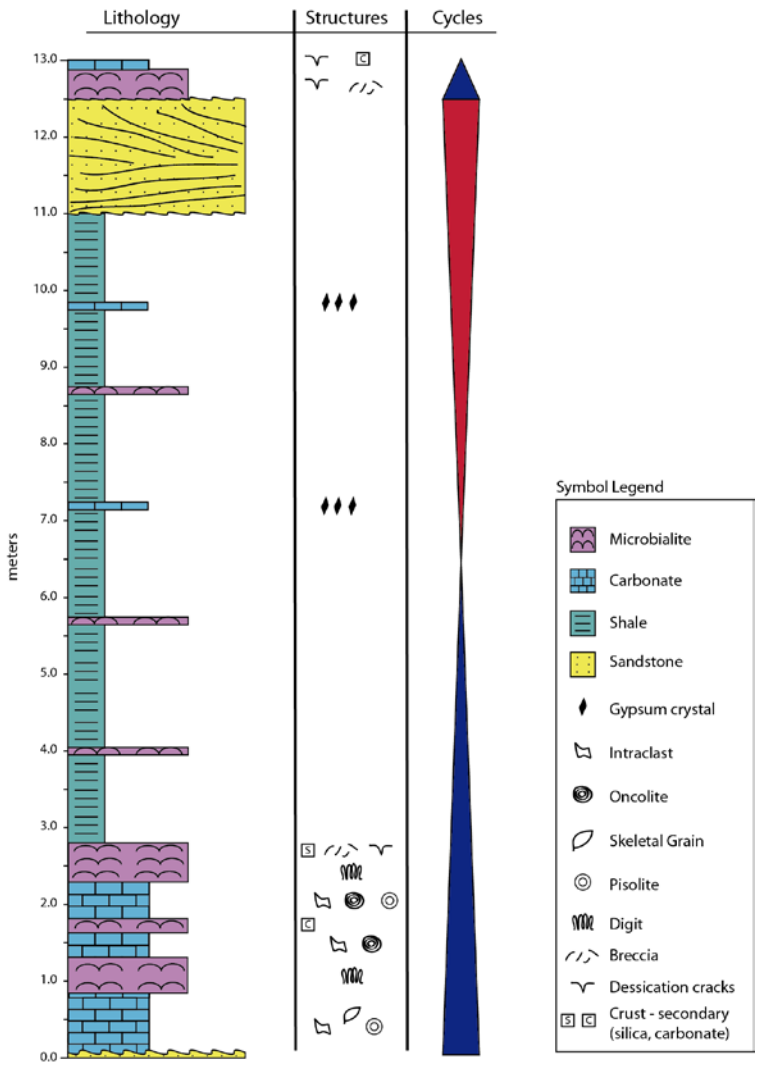

Figure III.3. Simplified stratigraphic section for units in the outcrop along Three Mile Canyon Road, showing lithology, sedimentary structures, grain types and the interpreted regressive-transgressive cycles. There are seven carbonate units interbedded with sandstone and shale deposits. The first unit is thicker and has a good lateral continuity of detrital and microbial carbonates throughout the outcrop. The passage from a transgressive period to the regressive periods was defined in the middle of a shale interval deposited before the first carbonate bed with gypsum crystal growth. It is based on the assumption that the maximum transgressive was reached at this stage and the lake water become more saturated in salts, favoring sulfate precipitation during rapid lake level falls, in a similar mechanism to the gypsum deposition in Dead Sea lakes proposed by Torfstein et al. (2008).

These shallow upward cycles formed during transgressive phases. In addition, changes in the proportion between microbialite and detrital carbonate, lateral changes in texture development and the relative lateral change in thickness in each cycle along the carbonate unit (figure III.6) indicate progradation of more proximal facies (detrital carbonate) on cycles 1 and 4 and retrogradation of more distal facies on cycles 2 and 3. Microbialites grew and spread toward proximal areas during transgressions, but the development of their textures were more expressive when the progradation of detrital carbonates was limited, as occurred during the cycles 2 and 3 (figure III.6). On top of each cycle there is evidence of subaerial exposure (figure III.5) and the microbialite textures are simpler (small textural components or planar stromatolite) and less porous. However during these periods microbialites still developed on proximal areas (except the lowest cycle that does not have microbialite, besides oncoids as grain component on detrital carbonates). This pattern indicates that at the end of shallowing upward cycles the sediments filled the accommodation space available for deposition, until the beginning of other transgression phase.

The table III.1 summarizes the framework components and characteristics of the main depositional textures in this carbonate unit. In terms of depositional texture, detrital carbonate is packstone and grainstone, with variable grain composition (e.g. intraclast, skeletal grains, insect egg, oncoid, pisoid and ooid) and microbialite units are stromatolite and thrombolite with differences in morphologic aspect (size and shape of framework components) and fabric. The frequency of each grain type in the detrital carbonate changes along the correlation diagram (figure III.6), but intraclasts are the

most common grains. Very fine, immature sand fills the pore space in grainstone deposited at the base of the lowest carbonate unit.

Microbial depositional textures, besides oncolite that is recognized as a carbonate grain, in this carbonate unit are thrombolite and stromatolite, which were differentiated by their fabrics. They were formed by peloid and carbonate crystalline precipitate that acted as building blocks, and minor amounts of trapped grains. Variable proportions and arrangements in these building blocks result in microfabric differences from peloidal shrubs, when the structure is formed mostly by peloids (figure III.7a) to mixed microfabric (figure III.7b) to crystal shrubs, when the structure is formed mostly by calcite crystals (figure III.7c). The mixed microfabric is dominant in the microbialite; the peloidal shrub microfabric occurs as layers in some stromatolite intervals or filling pores in thrombolites; and the crystal shrub only grew into the pore space as a diagenetic component.

The thrombolite texture (figures III.8a and III.8b) has branching and shrub fabrics without internal lamination and clotted aspect. Additionally, the arrangement of branches and shrubs is chaotic (figure III.8a) or irregularly layered (figure III.8b) with thin and small particles touching each other, forming an open framework that allows large pores without a clear orientation. This microfabric varies from peloid and crystalline mixed components to peloid layers linked by crystal bridges (figure III.8b). The size of branches and shrubs is variable, and a thrombolite layer may have a homogeneous particle size distribution or gradual changes in the particle size.

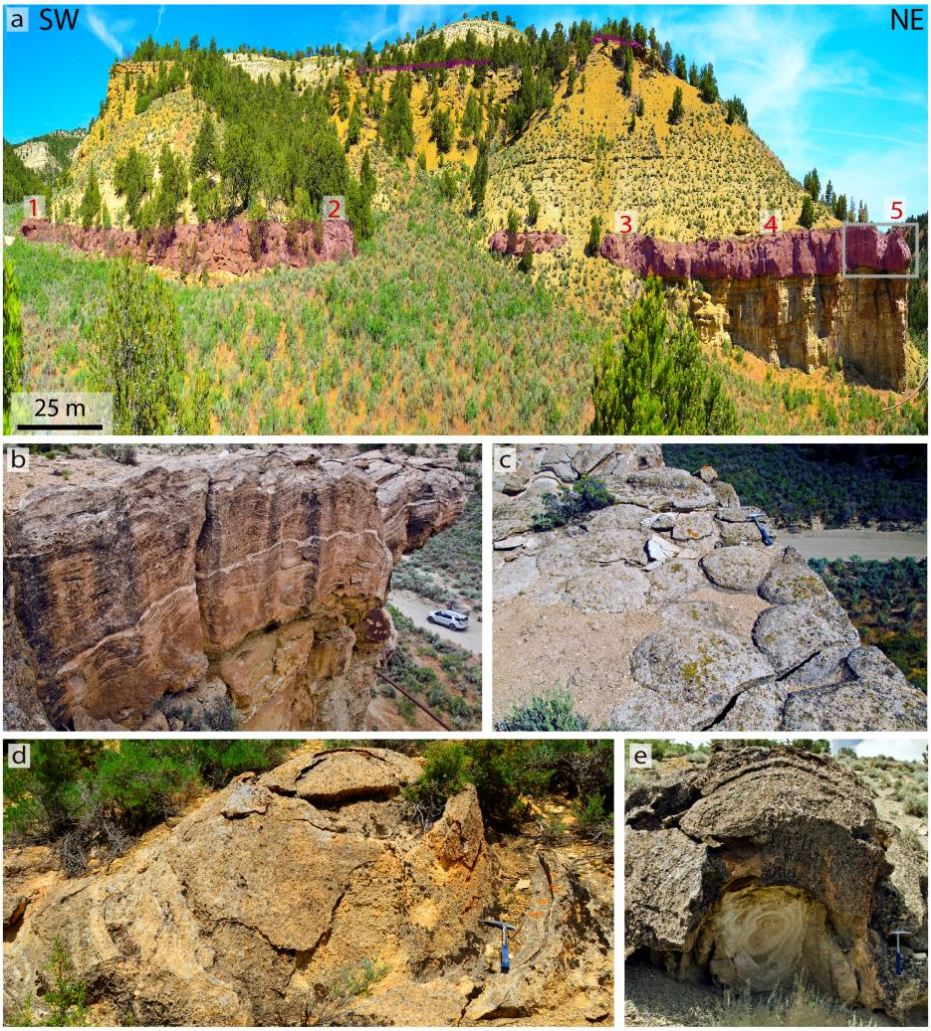

Figure III.4. Main microbialite external morphologies formed in this outcrop. (a) Panoramic image of the outcrop. The intervals highlighted in purple correspond to the microbialite build-ups and associated detrital carbonate deposits in the first carbonate unit. The numbers in red above the first interval are the location of the stratigraphic sections on the outcrop. The image has a 3x vertical exaggeration. (b) Laterally linked microbialite bioherms between the stratigraphic sections 4 and 5 (highlighted box on image (a). The white layer at the middle of the section is composed of intraclast packstone that represent a moment without microbialite growth. (c) Small microbialite heads formed on top of the section showed in the image b. They are coalesced in most areas, sometimes forming isolated depressions between them. (d) Meter-scale isolated microbialite head formed on top of the microbialite interval at section 1. Hammer for scale is 41 cm long. (e) Laterally linked microbialite at section 3. The center of this structure has thrombolite texture (light colors) and the outer layers formed a digitate stromatolite texture (dark colors). Hammer for scale is 41 cm long.

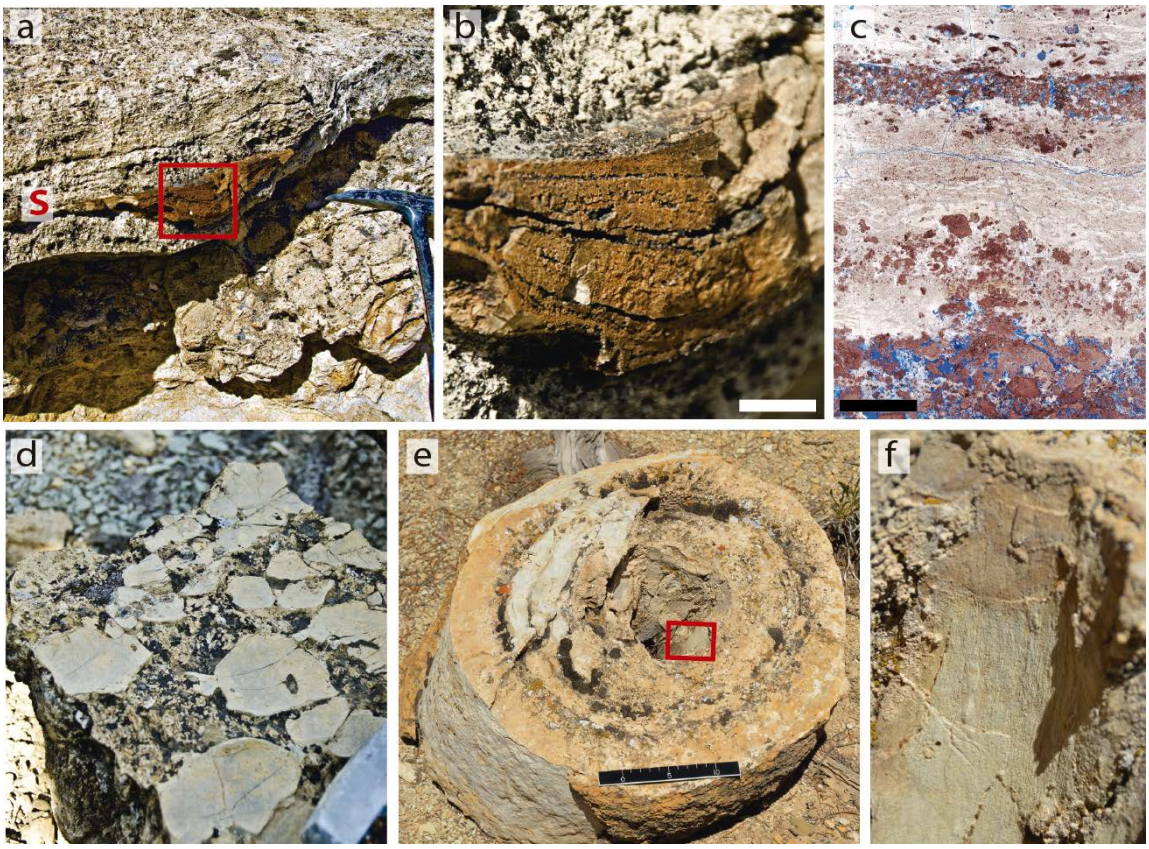

Figure III.5. Shallow-water and exposure sedimentary structures. (a) Caliche and partially silicified intraclast grainstone filling a small depression on the top of the lowest carbonate unit. The S on the image marks the silicified interval. (b) Close-up of the highlighted area in a. There is a noticeable stratification in this caliche/grainstone deposit. The cavities are grainstone layers more susceptible to dissolution and erosion. The bar on this image has a length of 1 cm. (c) Thin section image showing the caliche infiltration into the grainstone pore space and partial carbonate replacement by silica. The bar on this image has a length of 0.25 mm. (d) Intraclast chips of mudstone and desiccation cracks formed on the top of the first carbonate unit. (e) Tufa formed around a tree root on the top of the seventh carbonate unit. (f) Close-up image on the area highlighted in e, showing the root marks impressed on the carbonate surface.

Table III.1 Carbonate depositional textures, their framework components, fabric and pore system characteristics, in the Three Mile Canyon Road outcrop, Eocene Green River Formation.

Depositional Texture	**Framework Component**				**Fabric**	**Pore system**
	Type	*Shape*	*Size*	*Packing*		
Thrombolite	Shrubs	Complex	< 5 cm	Loose	Chaotic	Open, chaotic
	Branches	Complex	< 1 cm	Loose		
Stromatolite	Lamina	Simple	Not applicable	Tight	Horizontal	Tight, horizontal
	Digit	Simple	< 5 cm	Variable	Vertical	Open to tight; Vertical and horizontal
Grainstone	Grains	Variable	Variable	Variable	Chaotic	Open
Packstone	Grains Mud	Variable	Variable	Variable	Chaotic	Tight

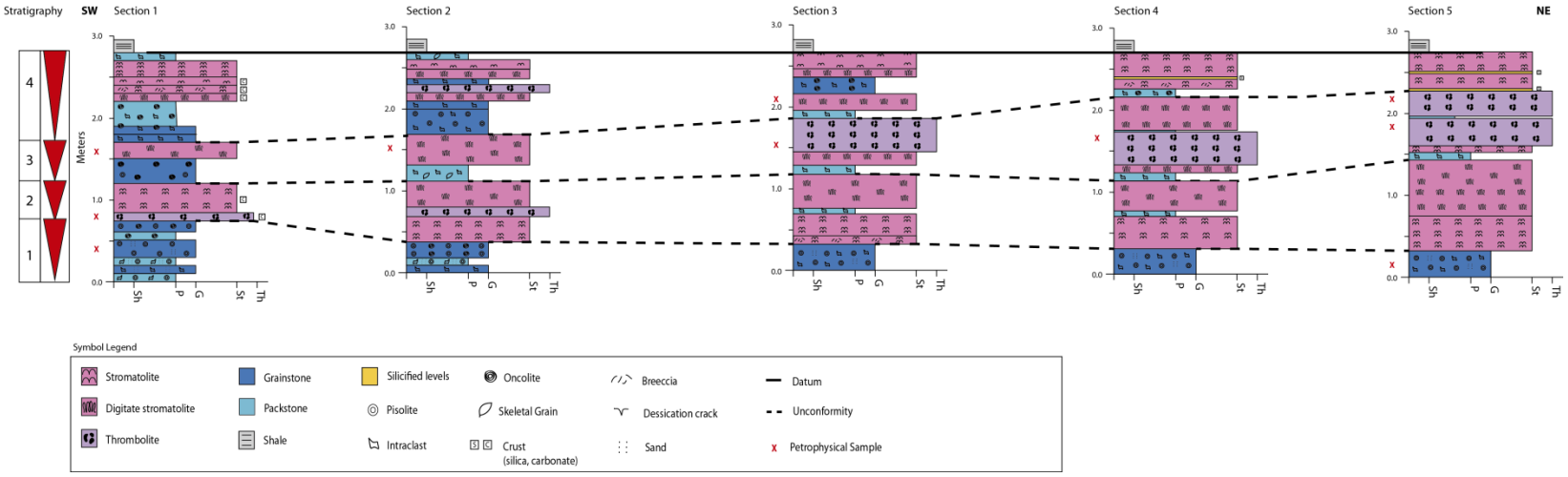

Figure III.6. Stratigraphic section for the first carbonate unit in this outcrop, showing the vertical and lateral distribution of facies, the depositional texture, grain and framework components and main unconformities. The microbialite and detrital carbonate intervals are laterally continuous, with internal and vertical changes in texture and petrophysical characteristics. Detrital carbonate deposits are more frequent at the area between sections 1 and 2, and microbialite deposits occur more often between the sections 3 and 5. The unconformities define the limits of different stratigraphic events. The texture scale of each section mnemonics are: Sh – shale, P – packstone, G – grainstone, St – stromatolite and Th – thrombolite.

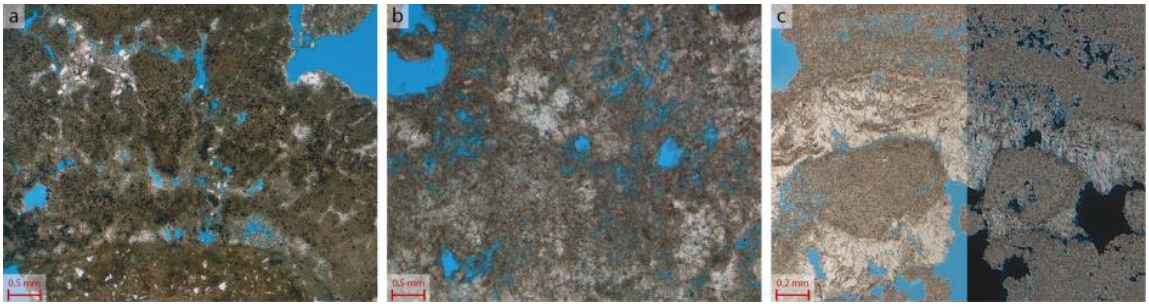

Figure III.7. Microbialite carbonate microfabrics. (a) Peloid and peloidal shrubs – structures formed by peloids. (b) Mixed microfabric with peloids, shrubs and crystalline carbonate precipitate. (c) Crystal shrubs – structures formed by calcite crystals (light color material filling the pore space on the image). This component was only identified in this unit as a diagenetic phase.

The stromatolite textures (figures III.8c and III.8d) dominant fabric is vertical digits (digitate) with internal laminations of peloid/mud, a crystalline phase and pore space, and variable height per width ratio. Planar fabric occurs with lower frequency, usually at the base or top of a microbialite interval. A more organized vertical framework forms a pore network that is mostly vertical, with horizontal connections occuring through thin layers in the digits. The digit packing in this texture also influences the pore system, with loose packing (figure III.8c) allowing larger pores, and tight packing reducing the pore space (figure III.8d).

The vertical transition between stromatolite and thrombolite layers is defined by sharp contacts. A thrombolite layer may form in the nuclei of a bioherm or continue laterally for a few meters. A thrombolite layer may gradually change into digitate stromatolite layers, which is the dominant microbial texture in this carbonate unit. The contact between microbialite and detrital carbonate is also sharp, but not erosive, where

thin planar stromatolite developed or the microbialite started to grow on top of a previous surface. Conversely, detrital grains usually fill the space between heads and digits in the stromatolite texture, and also fill cavities formed by erosion, desiccation and bioturbation of the bioherm surface.

Pore system characteristics of microbialites

In this Eocene microbialite carbonate build-up the primary porosity is well-preserved. Porous depositional textures are easily recognized and the relations between textural components (fabric and packing) and pore system are clear. Chaotic fabric and loose packing lead to well-developed pore systems (figures III.8a and III.8b), and organized fabric and tight packing lead to a closed pore system (figures III.8c and III.8d). Additionally, there is the effect of diagenetic dissolution on the enlargement of the primary pore system, as indicated by dissolved grains and moldic pores. However, these instances were few and this diagenetic effect secondary and had minimal effect on the development of the pore system in the microbialite carbonate.

Furthermore, the primary pore system was more affected by processes that reduced the pore space such as the pore filling by detrital sediment and the precipitation of diagenetic cements. Detrital sediment deposition (figures III.9a and III.9b), commonly fill the space between digitate textures (stromatolite more often), and also pores formed by erosive processes, reducing the pore space. The effects of diagenetic cements on the development of the final pore system are variable in terms of cementation intensity and number of cement phases. Most intervals have very little cementation, with cements only

partially filling the pore system. The temporal relationship between different cement phases was not detailed in this study.

The most important diagenetic component in volume and frequency is the formation of dolomite (figures III.9c, III.9d and III.9e), that replaced peloid and carbonate mud, and precipitated as crystals into pores. The second most important diagenetic event was the formation of crystal shrubs into pores and the pore filling with an organic material/clay mineral. These two phases occur as individual diagenetic phases very often, but sometimes they appear together (figure III.9f). Microcrystalline silica (figure III.9g) occurs in thrombolite textures, filling small pores and closing pore-throats of larger ones, but with minimal and localized effects on the pore system. Blocky calcite cement (figure III.9h) is common in grainstone beds and when present completely fills the available pore space.

Positive porosity versus permeability correlation trends (figure III.10) occur for both microbialite textures (stromatolite and thrombolite). These trends differ from the distribution observed for grainstone texture. The porosity varies from 17 to 30% in the microbialite textures and the permeability ranges from 3.75 md in digitate stromatolite texture to over 50000 md in the thrombolite texture. The well-developed pore system observed in thrombolite textures (figures III.8a and III.8b) result in higher permeability and porosity values than the values of the digitate stromatolite textures (figures III.8c and III.8d) that commonly have a tight pore system. Samples partially cemented or filled with detrital sediments have the lowest permeability and porosity values for each microbialite texture.

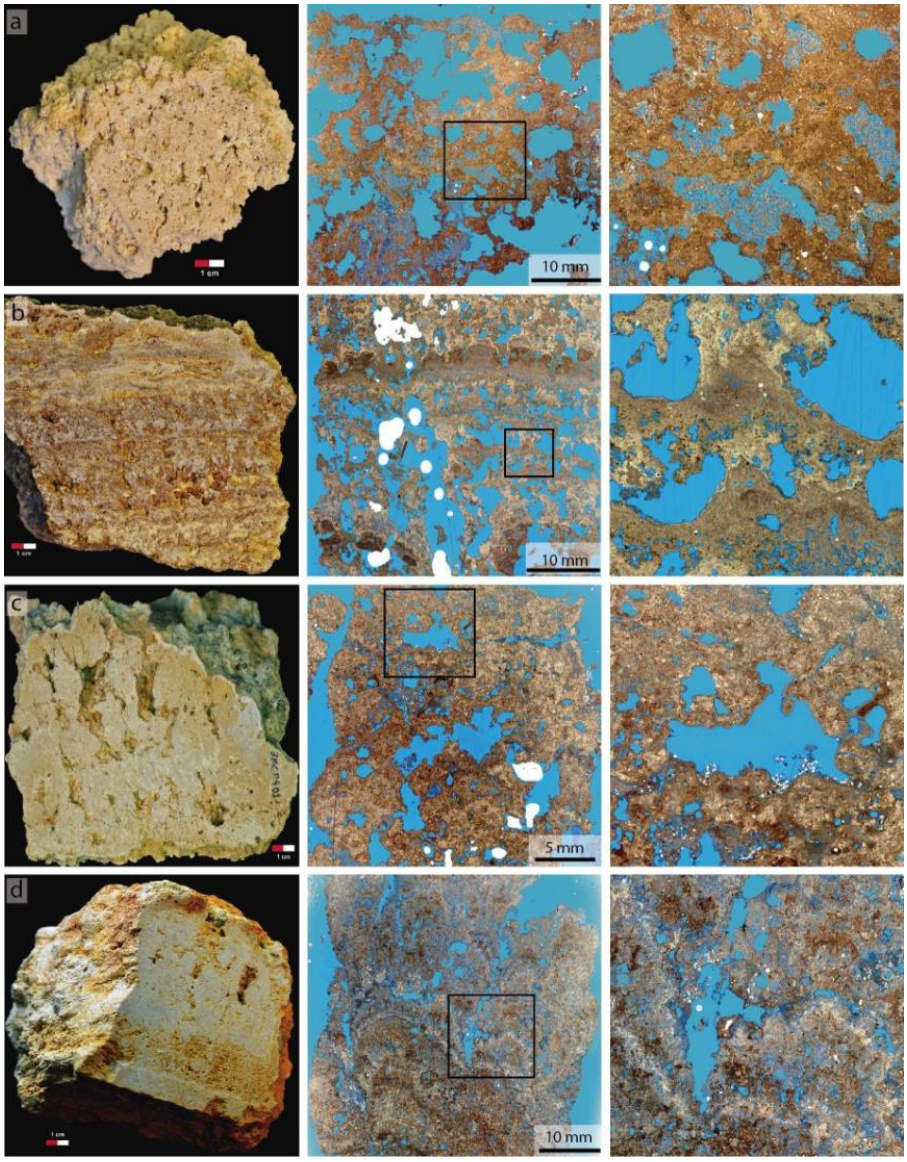

Figure III.8. Porous microbialite textures in the lowest carbonate unit. Each row is a separate texture. The images on left are hand samples, the middle images are high-resolution scans of thin sections, and the images on the right side close-ups on the areas marked by squares in the middle image. (a) Thrombolite texture formed by mixed peloid and crystalline carbonate, with chaotic shrub fabric and open pore system. (b) Thrombolite texture formed by peloid layers and crystalline carbonate bridges, with chaotic shrub and branches fabric and open pore system. (c) Digitate stromatolite texture formed by layers of mixed peloid and crystalline carbonate, with vertically oriented fabric, tight packing and a relatively open pore system. (d) Digitate stromatolite texture formed by layers of mixed peloid and crystalline carbonate, with vertically oriented fabric, tight packing and a closed pore system.

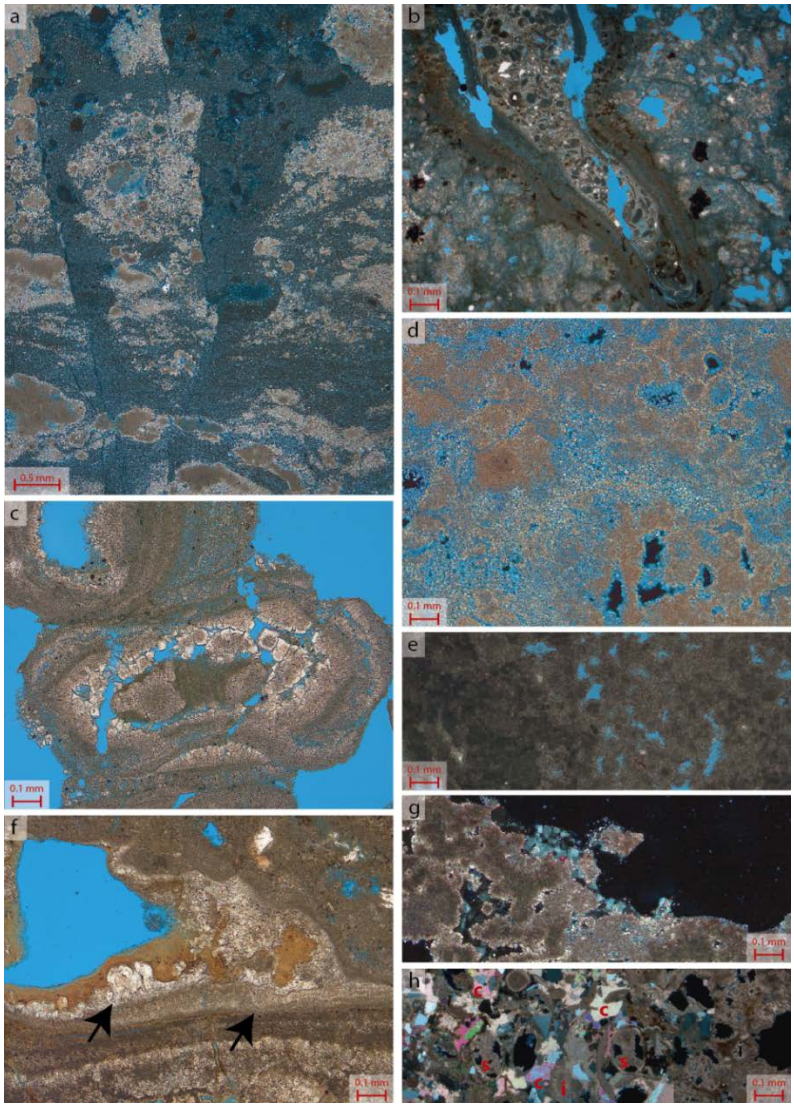

Figure III.9. Pore filling material and diagenetic cements. (a) Desiccation crack filled by detrital carbonate material partially replaced by silica (polarized light). (b) Bioturbation structure partially filled by intraclast skeletal grainstone (plane light) (c) Coarse dolomite with dirty nuclei formed in the dissolved pore space within an oncolite/pisolite grain (plane light). (d) Dolomite formed in pores between peloid shrubs and as replacement of carbonate mud (polarized light). (e) Dolomite formed around peloid and shrub filling the pore space between them (plane light). (f) Crystal shrubs (arrow) and amorphous material (greyish). They were precipitated around most part of the pore border (plane light) (g). Microcrystalline silica partially filling pores (polarized light). (h) Blocky calcite cement an intraclast, skeletal grainstone (polarized light). The components are labeled on the image as: c – cement, i – intraclast and s – skeletal grain

CT scan analysis (figure III.11) provided more detailed information on the relationships between the microbialite textures and their pore system. It is clear from the visual volume comparison that the pore system of thrombolite textures (figure III.11 – P3T and P5T) are more homogeneous and better connected than those formed in digitate stromatolite textures (figure III.11 – P1S and P2S) that have more isolated and vertically oriented pores. Additionally, the thrombolite texture has a higher number of larger pores per volume than the digit stromatolite texture, which has more than 80% of pores with radii less than to 0.25 mm (figure III.12). This difference explains the slightly higher porosity measured in thrombolite, with more space classified as pores as result of the open framework texture, when compared to the digitate stromatolite texture.

Another difference in the pore system of thrombolite and digit stromatolite textures is related to the number of pore throats (figure III.13). The digitate stromatolite texture pore system has a lesser amount of pores with 3 and 4 pore-throats, when compared to the thrombolite texture. Sample P3T has the higher number of connected pores with 3 and 4 pore-throats of all samples analyzed (figure III.13), which is also reflected in its exceptionally high permeability (50000 md) measured in this sample. The better pore connectivity of thrombolite textures also is characterized by higher values of connectivity density per volume in this texture than in the digitate stromatolite texture. This parameter has a strong positive correlation with permeability for the analyzed samples (figure III.14), indicating the strong control the microbial depositional texture has on its pore system.

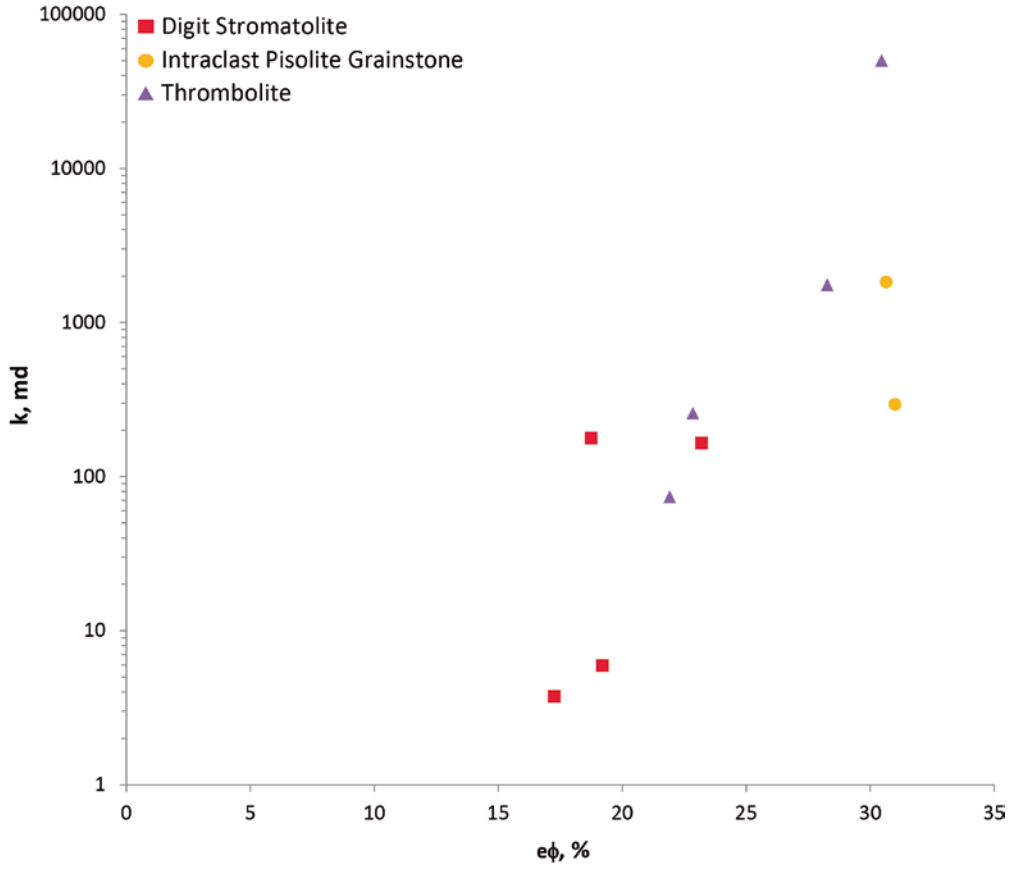

Figure III.10. Porosity versus permeability plot for the digitate stromatolite, thrombolite, and intraclast pisolite grainstone. The microbialite results show a positive correlation trend that is caused by changes in the pore system from closed to open as the texture packing becomes looser and the textures fabric more chaotic. The grainstone samples have a slight separation from the microbialite trend that could be caused by difference in the pore system between the detrital and microbialite carbonate.

Figure III.11. CT scans, rock/pore and pore system volumes. The rock components are showed as grey and white on the CT scans (left) and yellow and orange on the rock/pore volumes (center). White and orange colors represent denser material or with areas with less microporosity. The pores are represented in black on the CT scans and blue on the rendered volumes (right side). The red polygons on the CT images mark the limits of the volumes shown. The first two samples have thrombolite texture and the other two have digitate stromatolite texture. The thrombolite samples have a much higher pore volume when compared to the digitate stromatolite samples. The pore system connectivity is also better in the thrombolite samples than in the digit stromatolite samples. However, there are differences between samples with similar texture, as visible on the pore system volumes between samples P3T and P5T, and P1S and P2S. Sample P3T has the best pore system of all samples analyzed by CT, with a high proportion of well-connected pores. These characteristics result in very high permeability values for this sample (50000 darcys). Conversely, the pore system of sample P2S has more isolated pores that result in the lowest permeability values measured in these samples (3.75 millidarcys). The mnemonic of each sample indicates the section number (P1, P2, P3, P4 or P5) and its dominant depositional texture (T for thrombolite and S for digitate stromatolite).

Figure III.11. Continued.

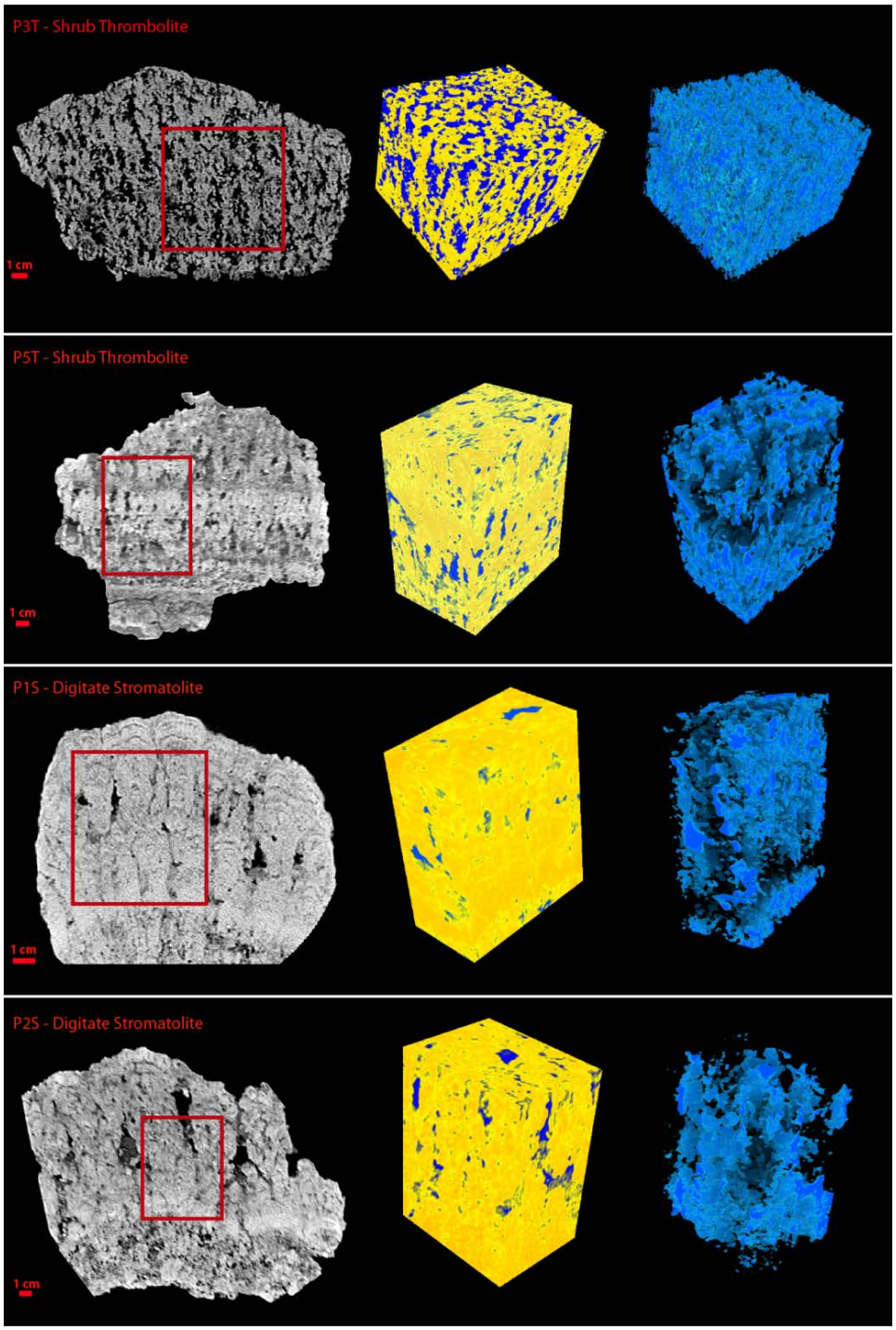

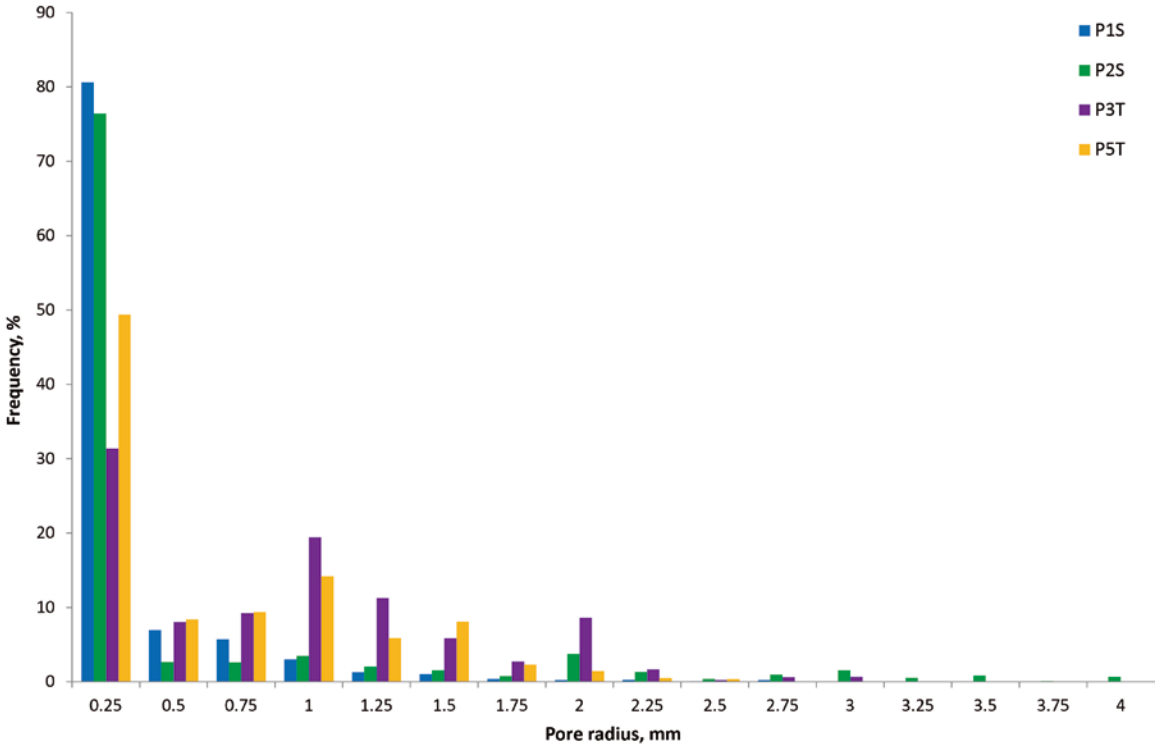

Figure III.12. Pore size distribution determined by CT image analysis for the samples P1S, P2S, P3T and P5T. The thrombolite samples have a higher frequency of large pores when compared with the digitate stromatolite samples, which are dominated by small pores. Pores sizes below 0.25 mm were below the CT equipment resolution. The mnemonic of each sample indicates the section number (P1, P2, P3 or P5) and its dominant depositional texture (T for thrombolite and S for digitate stromatolite).

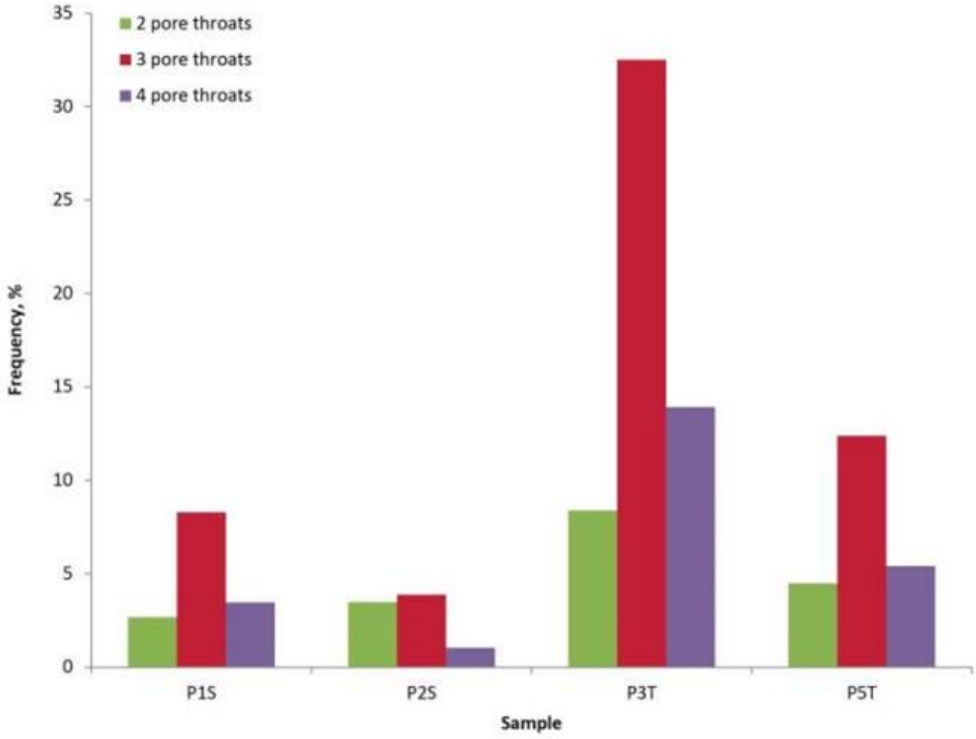

Figure III.13. Distribution of pores with 2, 3, and 4 pore-throats for the samples P1S, P2S, P3T and P5T. The samples with thrombolite texture have a higher number of connected pores, often connected by 3 and 4 pore-throats, in comparison to the samples with digitate stromatolite texture. The sample P3T has the higher number of connected pores, with 3 and 4 pore- throats of all samples analyzed, which helps to explain its very high permeability. The mnemonic of each sample indicates the section number (P1, P2, P3 or P5) and its dominant depositional texture (T for thrombolite and S for digitate stromatolite).

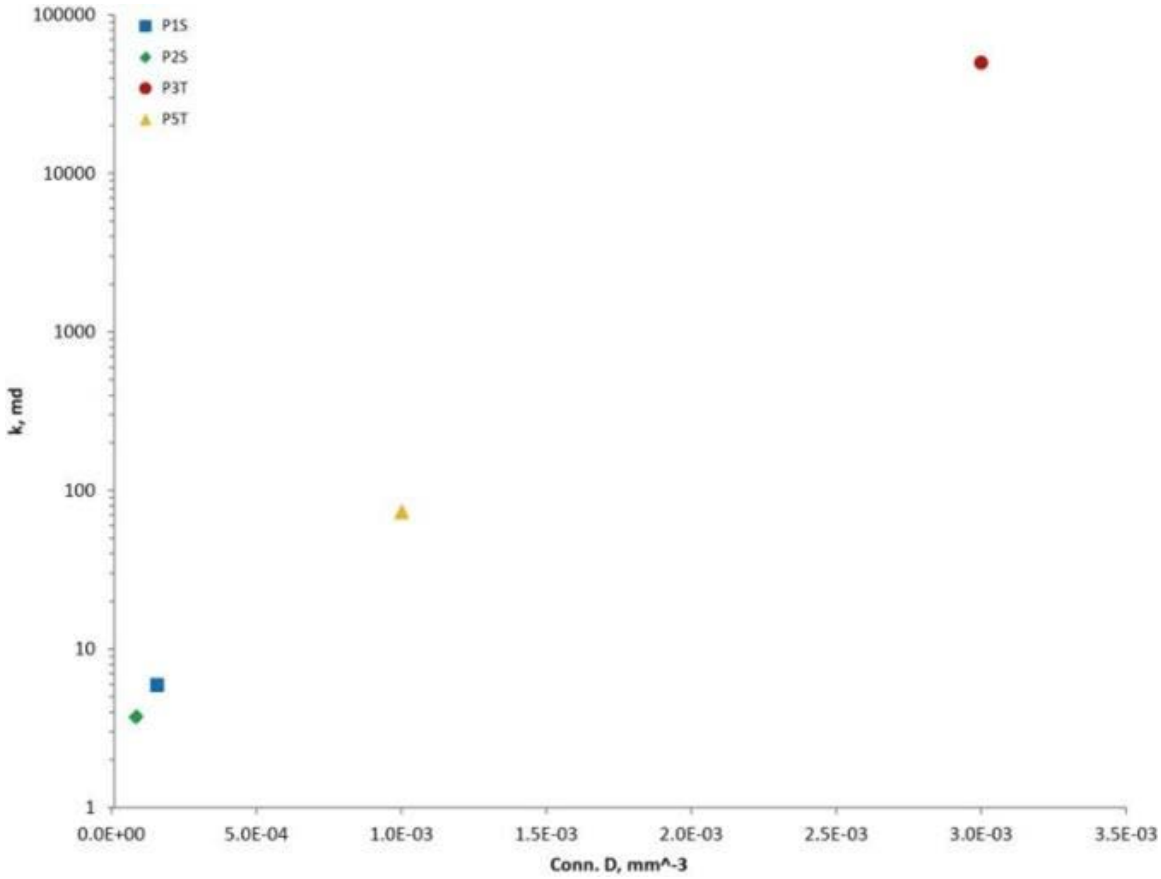

Figure III.14. Connectivity density per volume (Conn. D) versus permeability plot for the samples P1S, P2S, P3T and P5T, showing a strong positive correlation between the sample pore system connectivity and the permeability measured in plugs. The mnemonic of each sample indicates the section number (P1, P2, P3 or P5) and its dominant depositional texture (T for thrombolite and S for digitate stromatolite).

Discussion

Texture controls on pore system in the Eocene Green River Formation microbialites

Two microbial depositional textures (stromatolite and thrombolite) are identified in terms of sedimentary characteristics, morphometric aspects and pore space attributes in the Eocene Green River Formation. The relationship between texture and pore system that produces petrophysical differences are clear in the microbial carbonate (figures III.10, III.11, III.12, III.13 and III.14). The data suggest a strong depositional control on the development of the pore system and petrophysical properties expressed in terms of rock texture, fabric and environmental position.

The thrombolite texture has an open framework and a pore system formed by a chaotic organization of shrubs and branches (figures III.7a, III.7b and III.11) composed of peloid, carbonate mud and a crystalline carbonate phase. These characteristics result in better porosity and permeability (figure III.10), because it has a higher number of large pores and better connectivity (figures III.12, III.13 and III.14). Commonly, this pore system is free of detrital sediment in pores and it has low diagenetic cement content; the porosity is mostly primary, with localized secondary porosity formed by dissolution.

In contrast, the digitate stromatolite texture usually has a tighter framework and a pore system produced by a more organized microbial growth/carbonate precipitation fabric (figures III.7c and III.7d). The pore system in the digitate stromatolite texture (figures III.7c, III.7d and III.11) is characterized by small pores (submillimetre scale) and horizontal pores formed between each stromatolitic lamina and large vertical pores

(centimetre scale) formed between digits. However, the lamina related pore space is tight and the interdigit space commonly is filled with detrital sediments (figures III.9a, III.9b and III.11).

Reservoir quality lateral continuity in the Eocene Green River Formation microbialites

There is a high lateral continuity of microbialite deposits and depositional textures in this carbonate unit of the Eocene Green River Formation (figure III.6). The thicker intervals of both detrital and microbialite carbonate are continuous across tens of meters with minor changes in texture and fabric. The reservoir quality is similarly continuous, because it is linked to the dominant texture of a specific interval, however external factors such as a higher proportion of detrital sediments (e.g. intraclast packstone) as occurred between sections 3 and 4 (figure III.6), or diagenetic reduction of pore space, may reduce the expected reservoir quality of a specific interval.

Figure III.15 summarizes the main changes in reservoir quality in accordance to lateral shifts in facies and depositional textures along the studied carbonate unit. These interpretations are based on petrophysical measurements and petrographic porosity quantification of thin sections and visual estimates of textures on the outcrop. It is noticeable that the best microbialite texture in terms of open texture and reservoir quality formed during transgressions, when the microbialites had more space available for growth and less detrital sediments. During regressive periods, the detrital sediment influx was higher, therefore the thickness of the microbialite intervals was reduced and the microbialite texture was less developed and has a tighter pore system, resulting in worse reservoir quality.

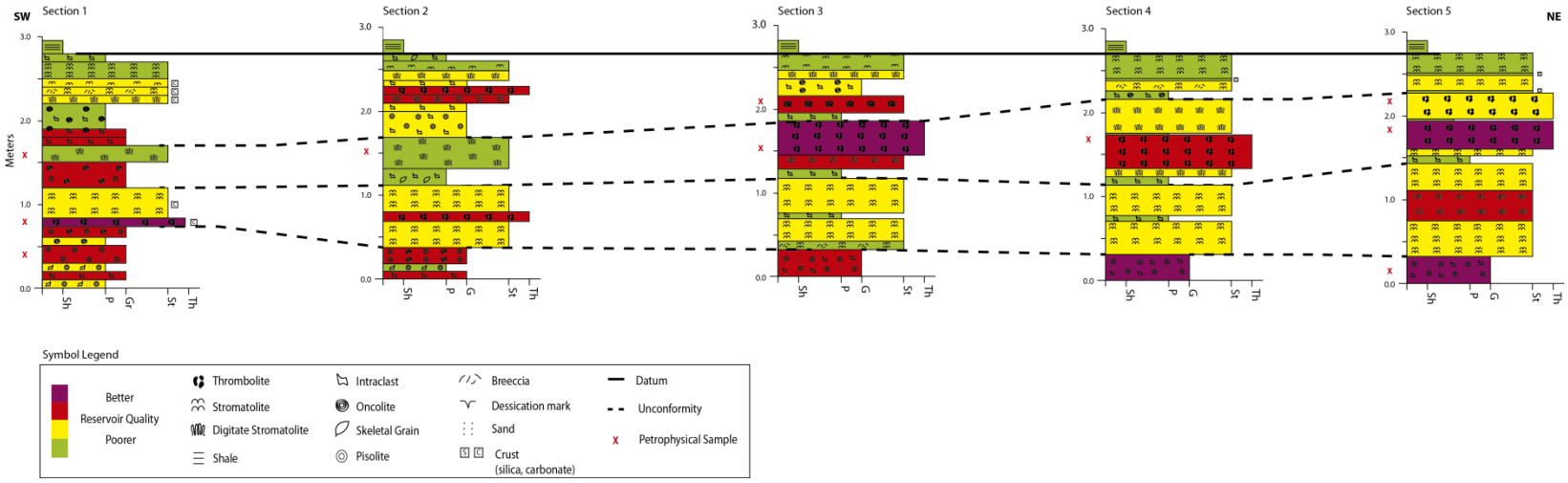

Figure III.15. Stratigraphic section of the first carbonate unit interpreted in terms of reservoir quality. Purple and red colors represent better reservoir intervals and green and yellow colors indicate poor reservoir intervals, considering the following permeability range: green < 10 md; yellow <100 md; red <1000 md and purple >1000 md. Intervals sampled for petrophysical analysis are marked with an x to the left of each measured section. All other intervals were classified based on the interpretation of thin sections, field descriptions and comparison to similar samples with petrophysical measurements and their textural characteristics. There is good lateral continuity in relation to the reservoir quality in this unit, since the texture controls the pore system and its porosity and permeability are well-defined for these microbialite deposits in the Eocene Green River Formation. The intervals with better reservoir quality are associated with thrombolite texture or digit stromatolite with open packing and low pore filing by detrital sediments. They occur more often on locations where the microbialite development was favored, and form layers that can be laterally correlated in terms of depositional characteristics and reservoir quality. The texture scale of each section mnemonics are: Sh – shale, P – packstone, G – grainstone, St – stromatolite and Th – thrombolite.

The thrombolite texture usually forms layers or nuclei of microbialite heads that change laterally to a digitate stromatolite texture, resulting in patches of excellent reservoir quality engulfed in intervals of good to moderate porosity and permeability (figure III.15 – sections 2, 4 and 5). The reservoir quality in the digit stromatolite texture is driven by its fabric characteristics. The digitate stromatolite texture with its loose packing results in intervals with better reservoir quality, whereas a tight packing in this texture worsens the reservoir quality. This texture is laterally continuous as result of coalesced microbialite bioherms. Despite the occurrence of diagenetic cements and pore filling by detrital sediments, the reservoir quality in this texture is also continuous, varying in accordance to changes in fabric and morphometric parameters such as digit size. The interbedding with detrital carbonate also reduces the reservoir quality in the digitate stromatolite texture, mostly because sediment fills available pores and reduces the connectivity of microbialite textures in these intervals (figure III.15 – sections 1, 2, 3 and 4).

Applicability of data to production

The results show that for this microbialite build-up in the Eocene Green River Formation the controls on porosity and permeability are strongly related to the depositional texture, fabric and the characteristics of the primary pore system. The thrombolite texture with its open pore system has excellent reservoir quality, but tighter textures, such as digitate stromatolite texture filled with detrital sediments, have poorer reservoir quality. Reservoir models for other microbialite deposits can be improved using similar constraints after the relationship between the depositional textures in

microbialites, pore system characteristics and their effects on porosity and permeability are defined.

This study also shows that the facies distribution in microbialite build-ups may be continuous across ten of meters with moderate changes in pore system characteristics and reservoir quality. The recognition of lateral continuity of both facies and reservoir quality in microbialite carbonate deposits demonstrates that it is possible to correlate intervals with similar depositional texture and petrophysical properties at a reservoir scale. Another important result is the association between depositional textures, reservoir quality and stratigraphy. In this Green River Formation microbialite, textures with well-developed pore system and better petrophysical properties formed during transgressions events, when the conditions for microbialite growth were enhanced.

Microbialites have highly variable depositional textures, fabrics, diagenesis, and pore systems characteristics between different deposits. The results of this study provide insights of the applicability of a pore system genetic characterization in microbialite reservoirs. However, they do not cover all microbialite textures, fabrics and diagenetic modifications already detailed on previous works (Parcell et al, 2002; Bohacs et al, 2013; Seard et al, 2013; Tonietto and Pope, 2013; Rezende and Pope, 2015). Therefore, to obtain a more robust and widespread understanding, other microbialite deposits must be fully analyzed in terms of their textures, pore systems and petrophysical properties.

Conclusions

Microbialite carbonate build-ups in the Eocene Green River Formation can have very high porosity and permeability values that result from open pore systems controlled by their depositional textures and fabric characteristics. The porosity in the microbialite is dominantly primary, locally reduced by diagenetic cements and enlarged by subsequent dissolution. The thrombolite texture in the studied carbonate unit has a more open pore system and better permeability when compared to the dominant digitate stromatolite texture. However, microbial textures with very low permeability also occur, usually related to tight pore systems formed in digitate stromatolite texture with organized fabric, tight packing and pore space reduced by sediment infiltration.

The thickness and textural characteristics of the microbialite intervals in this carbonate build-up are stratigraphically controlled. Microbialites grew and spread toward proximal areas during transgressions, but the development of their textures were more expressive when detrital carbonate was limited. Shallow-water and exposure structures and the change from digitate stromatolite to planar stromatolite textures on the top of microbialite layers at the end of each cycle suggest shallowing-upward deposition pattern. This information adds a predictive genetic character to the evaluation and reservoir modelling of microbialite reservoirs, positioning the intervals with better reservoir characteristics during transgressive phases.

The microbialite and detrital carbonate textures and their reservoir quality have good lateral continuity in this carbonate build-up. Some microbialite intervals are continuous across tens of meters and were mapped in five stratigraphic sections.

However, the thrombolite texture, which has the better permeability values, occurs only when the microbialite growth was favored. Therefore it is a more localized texture than the stromatolite texture that occur more often and are more continuous throughout the outcrop. These observations indicate that microbialite intervals can be correlated at the reservoir scale, in terms of depositional and petrophysical characteristics, but their characteristics may vary laterally due to changes in textures from stromatolite to thrombolite and vice versa.

REFERENCES

Ahr, W. M., 1973, The carbonate ramp: an alternative to the shelf model: Gulf Coast Association of Geological Societies Transactions, v. 23, p. 221-225.

Ahr, W. M., 2008, Geology of Carbonate Reservoirs, John Wiley & Sons, Inc., 277 p.

Akin, S., and A. R. Kovscek, 2003, Computed tomography in petroleum engineering research, *in* F. Mees, R. Swennen, M. Van Geet, and P. Jacobs, eds., Applications of X-ray computed tomography in the geosciences: Geological Society, London, Special Publications, v. 215, p. 23-28.

Al-Kharusi, A. S., and M. J. Blunt, 2008, Multiphase flow predictions from carbonate pore space images using extracted network models: Water Resources Research, v. 44. doi: 10.1029/2006wr005695

Alonso-Zarza, A. M., and L. H. Tanner, 2010, Carbonates in continental settings : facies, environments, and processes: Developments in sedimentology: Amsterdam ; London, Elsevier, 378 p.

Anselmetti, F. S., S. Luthi, and G. P. Eberli, 1998, Quantitative characterization of carbonate pore systems by digital image analysis: AAPG Bulletin, v. 82, p. 1815-1836.

Arai, M., 2009, South Atlantic Aptian paleogeography: a new model based on recent Brazilian micropaleontological data: Boletim de Geociências da Petrobras, v. 17, p. 331-351.

Araújo, C. C., P. A. Moretti Júnior, V. Madrucci, N. G. Carramal, A. Toczeck, and Â. B. Almeida, 2009, Aptian Carbonates of Carmopolis Field, Sergipe-Alagoas Basin: stratigraphy and depositional model: Boletim de Geociências da Petrobras, v. 17, p. 311-330.

Ashbridge, D. A., M. S. Thorne, M. L. Rivers, J. C. Muccino, and P. A. O'Day, 2003, Image optimization and analysis of synchrotron X-ray computed microtomography (C mu T) data: Computers & Geosciences, v. 29, p. 823-836. doi: 10.1016/S0098-3004(03)00081-5

Awramik, S. M., and P. H. Buchheim, 2012, The Quest for Microbialite Analogs to the South Atlantic Pre-Salt Carbonate Hydrocarbon Reservoirs of Africa and South America: Houston Geological Society Bulletin, v. 55, p. 21-25.

Baria, L. R., D. L. Stoudt, P. M. Harris, and P. D. Crevello, 1982, Upper Jurassic reefs of Smackover Formation, United States Gulf Coast: AAPG Bulletin, v. 66, p. 1449-1482.

Basan, P. B., B. D. Lowden, P. R. Whattler, and J. J. Attard, 1997, Pore-size data in petrophysics: a perspective on the measurement of pore geometry: Geological Society, London, Special Publications, v. 122, p. 47-67. doi: 10.1144/gsl.sp.1997.122.01.05

Beck, R. A., C. F. Vondra, J. E. Filkins, and J. D. Olander, 1988, Syntectonic sedimentation and Laramide basement thrusting, Cordilleran foreland; Timing of deformation, *in* C. J. Schmidt, and W. J. Perry Jr., eds., Interaction of the Rocky Mountain foreland and the Cordilleran thrust belt: Geological Sociey of America Memor, Geological Sociey of America, p. 465-488. doi: 10.1130/MEM171-p465

Beglinger, S. E., H. Doust, and S. Cloetingh, 2012, Relating petroleum system and play development to basin evolution: Brazilian South Atlantic margin: Petroleum Geoscience, v. 18, p. 315-336. doi: 10.1144/1354-079311-022

Bohacs, K., A. R. Carroll, J. E. Nede, and P. J. Mankirowicz, 2000, Lake-Basin Type, Source Potential, and Hydrocarbon Character: An Integrated Sequence-Stratigraphic-Geochemical Framework, *in* E. H. Gierlowski-Kordesch, and K. R. Kelts, eds., Lake Basins Through Space and Time: AAPG Studies in Geology, v. 46: Tulsa, American Association of Petroleum Geologists, p. 3-32.

Bohacs, K. M., K. Lamb-Wozniak, T. M. Demko, J. Eleson, O. McLaughlin, C. Lash, D. M. Cleveland, and S. Kaczmarek, 2013, Vertical and lateral distribution of lacustrine carbonate lithofacies at the parasequence scale in the Miocene Hot Spring limestone, Idaho: An analog addressing reservoir presence and quality: AAPG Bulletin, v. 97, p. 1967–1995. doi: 10.1306/07081312192

Bowers, M. C., R. Ehrlich, J. J. Howard, and W. E. Kenyon, 1995, Determination of Porosity Types from Nmr Data and Their Relationship to Porosity Types Derived from Thin-Section: Journal of Petroleum Science and Engineering, v. 13, p. 1-14.

Boyer, B. W., 1982, Green River laminites: Does the playa-lake model really invalidate the stratified-lake model?: Geology, v. 10, p. 321-324.

Bradley, W. H., 1964, Geology of the Green River and associated Eocene rocks in southwestern Wyoming and adjacent parts of Colorado and Utah, Professional Paper, United States Geological Survey, p. 86.

Bueno, G., 2004, Event diachronism in the South Atlantic rift: Boletim de Geociências da Petrobras, v. 12, p. 203-229.

Burne, R. V., and L. S. Moore, 1987, Microbialites: Organosedimentary Deposits of Benthic Microbial Communities: Palaios, v. 2, p. 241-254. doi: 10.2307/3514674

Campos Neto, O. P. d. A., W. S. Lima, and F. E. G. Cruz, 2007, Sergipe-Alagoas Basin: Boletim de Geociências da Petrobras, v. 15, p. 405-415.

Čapek, P., V. Hejtmánek, L. Brabec, A. Zikánová, and M. Kočiřík, 2009, Stochastic Reconstruction of Particulate Media Using Simulated Annealing: Improving Pore Connectivity: Transport in Porous Media, v. 76, p. 179-198. doi: 10.1007/s11242-008-9242-8

Carroll, A. R., and K. M. Bohacs, 1999, Stratigraphic classification of ancient lakes: Balancing tectonic and climatic controls: Geology, v. 27, p. 99-102.

Chafetz, H. S., 2013, Porosity in bacterially induced carbonates: Focus on micropores: AAPG Bulletin, v. 97, p. 2103-2111. doi: 10.1306/04231312173

Chafetz, H. S., and S. A. Guidry, 1999, Bacterial shrubs, crystal shrubs, and ray-crystal shrubs: bacterial vs. abiotic precipitation: Sedimentary Geology, v. 126, p. 57-74. doi: 10.1016/S0037-0738(99)00032-9

Choquette, P. W., and L. C. Pray, 1970, Geologic Nomenclature and Classification of Porosity in Sedimentary Carbonates: AAPG Bulletin, v. 54, p. 207-250.

Coimbra, M. M., C. G. Silva, C. F. Barbosa, and K. A. Mueller, 2000, Radiocarbon measurements of stromatolite heads and crusts at the Salgada Lagoon, Rio de Janeiro State, Brazil: Nuclear Instruments & Methods in Physics Research Section B-Beam Interactions with Materials and Atoms, v. 172, p. 592-596.

Conrad, R., M. Noll, P. Claus, M. Klose, W. R. Bastos, and A. Enrich-Prast, 2011, Stable carbon isotope discrimination and microbiology of methane formation in tropical anoxic lake sediments: Biogeosciences, v. 8, p. 795-814. doi: 10.5194/bg-8-795-2011

Corbett, P., F. Y. Hayashi, M. S. Alves, Z. Jiang, H. Wang, V. Demyanov, A. Machado, L. Borghi, and N. Srivastava, 2015, Microbial carbonates: a sampling and measurement challenge for petrophysics addressed by capturing the bioarchitectural components: Geological Society, London, Special Publications, v. 418. First published online February 26, 2015. doi: 10.1144/sp418.9

Desborough, G. A., 1978, A biogenic-chemical stratified lake model for the origin of oil shale of the Green River Formation: An alternative to the playa-lake model: Geological Society of America Bulletin, v. 89, p. 961-971. doi: 10.1130/0016-7606(1978)89<961:abslmf>2.0.co;2

Dias, G. T. M., 1981, Complexo deltaico do Rio Paraíba do Sul: Simpósio sobre o Quaternário do Brasil, p. 58-79.

Dias, G. T. M., and B. Kjerfve, 2009, Barriers and beach ridge systems of the Rio de Janeiro Coast, *in* S. Dillemburg, and P. Hesp, eds., Geology and geomorphology of Holocene coastal barriers of Brazil: Lectures notes in earth sciences: Berlin, Springer, p. 225-252.

Dias, J. L., 2005, Tectônica, estratigrafia e sedimentação no Andar Aptiano da margem leste brasileira: Boletim de Geociências da Petrobras, v. 13, p. 7-25.

Dickinson, W. R., M. A. Klute, M. J. Hayes, S. U. Janecke, E. R. Lundin, M. A. McKittrick, and M. D. Olivares, 1988, Paleogeographic and paleotectonic setting of Laramide sedimentary basins in the central Rocky Mountain region Geological Society of America Bulletin, v. 100, p. 1023-1039. doi: 10.1130/0016-7606(1988)100<1023:PAPSOL>2.3.CO;2

Dominguez, J. M. L., 2009, The coastal zone of Brazil, *in* S. Dillemburg, and P. Hesp, eds., Geology and geomorphology of Holocene coastal barriers of Brazil: Lectures notes in earth sciences: Berlin, Springer, p. 17-30.

Doube, M., M. M. Kłosowski, I. Arganda-Carreras, F. Cordeliéres, R. P. Dougherty, J. Jackson, B. Schmid, J. R. Hutchinson, and S. J. Shefelbine, 2010, BoneJ: free and extensible bone image analysis in ImageJ: Bone, v. 47, p. 1076-1079. doi: 10.1016/j.bone.2010.08.023

Dupraz, C., R. Pattisina, and E. P. Verrecchia, 2006, Translation of energy into morphology: Simulation of stromatolite morphospace using a stochastic model: Sedimentary Geology, v. 185, p. 185-203. doi: 10.1016/j.sedgeo.2005.12.012

Dupraz, C., R. P. Reid, O. Braissant, A. W. Decho, R. S. Norman, and P. T. Visscher, 2009, Processes of carbonate precipitation in modern microbial mats: Earth-Science Reviews, v. 96, p. 141-162. doi: DOI 10.1016/j.earscirev.2008.10.005

Dürrast, H., and S. Siegesmund, 1999, Correlation between rock fabrics and physical properties of carbonate reservoir rocks: International Journal of Earth Sciences, v. 88, p. 392-408. doi: 10.1007/s005310050274

Ehrlich, R., S. J. Crabtree, K. O. Horkowitz, and J. P. Horkowitz, 1991, Petrography and Reservoir Physics I: Objective Classification of Reservoir Porosity (1): AAPG Bulletin, v. 75, p. 1547-1562.

Fitch, P. J. R., M. A. Lovell, S. J. Davies, T. Pritchard, and P. K. Harvey, 2015, An integrated and quantitative approach to petrophysical heterogeneity: Marine and Petroleum Geology, v. 63, p. 82-96. doi: 10.1016/j.marpetgeo.2015.02.014

França, R. L., A. C. Del Rey, C. V. Tagliari, J. R. Brandão, and P. d. R. Fontanelli, 2007, Espírito Santo Basin: Boletim de Geociências da Petrobras, v. 15, p. 501-509.

Frantz, C. M., V. A. Petryshyn, P. J. Marenco, A. Tripati, W. M. Berelson, and F. A. Corsetti, 2014, Dramatic local environmental change during the Early Eocene Climatic Optimum detected using high resolution chemical analyses of Green River Formation stromatolites: Palaeogeography, Palaeoclimatology, Palaeoecology, v. 405, p. 1-15. doi: 10.1016/j.palaeo.2014.04.001

Glemser, C. T., 2007, Petrophysical and geochemical characterization of Midale Carbonates from the Weyburn Oilfield using synchrotron X-ray computed microtomography: Thesis (Master) thesis, University of Saskatchewan, Saskatoon, 103 p.

Gomes, P. O., B. Kilsdonk, T. Grow, J. Minken, and R. Baarragan, 2013, Tectonic evolution of the outer high of Santos basin, southern Sao Paulo Plateau, Brazil, and implications for hydrocarbon exploration, *in* D. Gao, ed., Tectonics and Sedimentation: Implications for Petroleum Systems: Memoirs, v. 100: Tulsa, OK, American Association of Petroleum Geologists, p. 125-142.

Grochau, M. H., E. Campos, D. Nadri, T. M. Müller, B. Clennell, and B. Gurevich, 2010, Sedimentary cyclicity from X-ray CT images in Campos Basin, offshore Brazil: The Leading Edge, v. 29, p. 808-813. doi: 10.1190/1.3462783

Harris, P. M. M., J. Ellis, and S. J. Purkis, 2013, Assessing the extent of carbonate deposition in early rift settings: AAPG Bulletin, v. 97, p. 27-60.

Hidajat, I., K. K. Mohanty, M. Flaum, and G. Hirasaki, 2004, Study of Vuggy Carbonates Using NMR and X-Ray CT Scanning: SPE Reservoir Evaluation & Engineering, v. 7, p. 365-377. doi: 10.2118/88995-pa

Hofmann, H. J., 1976, Chapter 2.5 Stromatoid Morphometrics, *in* M. R. Walter, ed., Developments in Sedimentology, v. Volume 20, Elsevier, p. 45-54. doi: 10.1016/S0070-4571(08)71128-2

Iespa, A. A. C., C. M. Damazio-Iespa, and L. B. F. Almeida, 2008, Microestratigrafia do Complexo Estromatólito, Trombólito e Oncoide Holocênico da Lagoa Salgada, Estado do Rio de Janeiro, Brasil: Revista de Geologia - Universidade Federal do Ceará, v. 22, p. 7-14.

Keighley, D., S. Flint, J. Howell, and A. Moscariello, 2003, Sequence Stratigraphy in Lacustrine Basins: A Model for part of the Green River Formation (Eocene), Southwest Uinta Basin, Utah, U.S.A.: Journal of Sedimentary Research, v. 73, p. 987-1006.

Kelts, K., and M. Talbot, 1990, Lacustrine Carbonates as Geochemical Archives of Environmental Change and Biotic/Abiotic Interactions, *in* M. Tilzer, and C. Serruya, eds., Large Lakes: Brock/Springer Series in Contemporary Bioscience, Springer Berlin Heidelberg, p. 288-315. doi: 10.1007/978-3-642-84077-7_15

Ketcham, R. A., and W. D. Carlson, 2001, Acquisition, optimization and interpretation of X-ray computed tomographic imagery: applications to the geosciences: Computers & Geosciences, v. 27, p. 381-400.

Ketcham, R. A., and G. J. Iturrino, 2005, Nondestructive high-resolution visualization and measurement of anisotropic effective porosity in complex lithologies using high-resolution X-ray computed tomography: Journal of Hydrology, v. 302, p. 92-106. doi: 10.1016/j.jhydrol.2004.06.037

Konhauser, K., 2007, Introduction to geomicrobiology: Malden, MA, Blackwell, 425 p.

Lee, T. C., R. L. Kashyap, and C. N. Chu, 1994, Building skeleton models via 3-D medial surface axis thinning algorithms: Graphical Models and Image Processing v. 56, p. 462-478. doi: 10.1006/cgip.1994.1042.

Lemos, R. M. T., 1995, Estudo das fácies deposicionais e das estruturas estromatolíticas da Lagoa Salgada - Rio de Janeiro: Master thesis, Universidade Federal Fluminense, Niterói, 122 p.

Lønøy, A., 2006, Making sense of carbonate pore systems: AAPG Bulletin, v. 90, p. 1381-1405. doi: 10.1306/03130605104

Lucia, F. J., 2007, Carbonate reservoir characterization : an integrated approach: Berlin ; New York, Springer, 336 p.

Luo, P., and H. G. Machel, 1995, Pore size and pore throat types in a heterogeneous dolostone reservoir, Devonian Grosmont Formation, Western Canada sedimentary basin: AAPG Bulletin, v. 79.

Mancini, E. A., J. C. Llinás, W. C. Parcell, M. Aurell, B. Bádenas, R. R. Leinfelder, and D. J. Benson, 2004, Upper Jurassic thrombolite reservoir play, northeastern Gulf of Mexico: AAPG Bulletin, v. 88, p. 1573-1602. doi: 10.1306/06210404017

Mancini, E. A., W. A. Morgan, P. M. Harris, and W. C. Parcell, 2013, Introduction: AAPG Hedberg Research Conference on Microbial Carbonate Reservoir Characterization—Conference summary and selected papers: AAPG Bulletin, v. 97, p. 1835–1847. doi: 10.1306/intro070913

Mancini, E. A., T. M. Puckett, and W. C. Parcell, 1999, Modeling of the burial and thermal histories of strata in the Mississippi Interior Salt Basin: Gulf Coast Association of Geological Societies Transactions, v. 49, p. 332-341.

McCreesh, C. A., R. Ehrlich, and S. J. Crabtree, 1991, Petrography and Reservoir Physics II: Relating Thin Section Porosity to Capillary Pressure, the Association Between Pore Types and Throat Size (1): AAPG Bulletin, v. 75, p. 1563-1578.

Mees, F., R. Swennen, M. Van Geet, and P. Jacobs, 2003, Applications of X-ray computed tomography in the geosciences, *in* F. Mees, R. Swennen, M. Van Geet, and P. Jacobs, eds., Applications of X-ray computed tomography in the geosciences: Geological Society Special Publication, v. 215: London, Geological Society, p. 1-6.

Melim, L. A., F. S. Anselmetti, and G. P. Eberli, 2001, The importance of pore type on permeability of Neogene carbonates, Great Bahama Bank, *in* R. N. Ginsburg, ed., Subsurface Geology of a Prograding Carbonate Platform Margin Great Bahama Bank: SEPM Special Publication: Tulsa, SEPM. doi: 10.2110/pec.01.70.

Monty, C. L. V., 1976, Chapter 5.1 The Origin and Development of Cryptalgal Fabrics, *in* M. R. Walter, ed., Stromatolites: Developments in Sedimentology, v. Volume 20: Amsterdam, Elsevier, p. 193-249. doi: 10.1016/S0070-4571(08)71137-3

Moore, C. H., 2001, Carbonate reservoirs : porosity evolution and diagenesis in a sequence stratigraphic framework: Developments in sedimentology: Amsterdam, Elsevier, 444 p.

Moreira, J. L. P., C. V. Madeira, J. A. Gil, and M. A. P. Machado, 2007, Santos Basin: Boletim de Geociências da Petrobras, v. 15, p. 531-549.

Morrill, C., E. E. Small, and L. C. Sloan, 2001, Modeling orbital forcing of lake level change: Lake Gosiute (Eocene), North America: Global and Planetary Change, v. 29, p. 57-76. doi: 10.1016/S0921-8181(00)00084-9

Morse, J. W., and F. T. Mackenzie, 1990, Geochemistry of sedimentary carbonates: Developments in sedimentology, v. 48: Amsterdam, Elservier, 706 p..

Nunn, J. A., A. D. Scardina, and R. H. Pilger, 1984, Thermal evolution of the north-central Gulf Coast: Tectonics, v. 3, p. 723-740.

Odgaard, A., and H. J. G. Gundersen, 1993, Quantification of connectivity in cancellous bone, with special emphasis on 3-D reconstructions: Bone, v. 14, p. 173-182. doi: 10.1016/8756-3282(93)90245-6.

Okabe, H., 2004, Pore-scale modelling of carbonates: Thesis (Ph D and D I C) thesis, Imperial College London, London, 142 p.

Okabe, H., and M. J. Blunt, 2007, Pore space reconstruction of vuggy carbonates using microtomography and multiple-point statistics: Water Resources Research, v. 43. doi: 10.1029/2006wr005680

Osmond, J. C., 2000, West Willow Creek Field: First Productive Lacustrine Stromatolite Mound in the Eocene Green River Formation, Uinta Basin, Utah: The Mountain Geologist, v. 37, p. 157-170.

Padhy, G. S., C. Lemaire, E. S. Amirtharaj, and M. A. Ioannidis, 2007, Size distribution in multiscale porous media as revealed by DDIF-NMR, mercury porosimetry and statistical image analysis: Colloids and Surfaces a-Physicochemical and Engineering Aspects, v. 300, p. 222-234. doi: 10.1016/j.colsurfa.2006.12.039

Parcell, W., 2002, Sequence stratigraphic controls on the development of microbial fabrics and growth forms-implications for reservoir quality distribution in the Upper Jurassic (Oxfordian) Smackover Formation, eastern Gulf Coast, USA: Carbonates and Evaporites, v. 17, p. 166-181. doi: 10.1007/bf03176483

Pieper, S., M. Halle, and R. Kikinis, 2004, 3D SLICER: Proceedings of the 1st IEEE International Symposium on Biomedical Imaging: From Nano to Macro, p. 632-635. doi:

Pieper, S., W. Lorensen, W. Schroeder, and R. Kikinis, 2006, The NA-MIC Kit: ITK, VTK, Pipelines, Grids and 3D Slicer as an Open Platform for the Medical Image Computing Community: Proceedings of the 3rd IEEE International Symposium on Biomedical Imaging: From Nano to Macro, p. 698-701.

Pietras, J., A. Carroll, and M. Rhodes, 2003, Lake basin response to tectonic drainage diversion: Eocene Green River Formation, Wyoming: Journal of Paleolimnology, v. 30, p. 115-125. doi: 10.1023/a:1025518015341

Pope, M. C., and J. P. Grotzinger, 2000, Controls on Fabric Development and Morphology of Tufas and Stromatolites, Uppermost Pethel Group (1.8 Ga), Great Slave Lake, Northwest Canada, *in* J. P. Grotzinger, and N. P. James, eds., Carbonate Sedimentation and Diagenesis in the Evolving Precambrian World: SEPM Special Publication: Tulsa, SEPM, p. 103-121. doi: 10.2110/pec.00.67.0103

Pueyo, J. J., A. Sáez, S. Giralt, B. L. Valero-Garcés, A. Moreno, R. Bao, A. Schwalb, C. Herrera, B. Klosowska, and C. Taberner, 2011, Carbonate and organic matter sedimentation and isotopic signatures in Lake Chungará, Chilean Altiplano, during the last 12.3 kyr: Palaeogeography, Palaeoclimatology, Palaeoecology, v. 307, p. 339-355. doi: 10.1016/j.palaeo.2011.05.036

Rainey, D. K., and B. Jones, 2009, Abiotic v. biotic controls on the development of the Farimont Hot Springs carbonate deposit, British Columbia, Canada.: Sedimentology, v. 56, p. 1832-1857. doi: 10.1111/j.1365-3091.2009.01059.x

Rezende, M. F., and M. C. Pope, 2015, Importance of depositional texture in pore characterization of subsalt microbialite carbonates, offshore Brazil, *in* D. W. J. Bosence, K. A. Gibbons, D. P. lemHeron, W. A. Morgan, T. Pritchard, and B. A. Vining, eds., Microbial Carbonates in Space and Time: Implications for Global Exploration and Production: Geological Society, London, Special Publications, v. 418. First published online February 26, 2015. doi: 10.1144/sp418.2

Rezende, M. F., S. N. Tonietto, and M. C. Pope, 2013, Three-dimensional pore connectivity evaluation in a Holocene and Jurassic microbialite buildup: AAPG Bulletin, v. 97, p. 2085-2101. doi: 10.1306/05141312171

Riding, R., 2000, Microbial carbonates: the geological record of calcified bacterial–algal mats and biofilms: Sedimentology, v. 47, p. 179-214. doi: 10.1046/j.1365-3091.2000.00003.x

Riding, R., 2011, Microbialites, stromatolites and thrombolites, *in* J. Reitner, and V. Thiel, eds., Encyclopedia of Geobiology: Encyclopedia of Earth Science Series: Heidelberg, Springer, p. 635-654.

Roehler, H. W., 1992, Correlation, composition, areal distribution, and thickness of Eocene stratigraphic units, Greater Green River Basin, Wyoming, Utah, and Colorado, Professional Paper, United States Geological Survey, p. 49.

Roehler, H. W., 1993, Eocene climates, depositional environments, and geography, greater Green River Basin, Wyoming, Utah, and Colorado, Professional Paper, United States Geological Survey, p. 74.

Sarg, J. F., Suriamin, K. Tanavsuu-Milkeviciene, and J. D. Humphrey, 2013, Lithofacies, stable isotopic composition, and stratigraphic evolution of microbial and associated carbonates, Green River Formation (Eocene), Piceance Basin, Colorado: AAPG Bulletin, v. 97, p. 1937–1966. doi: 10.1306/07031312188

Schmid, D. U., 1996, Marine Mikrobolite und Mikroinkrustierer aus dem Oberjura: Profil, v. 9, p. 101-251.

Seard, C., G. Camoin, J.-M. Rouchy, and A. Virgone, 2013, Composition, structure and evolution of a lacustrine carbonate margin dominated by microbialites: Case study from the Green River formation (Eocene; Wyoming, USA): Palaeogeography, Palaeoclimatology, Palaeoecology, v. 381–382, p. 128-144. doi: 10.1016/j.palaeo.2013.04.023

Sewall, J. O., and L. C. Sloan, 2006, Come a little bit closer: A high-resolution climate study of the early Paleogene Laramide foreland: Geology, v. 34, p. 81-84. doi: 10.1130/g22177.1

Silva e Silva, L. H., A. A. C. Iespa, and C. M. Damazio-Iespa, 2007, Considerações sobre Estromatólito do Tipo Domal da Lagoa Salgada, Estado do Rio de Janeiro, Brasil: Anuário do Instituto de Geociências - UFRJ, v. 30, p. 50-57.

Sloan, L. C., 1994, Equable climates during the early Eocene: Significance of regional paleogeography for North American climate: Geology, v. 22, p. 881-884.

Smith, M. E., A. R. Carroll, and B. S. Singer, 2008, Synoptic reconstruction of a major ancient lake system: Eocene Green River Formation, western United States: Geological Society of America Bulletin, v. 120, p. 54-84.

Srivastava, N. K., 1999, Lagoa Salgada (Rio de Janeiro) - Estromatólitos recentes, *in* C. Schobbenhaus, D. A. Campos, E. T. Queiroz, M. Winge, and M. Berbert-Born, eds., Sítios Geológicos e Paleontológicos do Brasil, v. 1: Brasília, DNPM/CPRM - Comissão Brasileira de Sítios Geológicos e Paleobiológicos (SIGEP), p. 203-209.

Sumner, D. Y., 2001, Microbial influences on local carbon isotopic rations and their preservation in carbonates: Astrobiology, v. 1, p. 57-70. doi: 10.1089/153110701750137431

Surdam, R. C., and K. Stanley, 1979, Lacustrine sedimentation during the culminating phase of Eocene Lake Gosiute, Wyoming (Green River Formation): Geological Society of America Bulletin, v. 90, p. 93-110.

Surdam, R. C., and K. O. Stanley, 1980, Effects of changes in drainage-basin boundaries on sedimentation in Eocene Lakes Gosiute and Uinta of Wyoming, Utah, and Colorado: Geology, v. 8, p. 135-139. doi: 10.1130/0091-7613(1980)8<135:eocidb>2.0.co;2

Swierenga, M., 2014, Depositional history and lateral variability of microbial carbonates, Three Mile Canyon and Evacuation Creek, Eastern Uinta Basin, Utah, Colorado School of Mines, Golden, Colorado, 94 p.

Talbot, M. R., and K. Kelts, 1990, Paleolimnological signatures from Carbon and Oxygen isotopi-ratios in carbonates from organic carbon-rich lacustrine deposits, *in* B. J. Katz, ed., Lacustrine Basin Exploration: Case Studies and Modern Analogs: Memoir, v. 50: Tulsa, American Association of Petroleum Geologists, p. 99-112.

Tänavsuu-Milkeviciene, K., and F. J. Sarg, 2012, Evolution of an organic-rich lake basin – stratigraphy, climate and tectonics: Piceance Creek basin, Eocene Green River Formation: Sedimentology, v. 59, p. 1735-1768. doi: 10.1111/j.1365-3091.2012.01324.x

Terra, G. J. S., A. R. Spadini, A. B. França, C. L. Sombra, E. E. Zambonato, L. C. d. S. Juschaks, L. M. Arienti, M. M. Erthal, M. Blauth, M. P. Franco, N. S. Matsuda, N. G. Carramal, P. A. M. Júnior, R. S. F. D'Avila, R. S. d. Souza, S. N. Tonietto, S. M. C. d. Anjos, V. S. Campinho, and W. R. Winter, 2009, Carbonate rock classification applied to brazilian sedimentary basins: Boletim de Geociências da Petrobras, v. 18, p. 9-29.

Tonietto, S. N., and M. C. Pope, 2013, Diagenetic evolution and its influence on petrophysical properties of the Jurassic Smackover Formation thrombolite and grainstone units of Little Cedar Creek Field, Alabama: Gulf Coast Association of Geological Societies Journal, v. 2, p. 68-84.

Torfstein, A., I. Gavrieli, A. Katz, Y. Kolodny, and M. Stein, 2008, Gypsum as a monitor of the paleo-limnological–hydrological conditions in Lake Lisan and the Dead Sea: Geochimica et Cosmochimica Acta, v. 72, p. 2491-2509. doi: 10.1016/j.gca.2008.02.015

Toriwaki, J., and T. Yonekura, 2002, Euler number and connectivity indexes of a three dimensional digital picture: Forma, v. 17, p. 183-209.

Tucker, M. E., and V. P. Wright, 1990, Carbonate sedimentology: Oxford, England, Blackwell Scientific Publications, 482 p.

Van Geet, M., D. Lagrou, and R. Swennen, 2003, Porosity measurements of sedimentary rocks by means of microfocus X-ray computed tomography (□CT), *in* F. Mees, R. Swennen, M. Van Geet, and P. Jacobs, eds., Applications of X-ray computed tomography in the geosciences: Geological Society Special Publication, v. 215: London, Geological Society, p. 51-60.

Vasconcelos, C., and J. A. McKenzie, 1997, Microbial mediation of modern dolomite precipitation and diagenesis under anoxic conditions (Lagoa Vermelha, Rio de Janeiro, Brazil): Journal of sedimentary Research, v. 67, p. 378-390.

Verwer, K., G. P. Eberli, and R. J. Weger, 2011, Effect of pore structure on electrical resistivity in carbonates: AAPG Bulletin, v. 95, p. 175-190. doi: 10.1306/06301010047

Winter, W. R., R. J. Jahnert, and A. B. França, 2007, Campos Basin: Boletim de Geociências da Petrobras, v. 15, p. 511-529.

Withjack, E. M., 1988, Computed Tomography for Rock-Property Determination and Fluid-Flow Visualization: SPE Formation Evaluation, v. 3, p. 696-704. doi: 10.2118/16951-pa

Wright, V. P., and A. Barnett, 2015, An abiotic model for the development of textures in some South Atlantic early Cretaceous lacustrine carbonates, *in* D. W. J. Bosence, K. A. Gibbons, D. P. lemHeron, W. A. Morgan, T. Pritchard, and B. A. Vining, eds., Microbial Carbonates in Space and Time: Implications for Global Exploration and Production: Geological Society, London, Special Publications, v. 418. First published online February 26, 2015. doi: 10.1144/sp418.3

Xu, B., J. Kamath, Y. C. Yortsos, and S. H. Lee, 1999, Use of Pore-Network Models to Simulate Laboratory Corefloods in a Heterogeneous Carbonate Sample: SPE Journal, v. 4, p. 178-186. doi: 10.2118/57664-pa

APPENDIX A

THE DEPOSITIONAL AND DIAGENETIC EFFECTS ON THE PORE SYSTEM OF BRAZILIAN SUBSALT MICROBIALITES EXPRESSED ON WELL-LOGS[3]

Abstract

Microbialites, besides their natural texture heterogeneity, can be interpreted using well logs. Textural controls on the microbialites pore system result in a negative correlation between gamma ray logs and porosity logs. The petrographic analysis and CT volumetric evaluation show that the pore system is better connected on large homogeneous microbial fabrics (e.g. large shrub stromatolites) compared to laminated or smaller heterogeneous fabrics.

Diagenetic modifications that reduced the porosity by dolomite and silica cements define intervals with large separation between porosity logs and the photoelectric factor log. Intervals with diagenetically enhanced pore systems commonly are associated with dissolution processes showing a positive correlation between the porosity logs and photoelectric factor. In the diagenetically enhanced pore systems the depositional trend between gamma ray logs and porosity logs is not present.

[3] This appendix adds supplemental data to Chapter II.

The differentiation between depositional and diagenetically controlled pore systems in microbialite carbonates units by petrographic and well log analysis may contribute to a better understanding of these reservoirs. The units detailed in this work indicate that intervals dominated by depositional or diagenetic characteristics have distinct petrographic and petrophysical characteristics, which can lead to different log signatures.

Introduction

The fabric and pore system of microbialite carbonates are controlled by depositional settings (Rezende et al., 2013; Rezende and Pope, 2015; Tonietto and Pope, 2013). However, these primary rock characteristics are diagenetically modified in different ways (dissolution and cementation) and degrees during subsequent burial, allowing a genetic classification of the carbonate pore system (Ahr, 2008). Consequently, units with the same initial primary characteristics may end up with very different pore systems and petrophysical characteristics (Rezende et al., 2013; Tonietto and Pope, 2013).

Subsalt microbialite carbonate units (Gomes et al, 2013; Rezende and Pope, 2015; Terra et al., 2009) were evaluated in six wells located in the Santos Basin, Brazil (figure II.1), using rock types defined by the dominant microbialite texture and well log signatures. Diagenetically modified intervals were then compared to these rock types to contrast the effects of dissolution and cementation on the primary pore system. The results suggest that it is reasonable to use well logs to classify microbialite carbonate

units, in terms of their textural, diagenetic and petrophysical characteristics, for further reservoir characterization.

Methods

Microbialite carbonate units in six wells from hydrocarbon reservoirs were sub-divided into rock types defined by their textural characteristics and different signatures on porosity, resistivity and lithological logs. These rock types also had their pore systems evaluated by petrography in terms of depositional and diagenetic history and CT scans for 3D structure. The information from log signatures, petrophysics measurements, petrographic and 3D pore system were integrated to understand how the microbial textures, diagenetic fabrics and pore systems are expressed on well logs.

Results

Better developed textures, such as large shrub microbialite, have higher porosity (Appendix, figure 1) and very low radioactivity (Appendix, figure 2). The effect of large pore structures of these better developed textures is also noted on the resistivity and density logs (Appendix, figure 3). Large pore structures result in lower resistivity in the water-bearing zones and lower density.

Textures with larger pore structure have higher acoustic slowness and porosity values estimated by Nuclear Magnetic Resonance (NMR) log (Appendix, figure 4), except in the authigenic clay-rich intervals. In these intervals the acoustic slowness is low because of the clays formed into pores. Higher concentration of mud and organic matter is common in lesser developed textures, which also reduces the acoustic slowness

(Appendix, figure 5). Interfingering effect between the main textural classes is caused by a high textural heterogeneity of these microbialite carbonate units.

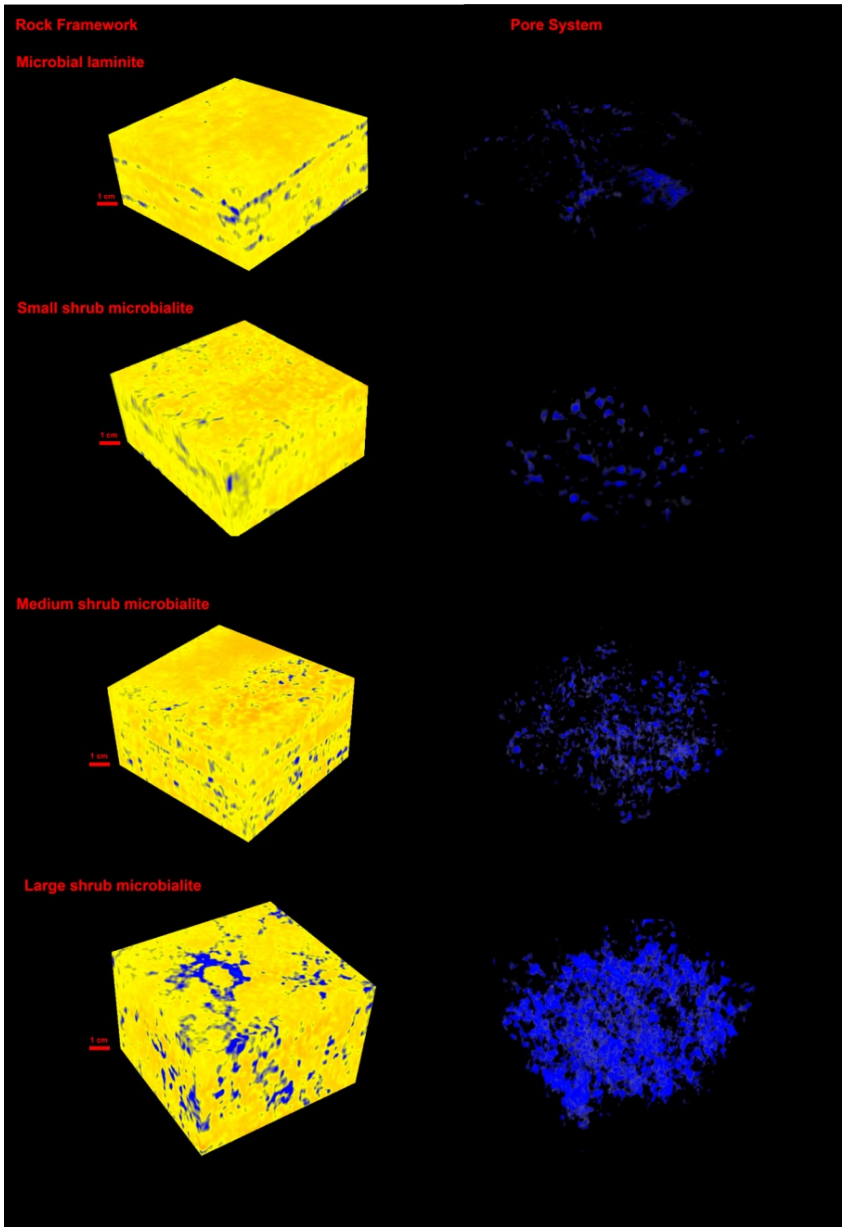

Appendix A, figure 1. CT rendered volumes for the rock framework and pore system of the microbial laminite, small shrub, medium shrub and large shrub microbialite textures in the subsalt carbonate deposits in Santos Basin. Orange color represents less porous particles, yellow color represents more microporous particles and blue color represents the pore system. The pore system is better developed, and changes from chaotic organization to horizontally oriented pores, on the large shrub microbialite textures and become worse towards the laminite, because of smaller pores and tight shrub packing.

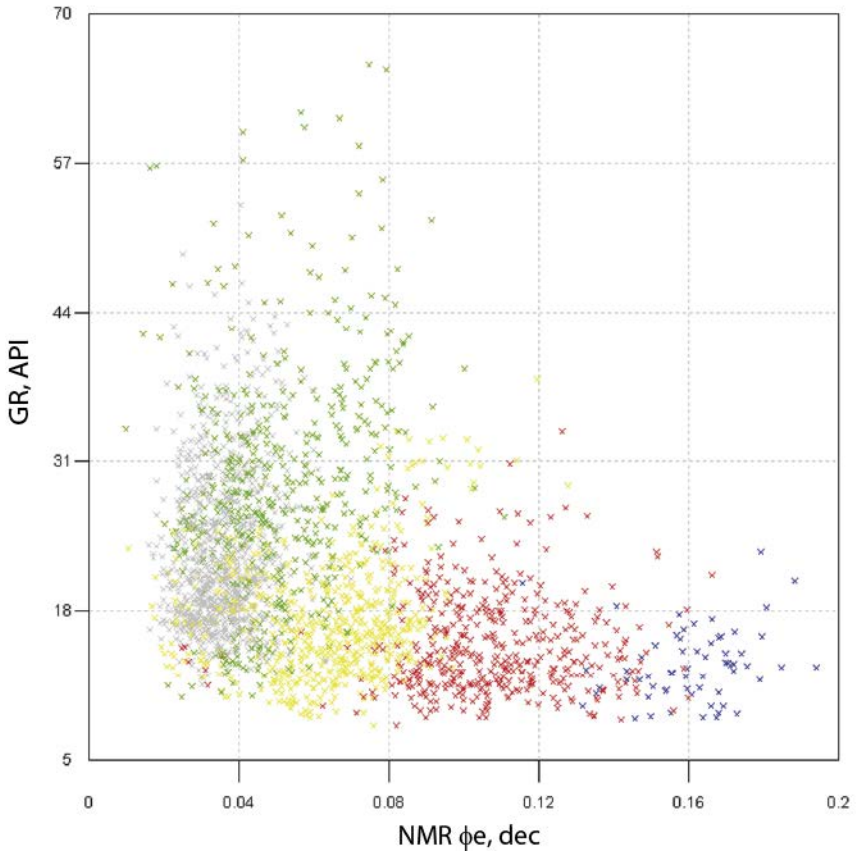

Appendix A, figure 2. NMR effective porosity v. gamma ray plot, showing that the large shrub microbialite (purple) and medium shrub microbialite (red) have higher porosity and lower natural radioactivity than the small shrub microbialite (yellow) and microbial laminites (green). The grey cluster is formed by samples located in intervals rich in authigenic clays that fill pores and reduces the porosity.

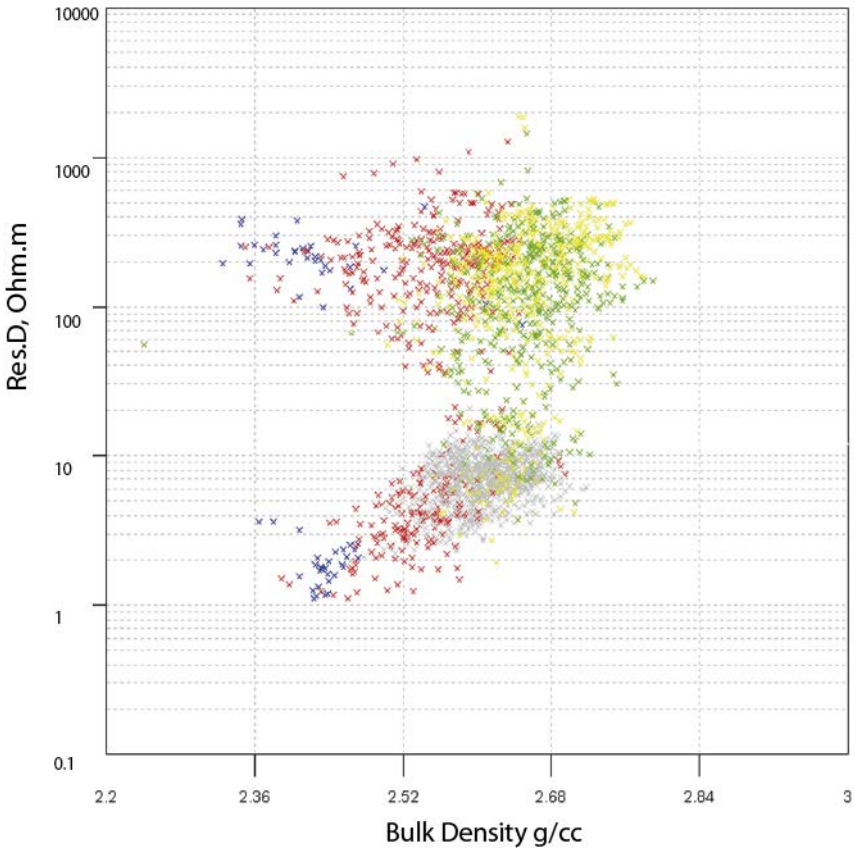

Appendix A, figure 3. Bulk density v. deep resistivity plot, showing the water-bearing zone below 20 Ohm.m and the oil bearing zone above 20 ohm.m. The large shrub microbialite (purple) and medium shrub microbialite (red) have lower bulk density values and lower natural resistivity in the water-bearing zone than the small shrub microbialite (yellow) and microbial laminites (green). On the oil-bearing zone the resistivity values are affected by the high resistivity of the oil, but a slight trend is present from lower resistivity values in the microbial laminite and small shrub microbialites towards higher resistivity values in the medium and large shrub microbialites. The grey cluster is formed by samples located in intervals rich in authigenic clays that fill pores, reduces the porosity and increases the water saturation.

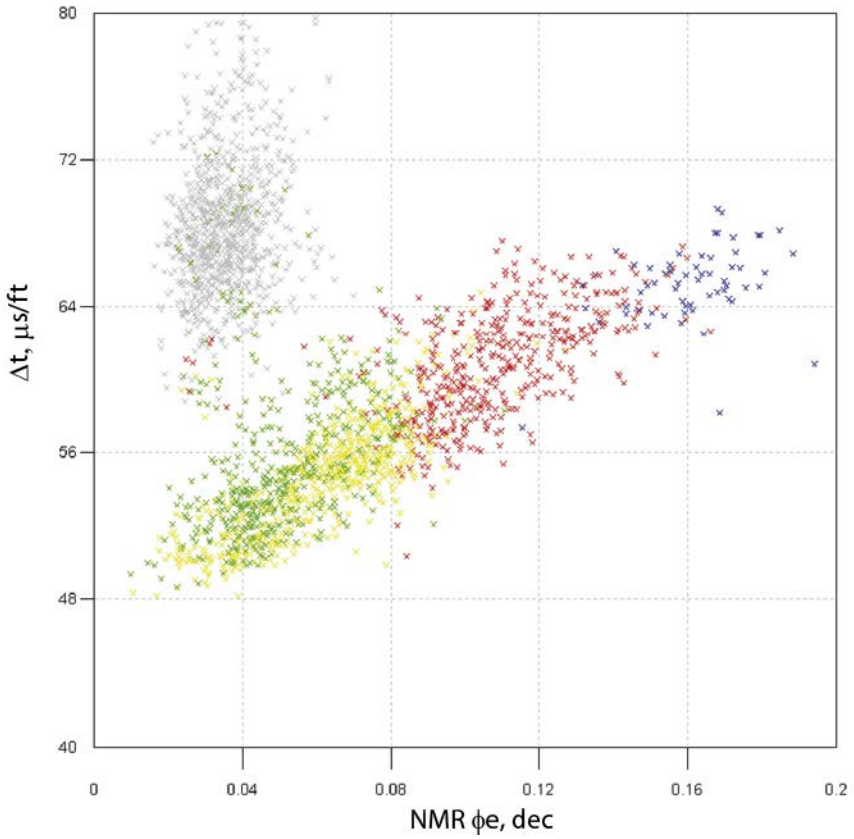

Appendix A, figure 4. NMR effective porosity v. acoustic slowness plot, showing that the large shrub microbialite (purple) and medium shrub microbialite (red) have higher porosity and higher acoustic slowness than the small shrub microbialite (yellow) and microbial laminites (green). The grey cluster is formed by samples located in intervals rich in authigenic clays that fill pores and reduces the porosity, but keep the acoustic slowness high, because of its microporous microstructure and high water saturation.

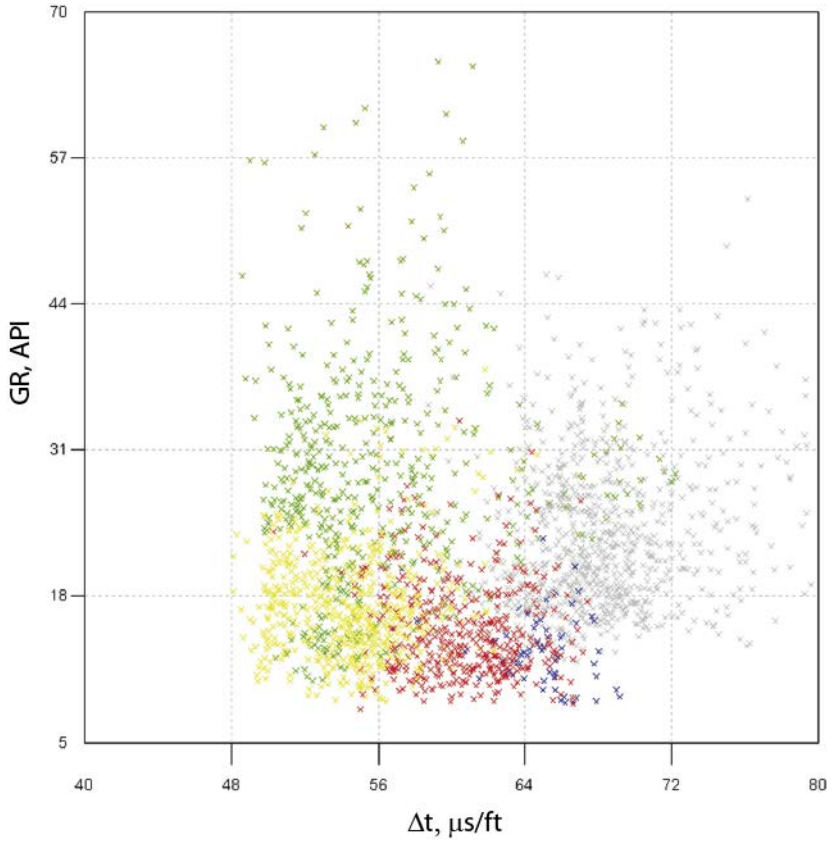

Appendix A, figure 5. Acoustic slowness v. gamma ray plot, showing that the large shrub microbialite (purple) and medium shrub microbialite (red) have higher acoustic slowness and lower natural radioactivity than the small shrub microbialite (yellow) and microbial laminites (green). The grey cluster is formed by samples located in intervals rich in authigenic clays that fill pores , reduces the porosity and increases the water saturation.

Besides the depositional controls on the rock properties, pore system characteristics and their effects on the well log measurements, there are two diagenetic patterns A and B that can identified by well logs. Pattern A represents intervals where the depositional control on the porosity is dominant, and the diagenesis acts enhancing or reducing the pore space. Pattern B represents intervals where the diagenetic control on the pore system is dominant. However, the textural changes still drives major changes in porosity.

These two diagenetic patterns and their resultant pore system are clearly defined on petrographic thin sections (Appendix figure 6). Pattern A is related to the primary porosity, which was enhanced by dissolution or reduced by cements. Pattern B is related to diagenetic pore systems formed by cementation and later dissolution of depositional particles. This different pore system formed by the pattern B results in lower permeability values when compared to the pore system formed by the Pattern A (Appendix figure 7).

Appendix figure 8 shows the correlation between NMR effective porosity and Photoelectric effect (PE) for these two diagenetic patterns. Pattern A has a positive correlation and Pattern B has a negative correlation. The gray data are the intervals in pattern A with strong cementation by dolomite or silica.

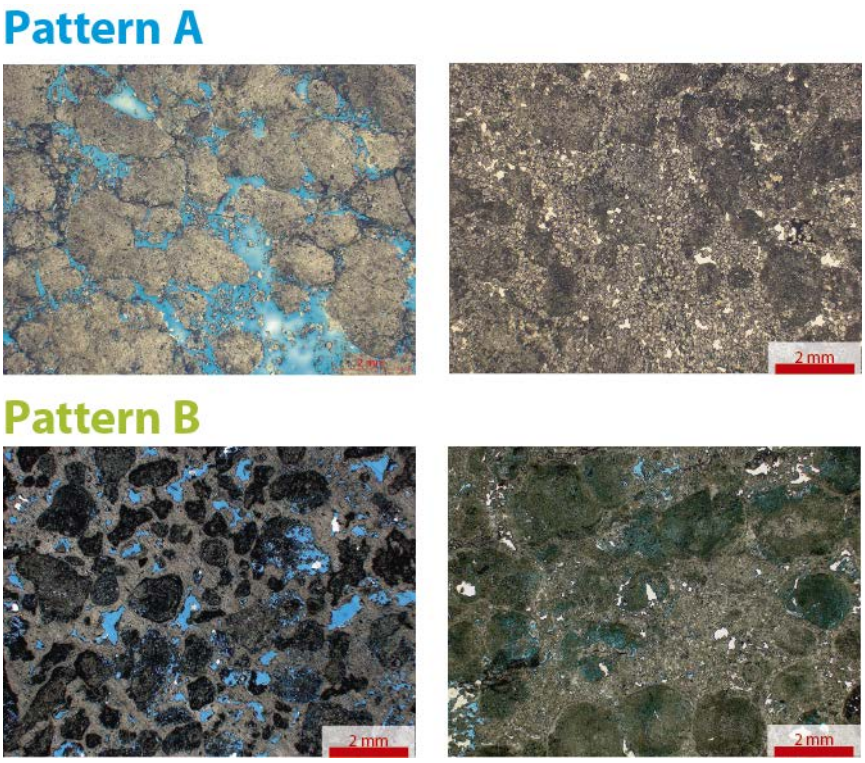

Appendix A, figure 6. Two diagenetic patterns characterized by differences in pore systems and mineral content. Pattern A has a pore system related to the depositional texture (left image). Dolomite and Silica are cement phases that reduces the porosity in this pattern (right image). Pattern B has a pore system (moldic pores and vugs) formed by selective dissolution of calcite particles in a rock that was previously cemented (left image). Intervals not affected by dissolution have low porosity (right image).

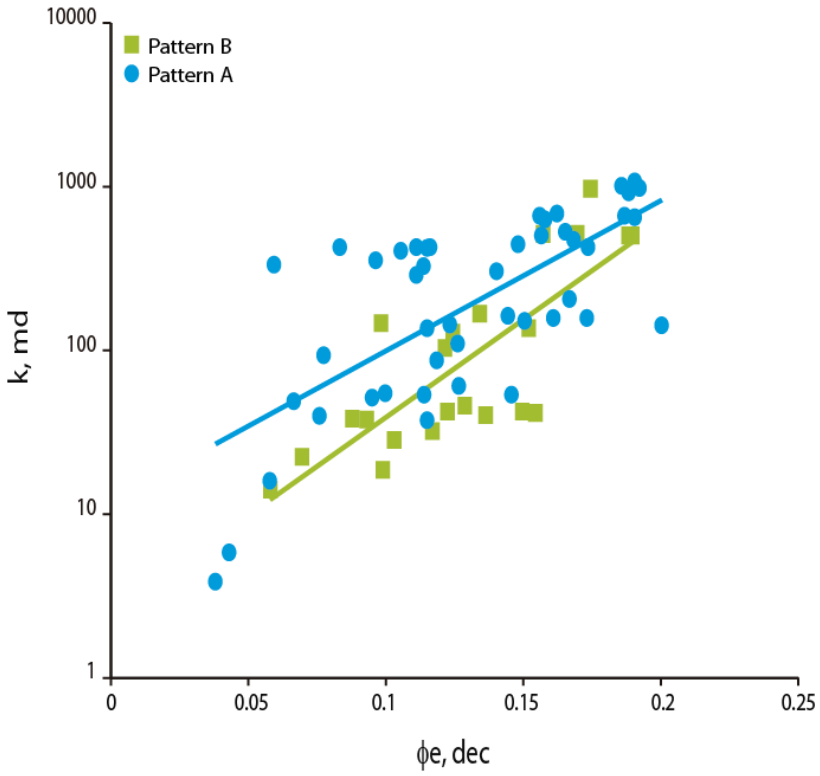

Appendix A, figure 7. Effective porosity v. permeability plot, showing that samples characterized by the pattern A have higher permeability values than samples characterized by the pattern B. All results in this plot were obtained from plugs sampled from cores.

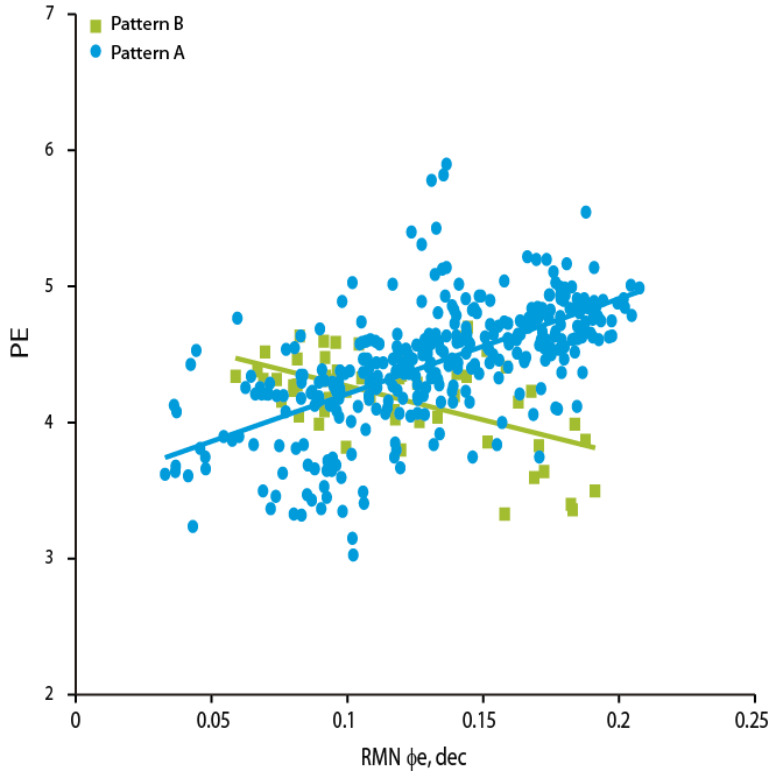

Appendix A, figure 8. NMR effective porosity v. PE plot, showing two opposite correlation trends for the diagenetic patterns A and B. Pattern A has a positive correlation trend between porosity and PE, which is defined by the association of open pore structure and calcite framework particles and closed pore structure and dolomite and/or silica cements. Pattern B has a negative correlation trend between porosity and PE, which is defined by the association of open pore structure (moldic pores and vugs) and dissolution of calcite framework particles and closed pore structure and the presence of calcite particles.

Discussion

Depositional patterns in well-logs

Depositional patterns in this subsalt microbialite carbonate units are identifiable on well-logs, which can be used to track shifts in facies and their related pore systems. The data indicate that better primary pore systems are related to better developed microbialite textures (Appendix, figure 1) with large particles and low concentration of mud and organic content. These patterns are useful to build conceptual reservoir models. These textures such as large shrub microbialite and medium shrub microbialite have low gamma ray and high acoustic slowness, except intervals rich in authigenic clays (Appendix, figures 2, 4 and 5). The larger and better connected pore system in these textures is identifiable by the deep resistivity log, which shows relatively lower values in the water-bearing zone for these textures than in microbial laminites and small shrub microbialites (Appendix, figure 3). However, different carbonate deposits may have different distribution of environments, facies and textures that lead to other log signatures.

Diagenetic patterns on well-logs

In these sub-salt carbonates, two diagenetic patterns A and B are observed as result of two different diagenetic pathways. Calcite rock framework, dolomite and silica cements, and dissolution processes resulted in totally distinct pore system characteristics (Appendix, figures 6 and 7). Pattern A is defined by interparticle porosity reduction by cements and interparticle porosity enhancement by dissolution. Pattern B is defined by

the generation of moldic and intraparticle porosity in intervals with strong cementation by silica or dolomite.

These changes in the pore system and mineral content allow the recognition of these two diagenetic patterns by well logs. Changes in the mineral content (e.g. calcite dissolution and dolomite precipitation) caused by the diagenetic processes related to these two patterns, result in different PE values. These values show a positive correlation for the pattern A and a negative correlation for the pattern B, when plotted against the porosity estimated by NMR logs (Appendix, figure 8). Therefore, it is possible to distinguish these two patterns by well logs. The integration of these diagenetic patterns with the primary depositional patterns allows a better differentiation of rock types with different log signatures and petrophysical characteristics.

Conclusions

Depositional patterns are expressed on lithological and porosity estimation logs in the sub-salt microbialite carbonate deposits. The environmental setting controls the depositional textures leading to different pore systems. These depositional patterns are the main identifiable element on the gamma ray and the porosity estimated by logs. They also impact the petrophysical characteristics of these microbialite carbonate deposits.

Two diagenetic patterns A and B control diagenetic enhanced and diagenetic reduced zones. They both are expressed on logs by changes in porosity and mineral composition. Both patterns result in low porosity values by silica and dolomite cements. Pattern A has higher porosity values when the cement content is low, whereas pattern B

the higher porosity values are related to moldic porosity in cemented intervals. These differences also lead to changes in porosity and permeability between these two diagenetic patterns.

Both depositional and diagenetic patterns can be integrated into reservoir models to define classes formed in similar environmental conditions, but with different diagenetic histories. Consequently, the petrophysical characteristics in these units can be better understood, once the genetic character of the pore system are properly defined. Each class can be later sub-divided to incorporate geologic and petrophysical details into the model when needed. As note of caution, complete rock-log integration is necessary to better define the depositional classes and diagenetic patterns in these microbial carbonate units.

APPENDIX B

MICROBIALITE TEXTURES FROM TWO OUTCROPS IN THE EOCENE GREEN RIVER FORMATION, IN WYOMING

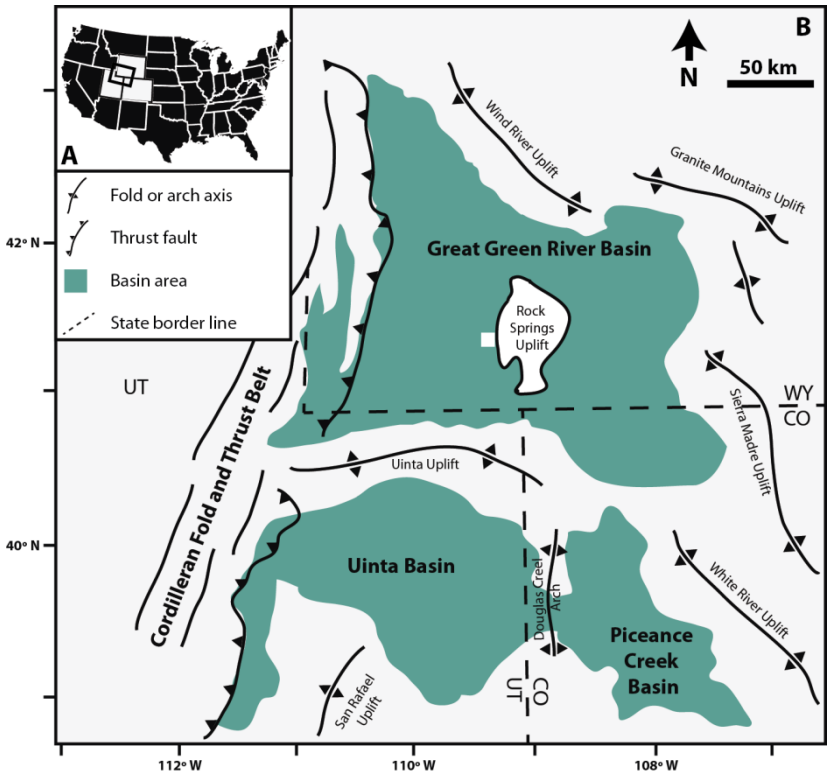

Appendix A, figure 1. Inset map A – United States map with the states where the Great Green River Basin, Uinta Basin and Piceance Creek Basin are located. B – Regional map with the areal distribution of the Eocene lake basins (Great Green River Basin, Uinta Basin and Piceance Creek Basin), major uplifts and tectonic lineaments (modified after Smith et al., 2008). The white square shows the outcrop location in Wyoming (north of Rock Spring) at 41° 58' 07" N, 109° 15' 05" W.

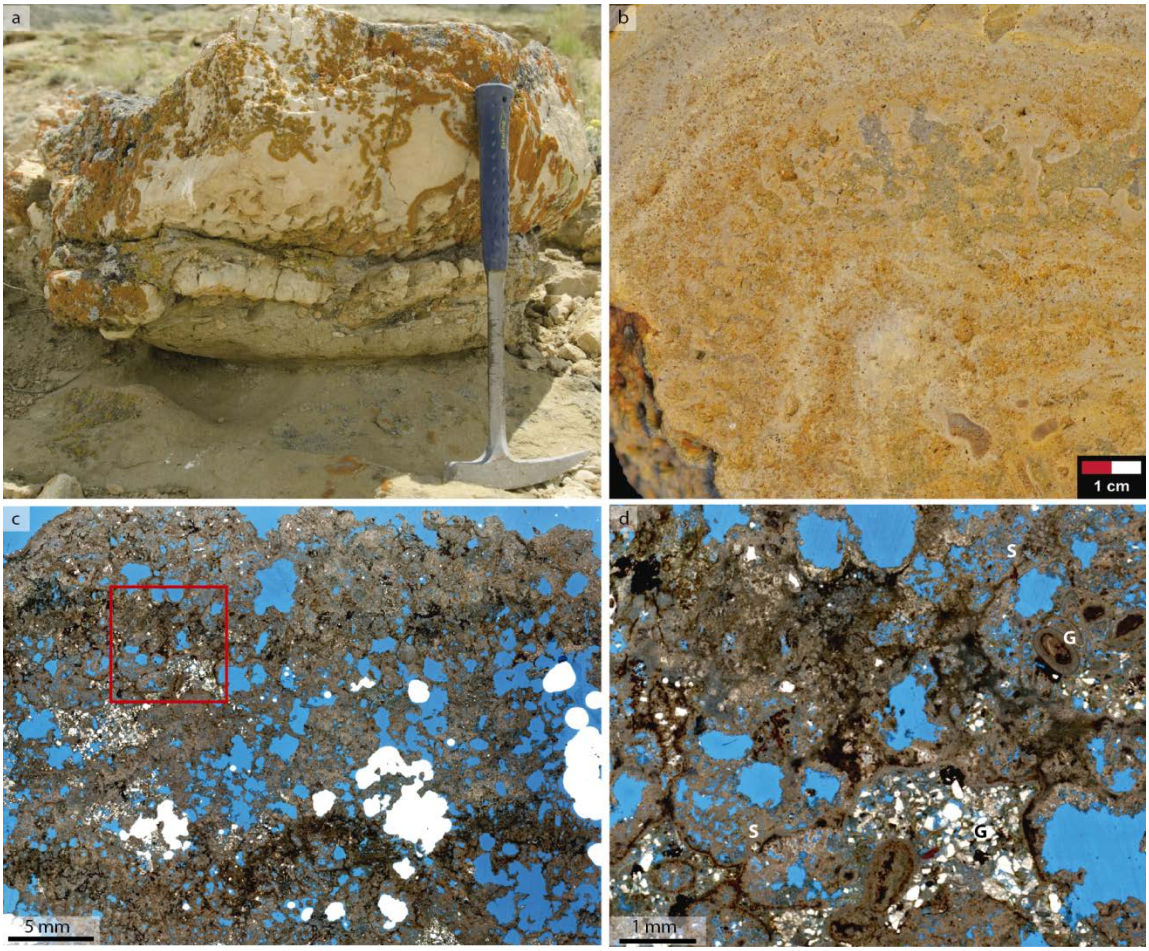

Appendix A, figure 2. a – Microbialite head composed of peloids, peloid shrubs and trapped grains (detrital carbonate and clastics). The heads are metric sized and occur scattered (some upside-down) in a cross stratified medium sandstone (Farson Sandstone). They developed on top of previous reliefs such as wood logs and other debris. b – Detail of thrombolite texture with complex 3D fabric capped by thinly laminated stromatolite texture. c – High-resolution image showing the complex and open fabric of the thrombolite texture formed by irregularly branches. c – Detail of the area marked on b (red square) showing the thrombolite texture framework of small peloids (S) shrubs and trapped grains (G). The black material is organic matter.

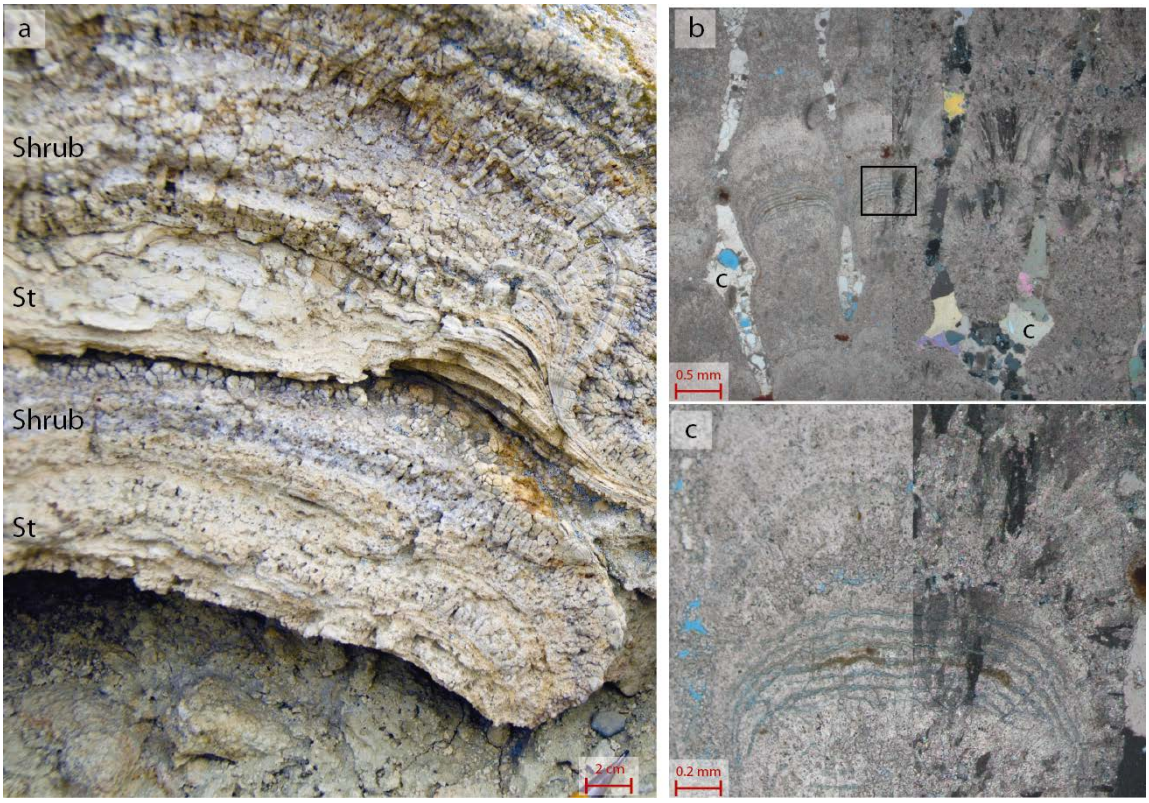

Appendix A, figure 3. a – Microbialite head composed of alternated layers of stromatolite (St) and shrub microbialite (Shrub). The heads form a 30 cm (average) thick layers interbedded with intraclast, oncolite grainstone that caps a shale/sandstone unit. b – Thin section image showing shrubs appearance. Darker colors are peloid rich intervals and light colors are crystalline phases intervals. The pore space is partially filled by blocky calcite cement (c). c – Close-up on the area marked with a black square in b. The shrubs are formed by alternations of thin carbonate and organic matter laminae, and vertically grown carbonate crystals. Pores formed between shrubs and between laminae. The left side of image is under cross-polarized light.

APPENDIX C

MERCURY INJECTION PORE THROAT RADIUS DISTRIBUTION

Company:	**Texas A&M University**	**Sample:**	**3MCP1S3A**	un-	Host Plug (1)	
Well:	**3 Miles CNY Utah**	Texture	Digitate Stromatolite	stressed	800psi	n/a
Location:	**Utah**	Klinkenberg Permeability, md:		N/A	5.93	-
File:	**HOU-140913**	Permeability to Air, md:		N/A	7.58	-
		Swanson Permeability, md:		6.18	-	-
		Porosity, fraction:		0.182	0.192	-
		maximum Sb/Pc, fraction:		0.0851		
(1) Sample contains vuggs.		R35, microns:		0.921		
		R50 (median pore throat radius):		0.449		

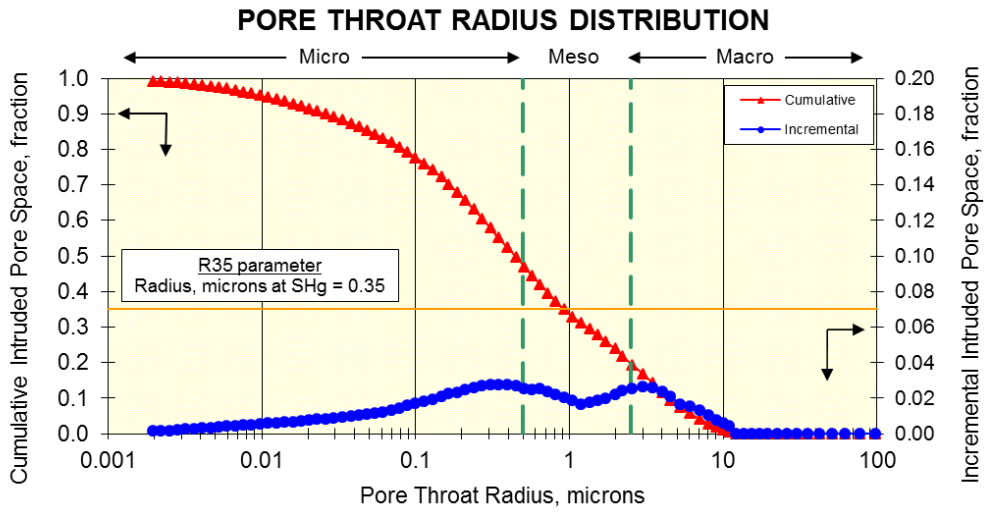

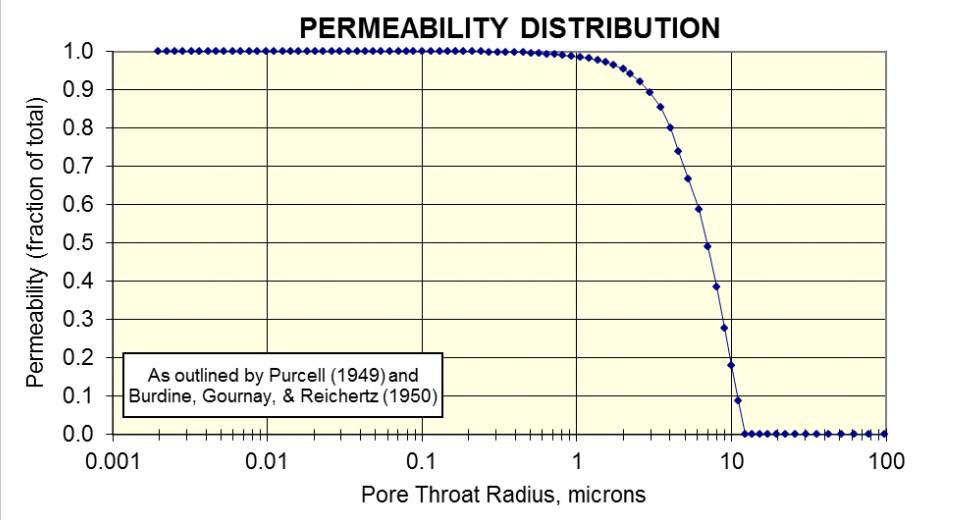

Company:	**Texas A&M University**	**Sample:**	3MCP1S5	un-	Host Plug (1)
Well:	**3 Miles CNY Utah**	Texture	Grainstone	stressed	800psi	n/a
Location:	**Utah**	Klinkenberg Permeability, md:		N/A	294.	-
File:	**HOU-140913**	Permeability to Air, md:		N/A	360.	-
		Swanson Permeability, md:		443.	-	-
		Porosity, fraction:		0.296	0.310	-
		maximum Sb/Pc, fraction:		1.06		
(1) Sample contains vuggs.		R35, microns:		7.22		
		R50 (median pore throat radius):		2.57		

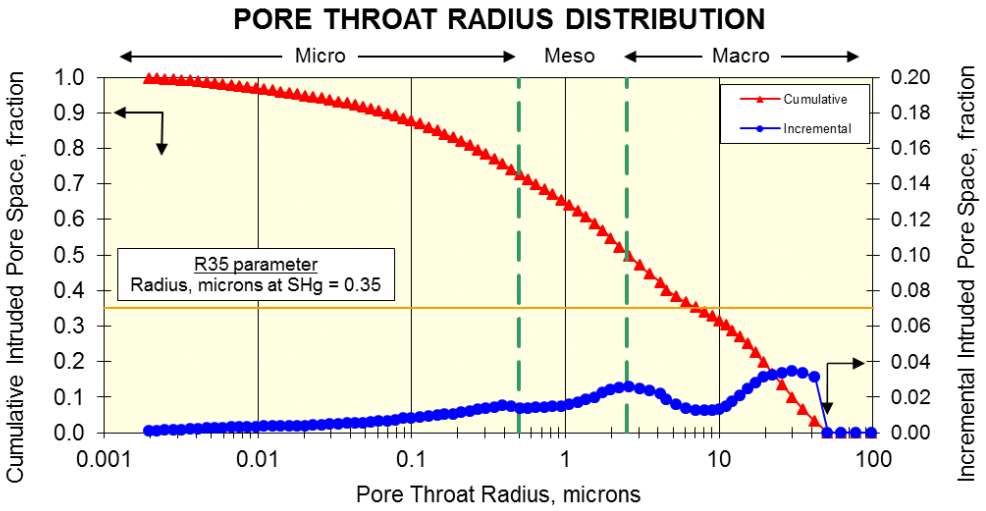

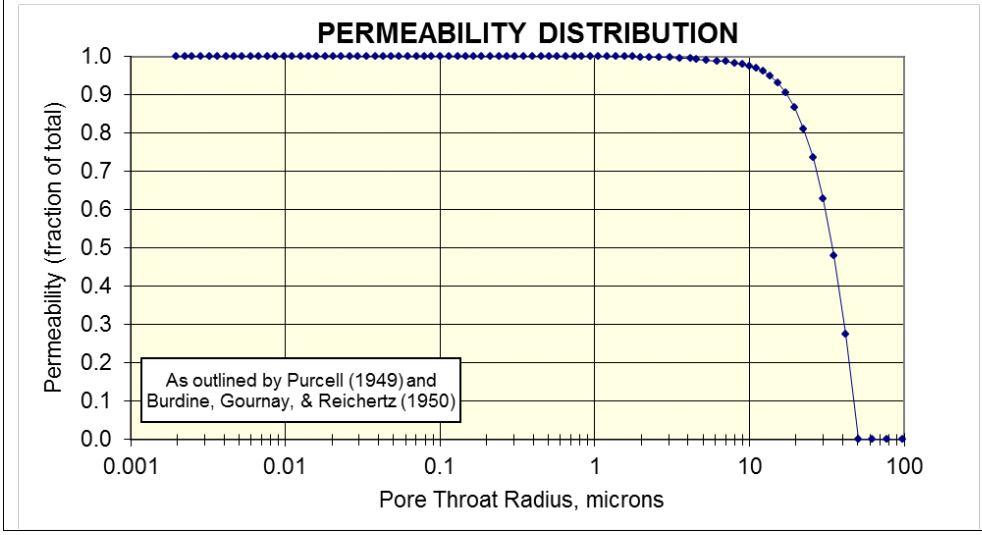

Company:	**Texas A&M University**	**Sample:**	**3MCP1S9A**	un-	Host Plug (1)
Well:	**3 Miles CNY Utah**	Texture:	Thrombolite	stressed	800psi / n/a
Location:	**Utah**	Klinkenberg Permeability, md:		N/A	1750. / -
File:	**HOU-140913**	Permeability to Air, md:		N/A	2350. / -
		Swanson Permeability, md:		807.	- / -
		Porosity, fraction:		0.252	0.283 / -
(1) Sample contains vuggs.		maximum Sb/Pc, fraction:		1.52	
		R35, microns:		11.9	
		R50 (median pore throat radius):		5.34	

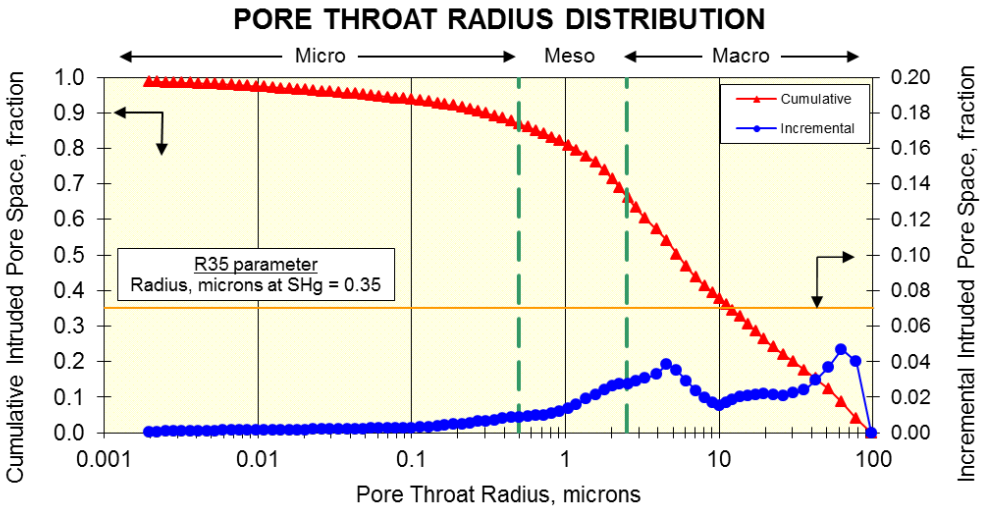

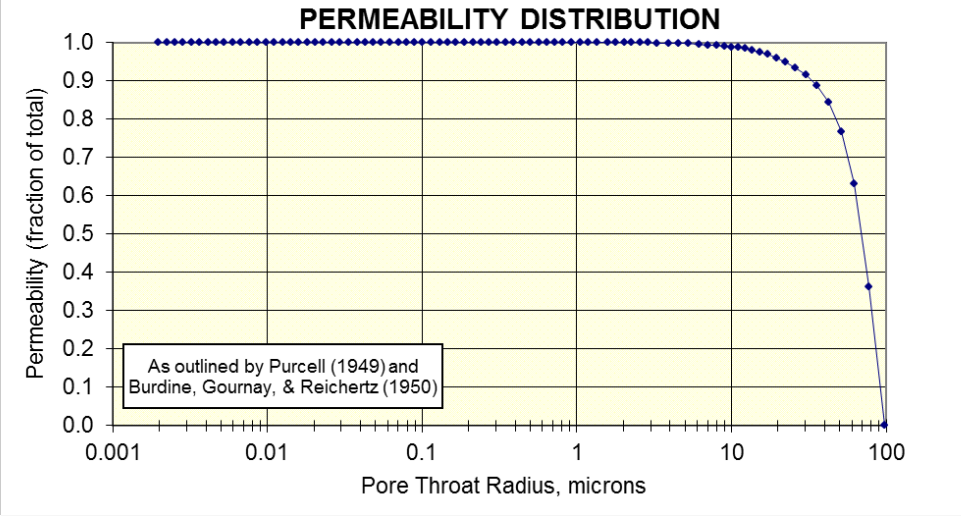

Company:	**Texas A&M University**	**Sample:**	**3MCP2S3**	un-	Host Plug (1)
Well:	**3 Miles CNY Utah**	Texture	Digitate Stromatolite	stressed	800psi	n/a
Location:	**Utah**	Klinkenberg Permeability, md:		N/A	3.75	-
File:	**HOU-140913**	Permeability to Air, md:		N/A	4.91	-
		Swanson Permeability, md:		7.64	-	-
		Porosity, fraction:		0.158	0.173	-
		maximum Sb/Pc, fraction:		0.0964		
(1) Sample contains vuggs.		R35, microns:		0.788		
		R50 (median pore throat radius):		0.240		

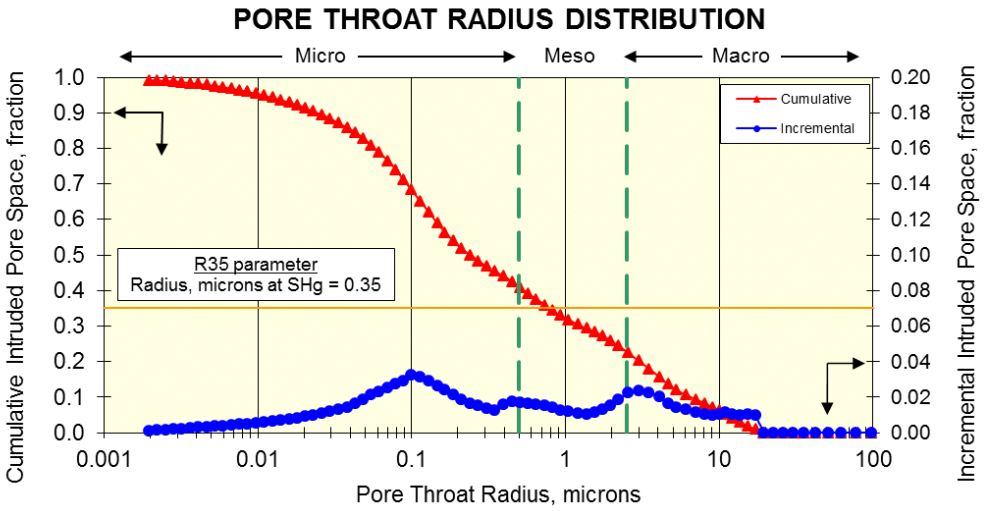

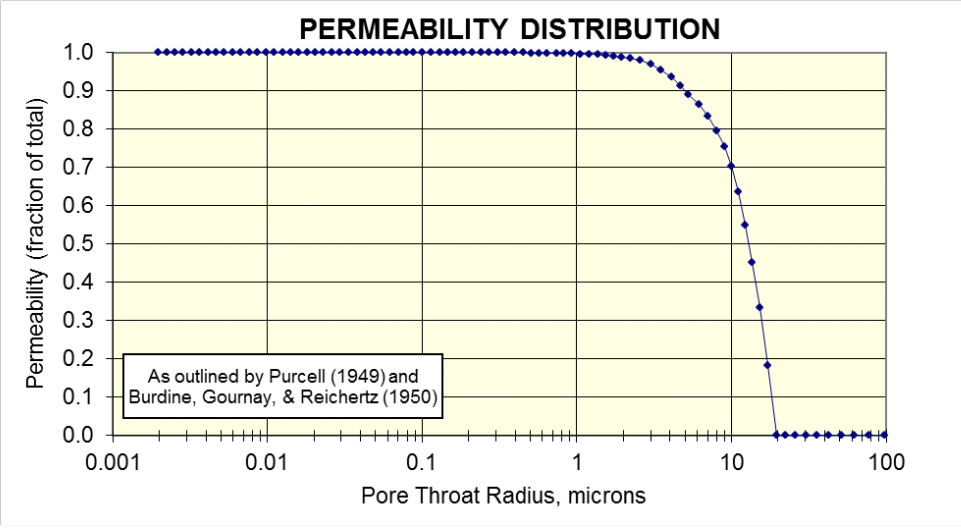

Company:	**Texas A&M University**
Well:	**3 Miles CNY Utah**
Location:	**Utah**
File:	**HOU-140913**

(1) Sample contains vuggs.

Sample:	**3MCP3S3**	un-	Host Plug (1)	
Texture	Thrombolite	stressed	800psi	n/a
Klinkenberg Permeability, md:		N/A	>50000	-
Permeability to Air, md:		N/A	>50000	-
Swanson Permeability, md:		447.	-	-
Porosity, fraction:		0.236	0.305	-
maximum Sb/Pc, fraction:		1.07		
R35, microns:		8.75		
R50 (median pore throat radius):		3.09		

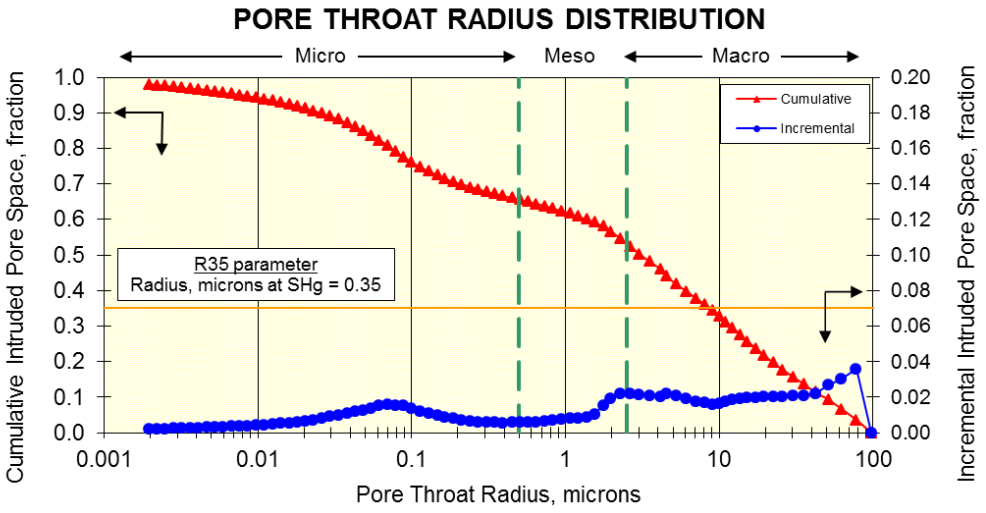

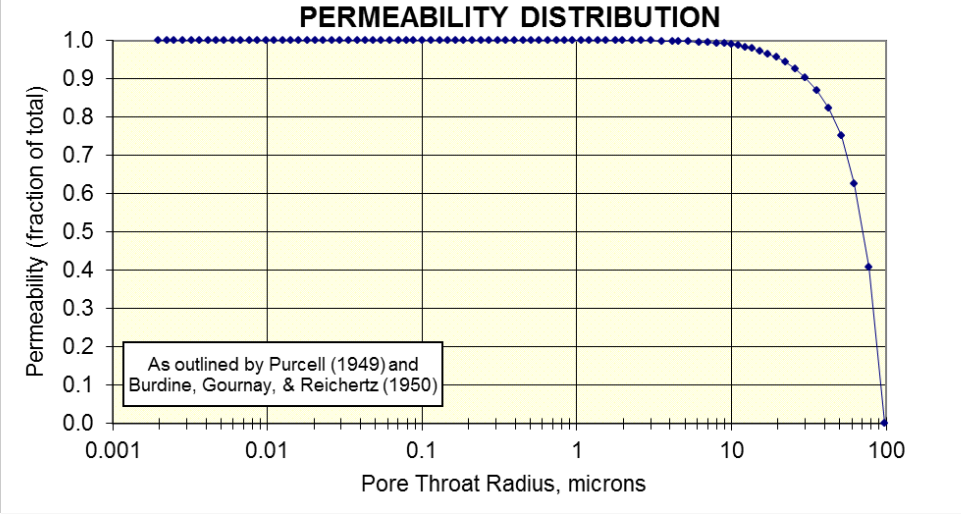

Company:	**Texas A&M University**	**Sample:**	3MCP3S3C	un-	Host Plug (1)
Well:	**3 Miles CNY Utah**	Texture	Digitate Stromatolite	stressed	800psi / n/a
Location:	**Utah**	Klinkenberg Permeability, md:		N/A	177. / -
File:	**HOU-140913**	Permeability to Air, md:		N/A	286. / -
		Swanson Permeability, md:		8.53	- / -
		Porosity, fraction:		0.126	0.188 / -
(1) Denotes fractured or chipped sample.		maximum Sb/Pc, fraction:		0.103	
Permeability and/or porosity may be optimistic.		R35, microns:		1.39	
Sample contains vuggs.		R50 (median pore throat radius):		0.476	

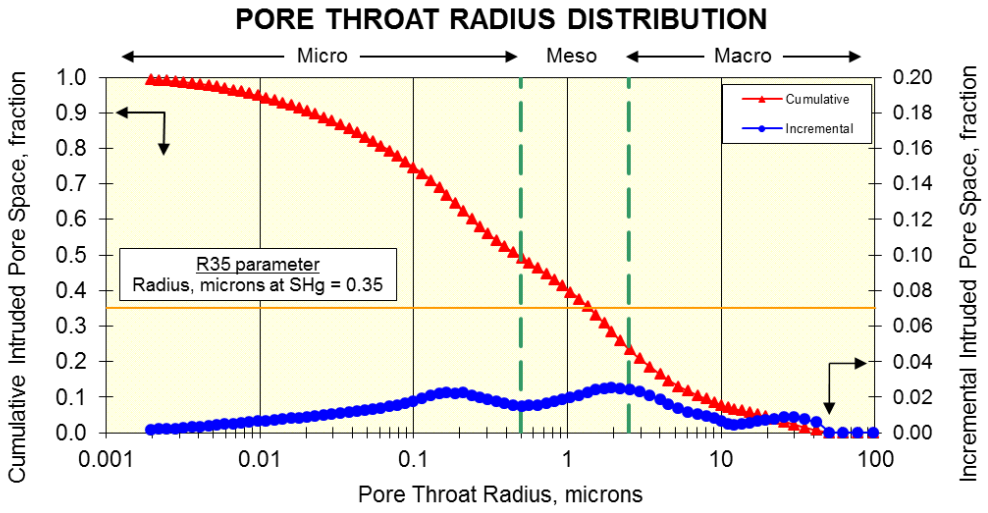

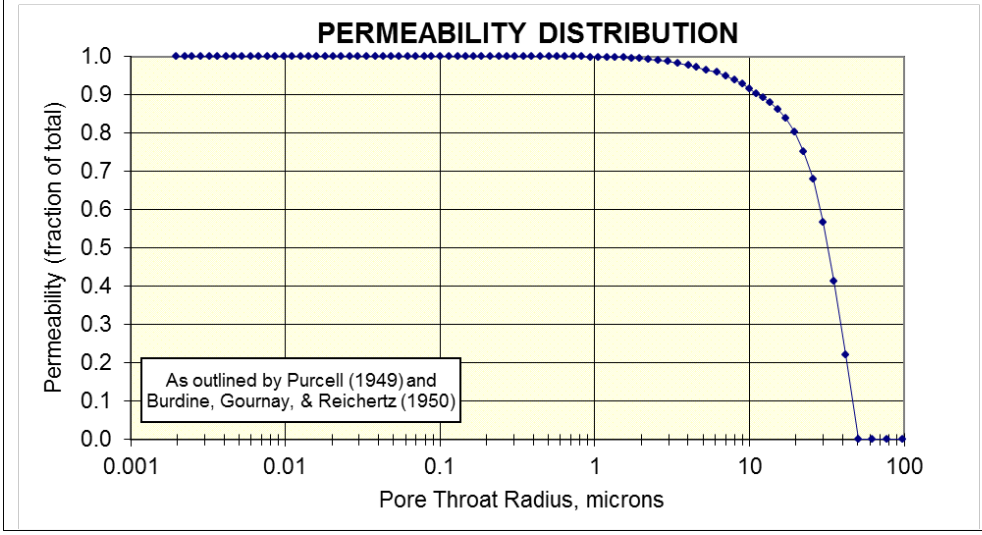

Company:	**Texas A&M University**	**Sample:**	**3MCP4S1**	un-	Host Plug (1)
Well:	**3 Miles CNY Utah**	Texture	Digitate Stromatolite	stressed	800psi	n/a
Location:	**Utah**	Klinkenberg Permeability, md:		N/A	165.	-
File:	**HOU-140913**	Permeability to Air, md:		N/A	231.	-
		Swanson Permeability, md:		38.3	-	-
		Porosity, fraction:		0.197	0.232	-
(1) Denotes fractured or chipped sample.		maximum Sb/Pc, fraction:		0.250		
Permeability and/or porosity may be optimistic.		R35, microns:		2.48		
Sample contains vuggs.		R50 (median pore throat radius):		0.917		

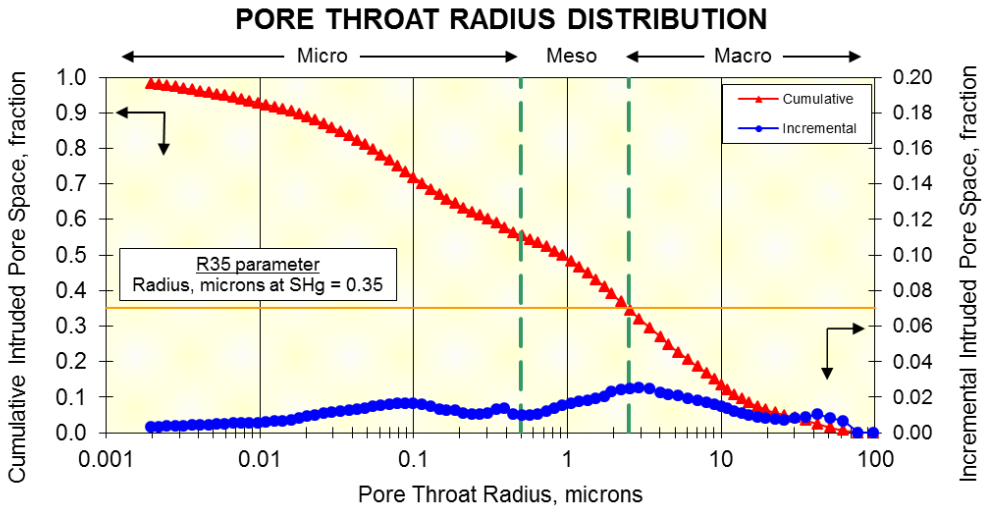

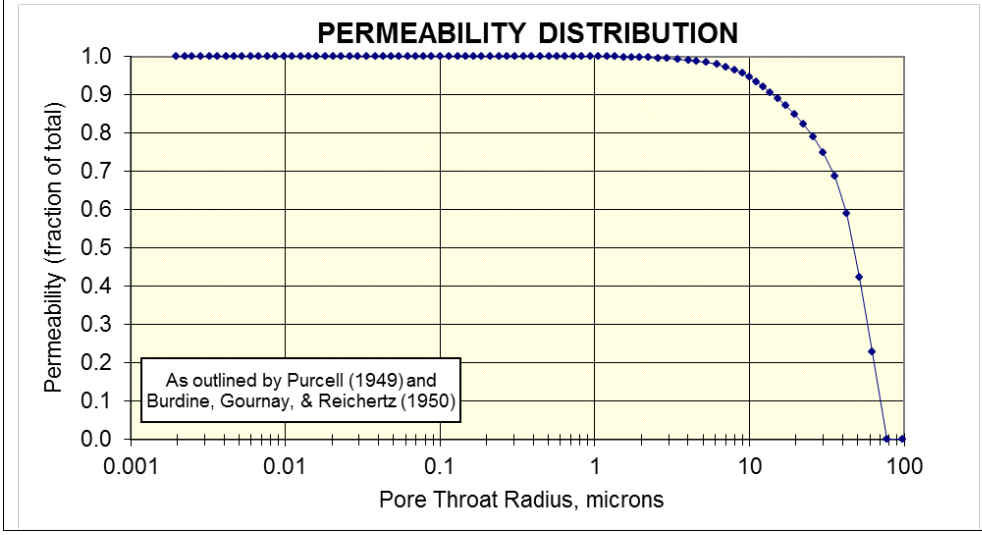

Company:	**Texas A&M University**	**Sample:**	3MCP5S1	un-	Host Plug (1)
Well:	**3 Miles CNY Utah**	Texture	Grainstone	stressed	800psi / n/a
Location:	**Utah**	Klinkenberg Permeability, md:		N/A	1830. / -
File:	**HOU-140913**	Permeability to Air, md:		N/A	2120. / -
		Swanson Permeability, md:		749.	- / -
		Porosity, fraction:		0.289	0.306 / -
		maximum Sb/Pc, fraction:		1.45	
(1) Sample contains vuggs.		R35, microns:		15.5	
		R50 (median pore throat radius):		9.53	

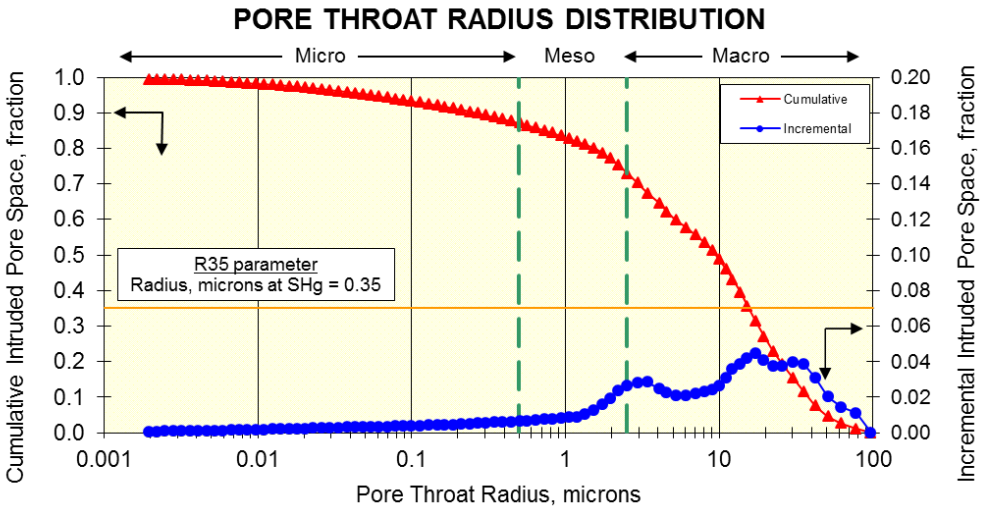

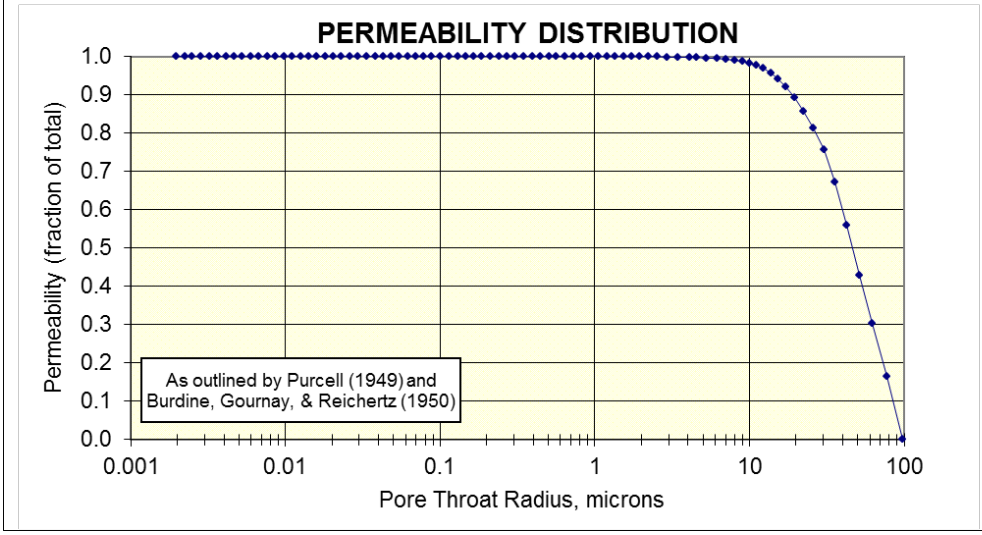

Company:	**Texas A&M University**	**Sample:**	3MCP5S4	un-	Host Plug (1)
Well:	**3 Miles CNY Utah**	Texture	Thrombolite	stressed	800psi / n/a
Location:	**Utah**	Klinkenberg Permeability, md:		N/A	258. / -
File:	**HOU-140913**	Permeability to Air, md:		N/A	378. / -
		Swanson Permeability, md:		255.	- / -
		Porosity, fraction:		0.191	0.228 / -
		maximum Sb/Pc, fraction:		0.767	
(1) Sample contains vuggs.		R35, microns:		3.80	
		R50 (median pore throat radius):		1.37	

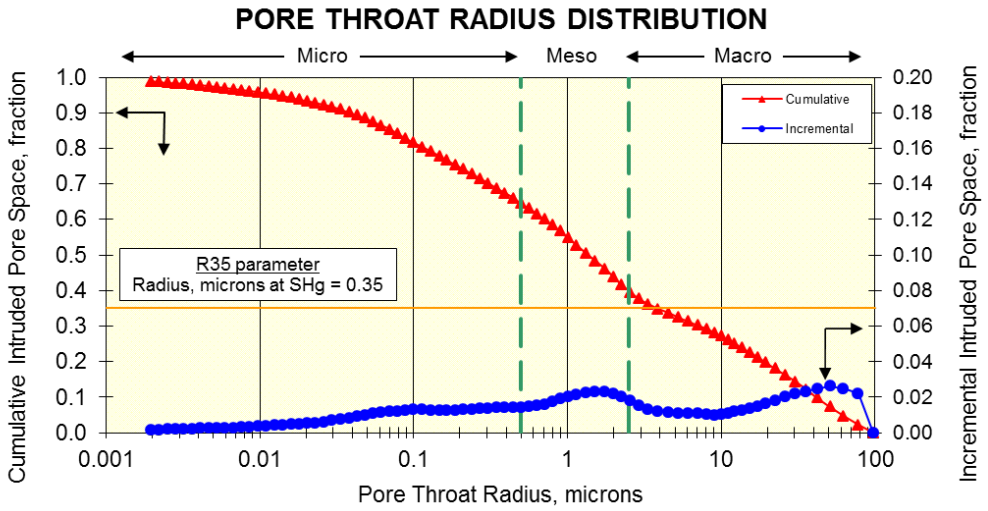

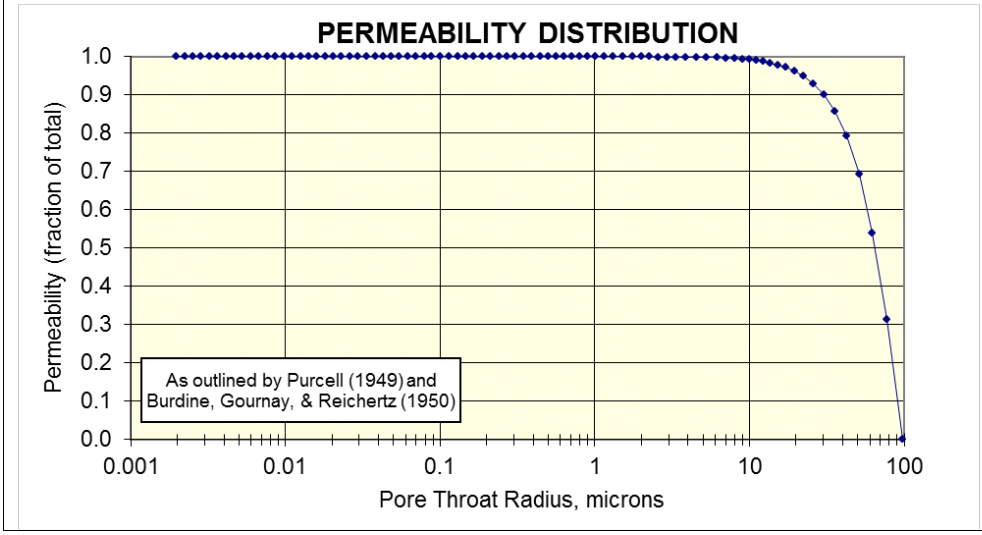

Company:	**Texas A&M University**	**Sample:**	3MCP5S7b	un-	Host Plug (1)
Well:	**3 Miles CNY Utah**	Texture	Thrombolite	stressed	800psi	n/a
Location:	**Utah**	Klinkenberg Permeability, md:		N/A	73.7	-
File:	**HOU-140913**	Permeability to Air, md:		N/A	110.	-
		Swanson Permeability, md:		44.1	-	-
		Porosity, fraction:		0.190	0.219	-
		maximum Sb/Pc, fraction:		0.272		
(1) Sample contains vuggs.		R35, microns:		1.94		
		R50 (median pore throat radius):		0.762